

**ROLE OF MITOCHONDRIAL CALCIUM UNIPORTER IN MITOCHONDRIAL MEMBRANE  
POTENTIAL INSTABILITY IN ISCHEMIA-REPERFUSION INJURY**

**by  
Deepthi Ashok**

**A dissertation submitted to Johns Hopkins University in conformity with the requirements for  
the degree of Doctor of Philosophy**

**Baltimore, Maryland  
June 2020**

## Abstract

Mitochondria exhibit non-stationary unstable membrane potential ( $\Delta\Psi_m$ ) when subjected to stress, such as during Ischemia/Reperfusion (I/R). Understanding mitochondrial instability in Ischemia Reperfusion injury is key to determining efficacy of interventions. Excess influx of mitochondrial  $\text{Ca}^{2+}$  and reactive oxygen species (ROS) accumulation are thought to be primary triggers of  $\Delta\Psi_m$  instability, but the underlying molecular mechanisms are still unclear.

The goal of this thesis is to understand the contributions of  $\text{mCa}^{2+}$  and ROS in triggering  $\Delta\Psi_m$  instability. For this purpose, it was important to first define and characterize oscillatory patterns of non-stationary mitochondrial  $\Delta\Psi_m$  instability. A data analysis tool was developed based on wavelet transform functions to automate analysis of time-series data from microscopy images to detect  $\Delta\Psi_m$  changes in an unbiased and reproducible manner. It is an ImageJ-MATLAB-based workflow called 'MitoWave' to unravel dynamic mitochondrial  $\Delta\Psi_m$  changes that occur during ischemia and reperfusion. Features such as, time-points of  $\Delta\Psi_m$  depolarization during I/R, area of mitochondrial clusters and time-resolved frequency components during reperfusion were determined per cell and per mitochondrial cluster with this tool.

We then used this tool to understand the role of  $\text{Ca}^{2+}$  and ROS in triggering  $\Delta\Psi_m$  instability. Physiologic  $\text{Ca}^{2+}$  entry via the Mitochondrial Calcium Uniporter (MCU) participates in energetic adaption to workload but is thought to contribute to cell death during I/R injury. We genetically knocked out the MCU to examine whether MCU-mediated  $\text{mCa}^{2+}$  uptake is required to trigger  $\Delta\Psi_m$  loss or oscillation during reperfusion in neonatal mouse ventricular myocyte (NMVM) monolayers. Our findings demonstrate that MCU knockout does not significantly alter  $\text{mCa}^{2+}$  import during I/R, nor does it affect  $\Delta\Psi_m$  recovery during Reperfusion. In contrast, blocking the

mitochondrial sodium-calcium exchange (mNCE) with CGP-37157 suppressed  $mCa^{2+}$  increase during Ischemia but did not affect  $\Delta\Psi_m$  recovery during reperfusion or the frequency of  $\Delta\Psi_m$  oscillations, confirming that mitochondrial  $\Delta\Psi_m$  instability on reperfusion is not triggered by  $mCa^{2+}$ . Interestingly, inhibition of mitochondrial electron transport and supplementation with antioxidants stabilized  $\Delta\Psi_m$  oscillations. The findings are consistent with  $mCa^{2+}$  overload being mediated by reverse-mode mNCE activity and support ROS-induced ROS release as the primary trigger of  $\Delta\Psi_m$  instability during reperfusion injury.

**Primary Reader and Advisor: Brian O'Rourke, PhD**

**Secondary Reader: David Kass, MD**

**Dedicated to my Amma, Appa, my sister Subha and my husband Amitabh**

## **Acknowledgements**

I cannot claim the joy and success I have in science as my own, because throughout my journey so far, I've had the support of enthusiastic and passionate individuals without whom I would not be where I am today.

First and foremost, I would like to thank my mentor Dr. Brian O'Rourke. It has been a humbling experience to work with a world-class mitochondrial expert such as Brian. He has taught me microscopy and all the nuances, which I consider a privilege, because not many professors are able to spend time at the bench helping you troubleshoot microscopy settings. It is not uncommon to see him donning a lab coat and tinkering with or setting up a microscope and it was an absolute joy to learn about all the workings from him. I am immensely grateful for all the times I've gone to him feeling stuck, and Brian would come up with a simple feasible solution. While his positive and encouraging attitude is what got me through the tough times in graduate school, his unassuming and generous persona made it easy for me to express my thoughts and questions, thus shaping me as an independent scientist. I always came from every meeting with Brian, happier and excited about doing experiments. Apart from my thesis work, I treasure all our conversations from quantum biology to the joys of going to Disneyland with kids. He is a true scientist. He is an incredibly supportive and enthusiastic person and I consider myself lucky to be mentored by him.

I am also so grateful to my dear friend Agnes Sidor. Since my first interaction with her, when she asked me if I knew what I'd be working on, I cherish every moment with her. It has my pleasure learning not just molecular biology from Agnes, but also about how to work through a problem logically and carefully. I admire her rational thought process and her meticulous work

ethic. In fact, it was one of our early conversations where Agnes told me an anecdote - Polish engineers who constructed bridges did such an impeccable job that they would stand under the bridge when it was being tested because they were so thorough and confident with their work. I have recollected this story multiple times over the years when I performed by own experiments. Do I feel confident about my results? Have I been thorough? Can I stand with my experiments like those Polish engineers? Agnes has definitely shaped my growth as a scientist and I consider myself richer for it.

Kyriakos Papanicolaou is the most generous person I know. This dissertation would not be possible if not for his immense help. He is an extremely hard-working person and one can always find him in the lab (with his t-shirt which he wears inside out) from 10:00 AM to 12:00 AM everyday. He is enthusiastic to help no matter what the problem is. He has been patient while teaching me protein quantification techniques. He has always been there to discuss every aspect of my project, he was my sounding board, he asked great questions that helped me clarify concepts in my mind and was often the person I went to for advice. I am grateful for his influence on my development as a scientist.

Ting Liu is a gifted and dedicated scientist whose appreciation and understanding of cardiac physiology is profound. I am in awe of his vast and intricate knowledge. I am fortunate to have learnt cardiac cell isolation techniques from him.

Michelle Wang and Lauren Parker were intelligent undergraduate researchers I had the pleasure of working with. They are the next generation of great scientists and physicians and seeing their enthusiasm and energy made me happy. I am so grateful for their time and presence in our lab.

I am also grateful to have the chance to work with and learn from An-Chi Wei, Swati Dey, Nattayaporn Apaijai, Rebeca Joca, Brian Foster, Sara Nathan, Samarjit Das and Barbara Roman. My time as a graduate student was enhanced because of these wonderful individuals and I am grateful to them.

Brian's lab has been my home, my place of joy, and my place of peace the past six years.

Outside of lab, I would like to extend my gratitude to my thesis committee members. David Kass and Mark Anderson, experts in cardiac physiology, have always offered great insight and support throughout graduate school. Rajini Rao, the chair of my committee has asked tough and insightful questions about my thesis, while always looking out for me giving me practical advice and encouragement. She is an inspiration.

I would also like to thank Colleen Graham and Leslie Lichter of the Cellular and Molecular Medicine Graduate program for their kindness and support throughout graduate school.

Special thanks to my dear friend Itzy Morales Pantoja. Though we met quite late in graduate school, we have become close friends because of our similar wavelengths. I cherish the Thursday early mornings we spent together drinking coffee and working on our theses. I am so glad and grateful to have her with me during this journey.

I am also so grateful to my mentors from my previous lab, Casey Quinlan, Adam Orr and Martin Brand. It was in this lab that I saw my biochemistry textbook come alive with experiments to understand mitochondrial biology. They were so supportive and gave me reliable advice and encouragement, without which I could not be here at a place like Hopkins.

Finally, I would like to thank my family.

I might have been 8 or 9 years old when my younger sister and I noticed that if we tried to stay really still, we couldn't. Our bodies had a rhythm that we couldn't stop even if we held our breath. At that time, we knew about our hearts but it was at that moment that we really appreciated what it meant by the heart pumping blood to the whole body. The heart rhythm resonated in the whole body. Was my sister's rhythm different from mine? Would this rhythm change if I scared my sister or chased her? While these questions might have been naïve, they were my earliest memories about being fascinated by the human body. My sister, Subha, was probably my earliest co-conspirator, with us collecting insects and bird shells and identifying them, to us doing 'science experiments' with anything we found around the house. My sister is a strong, creative and bright person and I look up to her immensely. Now she has a daughter, my little niece Tarini who has accelerated me to finish graduate school quickly so I can go visit her.

There are not enough words in the world to express my gratitude to my parents, my mother, Kalyani and my father, Ashok. My mother is a strong, practical and light-hearted person for whom there was no problem too big to solve. My father is an extremely hard-working person who worked everyday from 9AM-9PM. In fact, my father who is a physician is there at the front-lines battling COVID-19 in India. My parents are my role-models and my inspiration. They always encouraged and supported all my dreams. They gave me my first microscope when I was in grade 6. It is because of them that I could even dream to be here at Hopkins.

Finally, I'd like to express my gratitude to my husband Amitabh. He is my biggest advocate and my support. He made me realize that with patience, anyone can understand anything however complicated. My dream of a great education has been realized because of Amitabh.



## Table of Contents

ABSTRACT.....	ii
ACKNOWLEDGEMENTS.....	v
LIST OF TABLES.....	xi
LIST OF FIGURES.....	xii
<b>CHAPTER I: INTRODUCTION.....</b>	<b>1</b>
MITOCHONDRIAL OSCILLATIONS .....	4
MITOCHONDRIAL MEMBRANE POTENTIAL ( $\Delta\Psi_M$ ) .....	6
CONDITIONS THAT TRIGGER MITOCHONDRIAL OSCILLATIONS .....	8
MITOCHONDRIAL CHANNELS AND $\Delta\Psi_M$ INSTABILITY .....	9
MITOCHONDRIAL PERMEABILITY TRANSITION PORE (MPTP) .....	9
THE INNER MEMBRANE ANION CHANNEL (IMAC) AND TRANSLOCATOR PROTEIN (TSPO).....	11
MITOCHONDRIAL $Ca^{2+}$ IMPORT AND $\Delta\Psi_M$ INSTABILITY .....	12
GENETIC MANIPULATION OF MITOCHONDRIAL CALCIUM UNIPORTER AND ASSOCIATED SUBUNITS IN I/R INJURY .....	13
FACTORS AFFECTING $[Ca^{2+}]$ IN MITOCHONDRIA .....	16
$\Delta\Psi_M$ OSCILLATORY BEHAVIOR IN CARDIOMYOCYTE: SPATIAL CHARACTERISTICS AND IMPLICATIONS .....	18
HYPOTHESIS.....	20
<b>CHAPTER II: SPATIO-TEMPORAL ANALYSIS OF MITOCHONDRIAL MEMBRANE POTENTIAL FLUCTUATIONS DURING ISCHEMIA-REPERFUSION .....</b>	<b>21</b>
INTRODUCTION.....	21
METHODS: .....	23
RESULTS .....	34
DISCUSSION .....	45
<b>CHAPTER 3: MITOCHONDRIAL MEMBRANE POTENTIAL INSTABILITY PERSISTS IN ISCHEMIA/REPERFUSION INJURY IN MCU-KO CARDIOMYOCYTES .....</b>	<b>48</b>
INTRODUCTION.....	48
METHODS .....	50
RESULTS .....	56
DISCUSSION .....	80
CONCLUSIONS .....	86
<b>CHAPTER 4: FUTURE DIRECTIONS .....</b>	<b>87</b>
DOES ACTIVATING HYPOXIA INDUCIBLE FACTOR PRIOR TO I/R PREVENT MITOCHONDRIAL INSTABILITY? .....	87
MOTIVATION.....	87
RESULTS AND DISCUSSION:.....	87

**DOES KNOCKING OUT MITOCHONDRIAL  $\text{Na}^+/\text{Li}^+/\text{Ca}^{2+}$  EXCHANGER AFFECT  $\text{mCa}^{2+}$  IMPORT DURING ISCHEMIA/REPERFUSION? .....90**

**REFERENCES .....91**

**APPENDICES .....104**

**CURRICULUM VITAE .....128**

**List of Tables**

Table 1. Visual Observations during reperfusion..... 35

## List of Figures

Figure 1.1: Molecular mechanisms in Ischemia/Reperfusion: Cytosolic and Mitochondrial changes .....	3
Figure 1.2: Mitochondrial Membrane Potential generation .....	7
Figure 1.3: Multisubunit Mitochondrial Calcium Uniporter Complex .....	16
Figure 1.4: Mitochondrial Ca <sup>2+</sup> Influx/Efflux pathways.....	17
Figure 1.5: Hypothesis .....	20
Figure 2.1: Identification of Ischemic depolarization time.....	28
Figure 2.2: Mitochondria exhibit different $\Delta\Psi_m$ oscillatory behaviors upon reperfusion. ....	30
Figure 2.3: Schematic of Mito-wave analysis for $\Delta\Psi_m$ feature extraction. ....	32
Figure 2.4: Defining $\Delta\Psi_m$ Oscillatory patterns during reperfusion qualitatively and quantitatively:.....	36
Figure 2.5: Predominant frequencies exhibited by mitochondrial clusters during reperfusion. ....	39
Figure 2.6: Mitochondrial Cluster size and Frequency relationship.....	41
Figure 2.7: Time taken for $\Delta\Psi_m$ loss during Ischemia and Reperfusion .....	42
Figure 2.8: Relationship between Ischemic $\Delta\Psi_m$ depolarization time and Oscillatory behavior during Reperfusion .....	44
Figure 3.1: Methods and Protocol .....	52
Figure 3.2: Addition of Ad-Cre results in knockout of MCU in 5 days in NMVMs .....	58
Figure 3.3: Functional effects of MCU knockout; representative mCa <sup>2+</sup> transients in spontaneously beating MCU-WT and MCU-KO neonatal mouse ventricular myocytes.....	59
Figure 3.4: MCU is required for rapid Ca <sup>2+</sup> uptake into mitochondria .....	60
Figure 3.5: 4mtd3cpv (MitoCam) FRET probe calibration trace.....	61
Figure 3.6: Example traces of mCa <sup>2+</sup> during Ischemia/Reperfusion in MCU WT (top) and KO (bottom) monolayers.....	64
Figure 3.7: MCU knockout does not affect mitochondrial Ca <sup>2+</sup> import during Ischemia and Reperfusion, but blocking mNCE with CGP-37157 prevents mCa <sup>2+</sup> during Ischemia .....	65
Figure 3.8: CGP-37157 effect on Cytoplasmic Ca <sup>2+</sup> .....	66
Figure 3.9: MCU-KO does not protect against $\Delta\Psi_m$ loss during I/R, nor does CGP.....	70
Figure 3.10: Inhibiting mitochondrial electron transport chain component Complex I stabilizes $\Delta\Psi_m$ oscillations during Reperfusion in MCU-WT cells.....	73
Figure 3.11: Addition of cell-permeable Glutathione ethyl ester (GSHee) reduces and eventually stops $\Delta\Psi_m$ oscillations during reperfusion .....	75
Figure 3.12: Addition of CsA does not affect $\Delta\Psi_m$ oscillations.....	76
Figure 3.13: Empirical Cumulative Distribution Functions comparing different treatments on high-frequency $\Delta\Psi_m$ oscillators during reperfusion. ....	78
Figure 3.14: LDH Assay as a measure of cytotoxicity at the end of Reperfusion after Ischemia. ....	79
Figure 4: Addition of DMOG stabilizes $\Delta\Psi_m$ oscillations. ....	89

## CHAPTER I: Introduction

A Myocardial Infarction (MI) occurs when the blood flow to the heart is blocked by coronary occlusion, thus preventing the supply of blood to the ventricle. Ischemic Heart Disease is the leading cause of death world-wide (1). Angioplasty or stenting is done to restore normal blood flow to the myocardium. Reperfusion itself, while indispensable, causes injury, in part through production of Reactive Oxygen Species ROS. This injury causes a cascade of effects causing damage at the cellular level and the final tip over point occurs when the mitochondrial permeability transition occurs, releasing cytochrome c and pro-apoptotic factors into the cytosol(2).

### **Molecular Mechanisms of Ischemia and Reperfusion: cytosolic and mitochondrial changes in the cardiomyocyte**

During Ischemia, the lack of oxygen causes the myocyte to rely on anaerobic respiration, resulting in increased lactate production and decreased intracellular pH. While glycolysis may initially assist in energy production, it is not sustained, since acidification inhibits phosphofructokinase. There is a decrease in high-energy phosphate groups like creatine phosphate and ATP (3). Decrease in ATP inactivates the  $\text{Na}^+/\text{K}^+$  ATPase, increasing cytosolic  $\text{Na}^+$ . Acidification also prompts the  $\text{Na}^+/\text{H}^+$  exchanger to extrude  $\text{H}^+$  in exchange for  $\text{Na}^+$ , thus raising  $\text{Na}^+$  levels and leading to intracellular  $\text{Na}^+$  overload. As a consequence, the  $\text{Na}^+/\text{Ca}^{2+}$  exchanger (NCX) is forced to work in reverse, extruding  $\text{Na}^+$  while importing  $\text{Ca}^{2+}$ , leading to  $\text{Ca}^{2+}$  overload in the cell. Under these conditions of depleted ATP, xanthine is generated via xanthine oxidase,

a source of superoxide even under these low oxygen conditions. Lack of oxygen as the terminal electron acceptor in oxidative phosphorylation results in decreased ATP levels and accumulation of reducing equivalents in mitochondria. Ultimately, mitochondria are unable to maintain  $\Delta\Psi_m$ . Conditions of increased oxidative stress, along with dysregulation of matrix pH, mitochondrial  $\text{Ca}^{2+}$ , and ATP production, cause the mitochondria during Ischemia to become increasingly impaired. The extent of mitochondrial damage during Ischemia heavily influences recovery during reperfusion. (4),(5),(6),(3). Under the acidic conditions of ischemia, the mitochondrial permeability transition pore does not open, but it is primed for opening on reperfusion, and the cardiomyocyte undergoes hypercontracture.

During Reperfusion, the restoration of oxygen supply allows the electron transport chain to be activated, thus restoring NADH oxidation, proton pumping and  $\Delta\Psi_m$ . The Na-K<sup>+</sup> ATPase and NCX get reactivated and Na<sup>+</sup> is extruded. However, extrusion of Na<sup>+</sup> via NCX promotes  $\text{Ca}^{2+}$  entry. Restoration of  $\Delta\Psi_m$  also allows  $\text{Ca}^{2+}$  entry into the mitochondria, which can cause m $\text{Ca}^{2+}$  overload. pH returns to normal and the Na<sup>+</sup>/H<sup>+</sup> exchanger allows extrusion of H<sup>+</sup>. The sudden shutdown (Ischemia) and start-up (reperfusion) of Oxidative Phosphorylation results in impaired redox balance, mitochondrial ROS accumulation and the activation of energy dissipating ion channel. Production of excess ROS, along with influx of  $\text{Ca}^{2+}$  and restoration of pH, makes conditions favorable for mPTP opening, which can trigger cell death. (7), (8), (9), (2). (Figure 1.1)

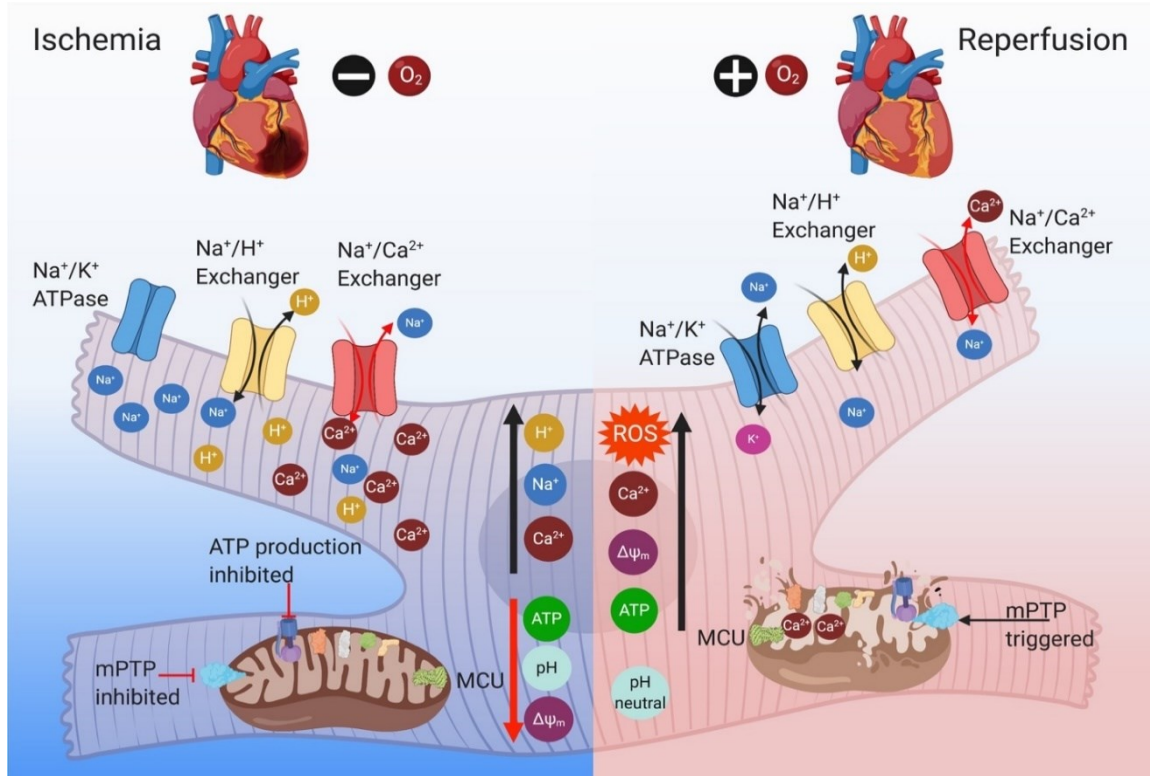


**Figure 1.1: Molecular mechanisms in Ischemia/Reperfusion: Cytosolic and Mitochondrial changes**

During Ischemia, the lack of oxygen causes the cardiomyocyte to rely on anaerobic respiration instead of oxidative phosphorylation. This increases lactate production and decreases the pH. A decrease of ATP inhibits Na<sup>+</sup>/K<sup>+</sup> ATPase, therefore increasing cytosolic Na<sup>+</sup>. Acidification causes Na<sup>+</sup>/H<sup>+</sup> exchanger to extrude H<sup>+</sup> and allow Na<sup>+</sup> in, increasing of Na<sup>+</sup> further. Together with loss of ΔΨ<sub>m</sub>, this favors reverse-mode Na<sup>+</sup>/Ca<sup>2+</sup> exchange activity, increasing cytosolic Ca<sup>2+</sup>. Under low pH, the mitochondrial permeability transition pore (mPTP) is inhibited. During reperfusion, the mitochondrial oxidative phosphorylation system is suddenly restarted leading to some ATP production along with increasing Reactive Oxygen Species. ATP production allows activation of the Na<sup>+</sup>/K<sup>+</sup> pump, which can facilitate forward-mode plasmalemmal Na<sup>+</sup>/Ca<sup>2+</sup> exchange, and SR Ca<sup>2+</sup> pump activity, extruding Na<sup>+</sup> and lowering Ca<sup>2+</sup>; however, additional mitochondrial Ca<sup>2+</sup> loading can occur as ΔΨ<sub>m</sub> is restored. Recovery of pH, an increase in ROS, and mCa<sup>2+</sup> loading can trigger mPTP opening and cell death.

## Mitochondrial Oscillations

Oscillatory behavior of mitochondria was discovered as early as 1965 by several groups(10),(11),(12),(13). Mitochondrial oscillations in ion fluxes and metabolic components, such as NADH, ROS,  $\text{Ca}^{2+}$ , pH, and  $\Delta\Psi_m$  were observed. In response to stress, mitochondria exhibit various phenotypes that can be qualitatively and quantitatively measured such as changes in morphology, membrane potential, oxygen consumption, reactive oxygen species generation, mitochondrial DNA transcription and translation.

Mitochondrial instability is a hallmark of pathological stress. Mitochondria are at the heart of ATP supply insufficiency causing electrophysiological changes, accumulation of excess  $\text{Ca}^{2+}$  and  $\text{Na}^+$  and excess ROS production under pathological conditions. Abrupt changes in mitochondrial membrane potentials, known as membrane potential oscillations are a reproducible phenomenon occurring under stress. They have been extensively studied in cardiac mitochondria by our group (14), (15),(16)

Oscillations can be thought of as a read-out for the complex non-linear dynamic mitochondrial system. Studying oscillatory properties in terms of frequency, amplitude and coherence between oscillators under different conditions helps to reveal the important regulators of the mitochondrial system. Our lab was the first to demonstrate that mitochondrial  $\Delta\Psi_m$  heterogeneity has pathological consequences in ventricular fibrillation and tachycardia (17). Mitochondrial oscillations, when triggered under pathological conditions, scale up and trigger myocardium-level arrhythmias and precipitate sudden death (18).

To understand the mechanism of mitochondrial oscillations, several questions need to be answered. First, how do we quantify and characterize mitochondrial oscillations when they

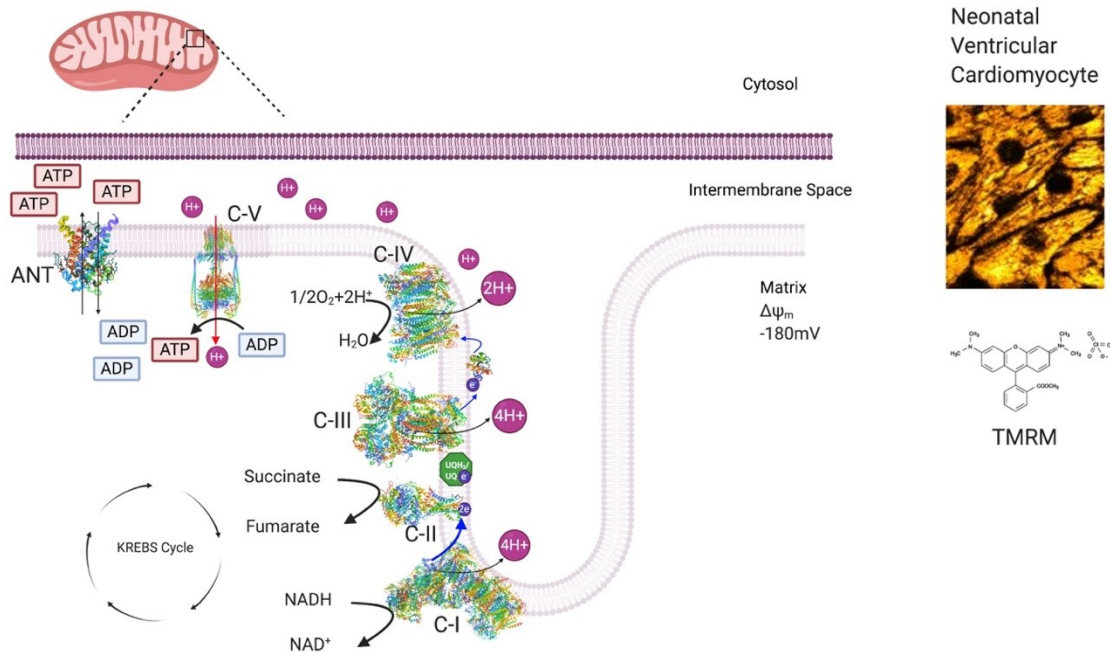


exhibit variable non-stationary behavior? Can we predict the occurrence of mitochondrial oscillation prior to their onset based on initial conditions? What positive and negative feedback loops control oscillatory behavior? And the most important question: Can we tune these feedback loops and control oscillations to prevent pathology? This thesis attempts to answer these questions by first presenting the background on the origin of mitochondrial oscillations under physiological and pathological conditions (in Chapter I). Characterizing oscillatory patterns of non-stationary mitochondrial  $\Delta\Psi_m$  instability is advanced by developing a new data analysis method using wavelet transform functions (described in Chapter II). For this, we developed 'MitoWave', an ImageJ and MATLAB based image-processing workflow, for extracting predominant frequencies, timepoints at which these frequencies are exhibited, and the area of oscillating mitochondrial clusters. We employed this tool to test potential candidates that could be 'regulators' (positive or negative) of ischemia-induced  $\Delta\Psi_m$  oscillations. We genetically knocked out the mitochondrial  $\text{Ca}^{2+}$  uniporter responsible for  $\text{Ca}^{2+}$  import into the mitochondria and boosted the antioxidant capacity of cardiomyocytes subjected to in vitro Ischemia/Reperfusion injury and analyzed the  $\Delta\Psi_m$  oscillatory response (described in Chapter III).

## Mitochondrial Membrane Potential ( $\Delta\Psi_m$ )

The principal function of the mitochondria is generation of ATP through oxidative phosphorylation. Electrons released from reducing pyridine nucleotide equivalents (NADH and  $\text{FADH}_2$ ) are faithfully transferred via the electron transport chain (ETC) complexes (Complex I-IV) to  $\text{O}_2$ . While three of the ETC complexes (I, II and IV) pump  $\text{H}^+$  across the mitochondrial inner membrane, complex II (succinate dehydrogenase) does not. Pumping of protons produces an electrochemical gradient across the inner membrane with a proton motive force of  $\sim 180\text{mV}$ . A rotary catalysis mechanism by the ATP synthase (19) harnesses the proton motive force generated by the electrochemical gradient and couples it to ATP production. (Figure 1.2)

A portion of the electrons entering the electron transport chain may be diverted to the single electron reduction of oxygen to generate superoxide, particularly when the ETC is defective or impaired. Superoxide is typically scavenged by Superoxide Dismutase to generate the reactive oxygen species, hydrogen peroxide ( $\text{H}_2\text{O}_2$ ), which is then detoxified by peroxidase enzymes. In the ROS-induced ROS release hypothesis, disruption in the balance of ROS production and scavenging triggers the activation of energy dissipating channels that cause mitochondrial depolarization and an additional burst of ROS. This can happen cyclically during mitochondrial oscillation.



**Figure 1.2: Mitochondrial Membrane Potential generation**

(A) The mitochondrial respiratory chain consists of proton translocating complexes (I, III and IV) that couple proton pumping to electron flow. Reducing equivalents (NADH and FADH<sub>2</sub>) feed electrons into complex I and II. Complex I transfers 2e<sup>-</sup> to the Ubiquinone pool (UQ) and pumps 4H<sup>+</sup>, Complex II transfers 2e<sup>-</sup> to the UQ pool without pumping any protons. Complex III translocates 2e<sup>-</sup> and 4H<sup>+</sup>. Complex IV translocates 2H<sup>+</sup> and 2e<sup>-</sup> while reducing 1/2 O<sub>2</sub> to H<sub>2</sub>O. Thus, pumping of protons generates the proton motive force that is used by ATP synthase for ATP production. (Adapted from (19)) (B) TMRM is a lipophilic cationic dye that sequesters into energized mitochondria. Here, Neonatal ventricular myocytes have TMRM sequestered in them indicating polarized mitochondria.

Protein structures from obtained from PDB: Complex I (5XTD)(20), Complex II (6MYO), Complex III (1BGY)(21), Complex IV (1OCC)(22), ATP Synthase (6QUM) (23)

## Conditions that trigger mitochondrial oscillations

Some of the earliest studies in our lab showed that when guinea-pig cardiomyocytes were subjected to fuel substrate deprivation (glucose starved), their sarcolemmal KATP channel currents displayed oscillations. This was correlated with cycles of oxidation and reduction of NADH. Increases in sarcolemmal KATP current followed the decrease of NADH, indicating that it was the change in energy metabolism that initiated the change in sarcolemmal KATP current. These oscillations helped reduce energy consumption by reducing action potential duration and thus facilitated oscillations in action potential duration. (24). A mitochondrial origin for the oscillations was established when Romashko et. al found that oxidation-reduction cycles of mitochondrial flavoproteins were correlated with mitochondrial membrane potential depolarization and repolarization. These redox phenomena could encompass the whole myocyte or large clusters of mitochondria. Redox waves were found to propagate from one myocyte to another, highlighting the importance of synchronization of mitochondrial network in the redox-wave phenomena (25). Subsequent studies revealed that uncoupled mitochondria consume intracellular ATP stores thus resulting in low ATP/ADP ratio. This activates the ATP-sensitive K<sup>+</sup> channel, affecting the action potential of the cardiomyocyte, thus linking mitochondrial metabolism to cardiomyocyte excitability (26).

Aon et. al found that photooxidation of a small cluster of mitochondria in a cardiomyocyte could reliably trigger  $\Delta\Psi_m$ , NADH and ROS oscillations in the whole cell. (14). The main driver for mitochondrial instability was found to be ROS (27). Experiments with glutathione depletion also confirmed the main role ROS plays in triggering  $\Delta\Psi_m$  instability (28). ROS are formed when electrons leak from the ETC and are not scavenged by ROS scavenging mechanisms in the

intermembrane space (cytochrome c and Cu/Zn-SOD) and in the matrix (Mn-SOD) (29) . These ROS can further cause damage by interacting with membranes and other proteins. They can thus escape through membranes and damage nearby organelles, through a phenomenon called ROS Induced ROS release (RIRR) (30). When the antioxidant defenses are overwhelmed, ROS accumulation beyond a certain threshold occurs and causes the mitochondrial network to approach a 'critical' level. This phenomenon is called mitochondrial criticality (31). When criticality occurs, excess ROS is released through a channel in the mitochondrial inner membrane and causes instability of neighboring mitochondria. Other labs have observed superoxide oscillations occurring in single or small clusters of mitochondria and termed them 'mitoflashes'(32). This interpretation has been questioned because the mt-cpYFP probe used as an indicator for superoxide is also known to be sensitive to changes in pH, leading some to refer to the oscillatory behavior as pH transients (33). Whether all of these phenomena occur by different mechanisms or are the same fundamental process remains to be determined but all appear to involve RIRR.

### **Mitochondrial channels and $\Delta\Psi_m$ instability**

#### **Mitochondrial Permeability transition pore (mPTP)**

The mitochondrial permeability transition pore is a non-specific large conductance pore located in the inner mitochondrial membrane that is normally closed (34). A physiological role for the mPTP, which is not firmly established, is that it may contribute to ion homeostasis when it opens transiently (35). Nevertheless, a pathological role in Ischemia/Reperfusion injury has been consistently observed (36). The molecular identity of the mPTP is currently debated, but

Cyclophilin D, Adenine Nucleotide Translocator, Phosphate Carrier, Bax and Bak are believed to be involved in the modulation of the mPTP, with the ATP synthase potentially comprising the pore domain (37). It is a large conductance channel of 0.9-1.3 nS that allows non-specific solutes up to 1.5kDa when open. Optimal conditions for the mitochondrial permeability transition to occur are: high  $\text{Ca}^{2+}$ , oxidative stress (if matrix NADH and Glutathione are oxidized, or high ROS), elevated Pi and an optimal pH of above 7. Conditions that prevent mPTP opening are low pH, high proton motive force, Cyclosporine A (CsA), which binds to Cyclophilin D and Bongkreikic Acid (BKA) which inhibits the ANT (34).

Given the established role of mPTP in I/R injury, it seemed like an obvious candidate for its role in triggering  $\Delta\Psi_m$  instability. Classical mPTP is defined as one that is blocked by CsA and high  $\text{Ca}^{2+}$ . However, studies from our lab show that addition of CsA did not affect  $\Delta\Psi_m$  oscillations in guinea pig cardiomyocytes. Also, if mPTP was involved in these oscillations, the opening of the pore should allow large molecules (up to 1.5kDa) to pass through. Both CM-DCF (of  $\sim 600\text{Da}$ ) and Calcein (of  $\sim 622\text{ Da}$ ) were not released from the mitochondrial matrix during  $\Delta\Psi_m$  oscillations. Further, addition of 1mM EGTA to chelate  $\text{Ca}^{2+}$ , or cellular  $\text{Ca}^{2+}$  depletion, did not affect laser-flash induced  $\Delta\Psi_m$  oscillations, showing that  $\text{Ca}^{2+}$  was not a major factor in triggering oscillations (14). Further, CsA did not have any effect on arrhythmias after ischemia (17). Thus, from these studies, it indicated that mPTP was not involved in  $\Delta\Psi_m$  oscillations.

## **The Inner Membrane Anion Channel (IMAC) and Translocator protein (TSPO)**

An Inner Membrane Anion Channel (IMAC) in mitochondria was described in the 1980s (38) as a partially anion-selective pore that was sensitive to variety of amphipathic compounds. Although the molecular identity of IMAC is currently unknown, based on pharmacological evidence, we proposed that IMAC plays a role in  $\Delta\Psi_m$  instability and Action Potential Duration reduction under stress. IMAC is permeable to a number of inorganic anions ( $\text{NO}_3^-$ ,  $\text{Cl}^-$ , Pi, superoxides) and organic anions (oxaloacetate, citrate, malate,  $\text{ATP}^{4-}$ ). In mitoplast patch clamp studies, a method for direct assessment of channels in the inner membrane, a prominent anion channel with a conductance of 108pS has been reported.  $\text{Mg}^{2+}$  and low pH decrease the probability of opening of this channel (O'Rourke, 2007) (39). The TSPO, previously known as the peripheral benzodiazepine receptor for its high affinity for certain benzodiazepines and isoquinoline carboxamides, is now termed the mitochondrial translocator protein (40). Although it is located in the outer membrane in association with the voltage-dependent anion channel VDAC, it is thought to regulate IMAC and/or the mPTP. Another physiological role of TSPO is the regulation of cholesterol transport across the inner membrane and steroidogenesis. Although there are similarities in the pharmacological regulators of TSPO and IMAC, their relationship to each other is unclear. For example, the benzodiazepine, 4'-chlorodiazepam, inhibits IMAC flux (isolated mitochondria), as well as cellular mitochondrial depolarization under oxidative stress, and it is proposed that IMAC is the first to response to oxidative stress, while mPTP activates under more prolonged stress conditions (28), (41). During ischemia-reperfusion, 4'-chlorodiazepam prevented ischemia-induced AP duration (APD) shortening and inexcitability, while the TSPO agonist FGIN-1-27 promoted APD shortening and conduction failure with

ischemia (17)(42). Cardiac-specific knockdown of TSPO in rats was also protective against arrhythmias after Ischemia in hypertensive rats (43). Since TSPO and IMAC are close to each other, and antagonists for TSPO, 4'-chlorodiazepam and PK11195, are known to block IMAC, genetic manipulation studies might be better at dissecting the exact mechanism of triggering  $\Delta\Psi_m$  instability and the chronology of the cascading events.

### **Mitochondrial $\text{Ca}^{2+}$ import and $\Delta\Psi_m$ instability**

$\text{Ca}^{2+}$  plays an important role in relaying cytosolic signals for energy demand to the mitochondria (44).  $\text{Ca}^{2+}$  is responsible for activating three enzymes involved in the Krebs cycle, namely the pyruvate dehydrogenase complex, isocitrate dehydrogenase and alpha-ketoglutarate dehydrogenase, which contributes to an increase in NADH production to match NADH oxidation during increased metabolic demand (45). While mitochondria have a large capacity for buffering  $\text{Ca}^{2+}$  by forming calcium phosphate complexes (46), excess  $\text{Ca}^{2+}$  influx into mitochondria is pathological. When excess  $\text{Ca}^{2+}$  influx occurs along with excess ROS production in mitochondria, conditions are optimal for mPTP to occur. Under pathological conditions such as Ischemia/Reperfusion injury, ion imbalance occurs and an increase in m $\text{Ca}^{2+}$  is observed (9). In isolated cardiomyocytes undergoing hypoxia/reoxygenation or anoxia/reoxygenation, those that accumulated 250-300nM of m $\text{Ca}^{2+}$  hypercontracted upon reperfusion (47), (48).  $\text{Ca}^{2+}$  import into mitochondria unconditionally requires  $\Delta\Psi_m$  (at -180mv or very close to it). Without  $\Delta\Psi_m$   $\text{Ca}^{2+}$  does not enter mitochondria. But  $\text{Ca}^{2+}$  import into mitochondria is necessary for maintaining  $\Delta\Psi_m$ . Therefore  $\text{Ca}^{2+}$  and  $\Delta\Psi_m$  are intricately coupled (49). While the role of  $\text{Ca}^{2+}$  in cell death has



been established, its role in  $\Delta\Psi_m$  instability is still unclear. In chapter 3 of this thesis, we use a genetic knock-out model of the mitochondrial calcium uniporter to dissect out the role of  $\text{Ca}^{2+}$  and the role of Mitochondrial Calcium Uniporter in  $\Delta\Psi_m$  instability.

### **Genetic Manipulation of Mitochondrial Calcium Uniporter and associated subunits in I/R injury**

The Mitochondrial Calcium uniporter is one of the main modes through which  $\text{Ca}^{2+}$  enters the mitochondria (50) (51). Molecular identification of the **MCU** pore by two independent groups in 2011 (52)(53), has allowed for several researchers to evaluate the role of MCU in pathological conditions via genetic manipulation.

The mitochondrial calcium uniporter (MCU) is a multisubunit complex, consisting of five other proteins (identified so far) that is associated with the pore (Figure 1.3). The MCU is a 40kDa protein consisting of two coil-coil domains and two transmembrane domains separated by a short loop enriched in acidic residues. The MCU can oligomerize to form a tetramer or hetero-oligomerize with its paralog MCUB. MCUB has an amino-acid substitution in the loop region (E256V), which removes a negative charge and thus depress  $\text{Ca}^{2+}$  uptake by the mitochondria (54).

Mice with global MCU knockout (MCU-gKO) were generated by a gene-trap method. They are smaller in size and exhibit no other outward phenotype. (55). Rapid  $\text{mCa}^{2+}$  uptake was severely affected, as expected. Mitochondria isolated from skeletal (55) and cardiac muscle (56) from these mice have 25% of the  $\text{Ca}^{2+}$  levels as WT mice; it was not zero as expected. There were no differences in cell viability between WT and gKO MEFs when challenged with cell-death inducing reagents like hydrogen peroxide (oxidative stress), tunicamycin (ER stress), doxorubicin

(DNA damage), c2-ceramide (activates apoptotic and necrotic pathways, thapsigargin (affects ER  $\text{Ca}^{2+}$  uptake) and there were no changes in cytochrome C levels upon hydrogen peroxide addition (apoptosis, I/R injury or protection effect), but MCU-gKO MEFs did not exhibit  $\text{Ca}^{2+}$  induced mPTP opening. MCU-gKO does not affect overall cardiac function at baseline and does not confer protection against I/R injury, (55). Acute knockdown of MCU in cells like NRVMs showed an increase in cytosolic  $\text{Ca}^{2+}$  levels and a reduction in beat-to-beat  $\text{mCa}^{2+}$  uptake (57).

Cardiac specific KO (MCU-cKO) were generated by subjecting  $\text{MCU}^{\text{fl/fl-MCM}}$  mice to a tamoxifen diet for four weeks (58), (59). There were no differences in the general phenotype of the mice.  $\text{mCa}^{2+}$  levels in mitochondria isolated from the heart and from permeabilized cardiac cells were the same between WT and MCU-cKO. But acute  $\text{mCa}^{2+}$  uptake was reduced in cardiac-specific KO, similar to the other studies and showed reduced oxygen consumption rate in response to isoproterenol (58). They also found reduction in  $\text{Ca}^{2+}$  induced mPTP opening in mitochondria isolated from MCU-cKO heart, where the mitochondria failed to swell with a  $\text{Ca}^{2+}$  bolus of  $500\mu\text{M}$ . They observed a 50% decrease in infarct size in MCU-cKO compared to WT (59).

Another example with contrasting protection against I/R injury is seen in two studies with genetic manipulation of **MCUb**. It is the dominant negative paralog of MCU, which can depress  $\text{Ca}^{2+}$  influx into mitochondria. Cardiac specific knock-in of dominant negative MCU (MCUb) (making the pore essentially non-functional) did not confer protection in I/R injury (60). However, Lambert et.al created a mouse line that conditionally expresses M $\text{CUB}$  in the heart. They treated mice for 4 days to a tamoxifen diet to allow overexpression of M $\text{CUB}$ . Mice with increased M $\text{CUB}$  expression, showed protection against I/R injury (61). In both these studies, acute  $\text{mCa}^{2+}$  influx was abolished when M $\text{CUB}$  expression increased.

**MICU1 and MICU2** are EF-hand containing proteins present in the intermembrane space that modulate the open probability of MCU, acting as gatekeepers. MICU2 responds to low  $[Ca^{2+}] < 1\mu M$  to suppress MCU activity (62)(63) and at high  $[Ca^{2+}]$ ,  $Ca^{2+}$  binds to MICU1 and causes a conformational change to “open” the pore (64)(65) (66). Knockout out MICU1 in whole body results in mice with severe neurological and myopathic defects and in 70% perinatal deaths. Mice that survive improve over time (67). Knockdown or knockout of MICU1 causes constitutive  $Ca^{2+}$  overload at baseline conditions. Knockout of MICU1 results in high  $Ca^{2+}$  uptake rates under low  $Ca^{2+}$  conditions and reduces  $Ca^{2+}$  uptake rate under high  $Ca^{2+}$  conditions. MICU2 knockout mice are born in mendelian ratios and survive more than 18 months. MICU2 knockout mitochondria exhibit slower rate of  $mCa^{2+}$  uptake at high  $[Ca^{2+}]$  pulse and take up  $Ca^{2+}$  more rapidly under low  $[Ca^{2+}]$  pulse. (68). These results are in line with the expected function of MICU1 and MICU2 as the MCU gatekeeper.

Essential MCU Regulator, **EMRE**, located on the inner membrane is essential for MCU's  $Ca^{2+}$  channel activity to keep MICU1/2 dimer attached to the MCU (69). When EMRE KO is generated in C57BL/6N, it results in embryonic lethality. EMRE KO mice are born with less frequency when generated in a mixed background, crossed with CD1. These mice have slightly lower body weight, but otherwise healthy phenotype (70). Knocking out EMRE, abolishes rapid  $Ca^{2+}$  uptake even if MCU is overexpressed (69). EMRE knockout does not affect I/R injury(70).

Mitochondrial Calcium Uniporter Regulator 1, **MCUR1**, associates with MCU and regulates the Ruthenium sensitive mitochondrial  $Ca^{2+}$  uptake (71). Pups were born in the expected mendelian ratios. Lower  $mCa^{2+}$  uptake was observed in MCUR1 KO cardiac mitochondria (72).

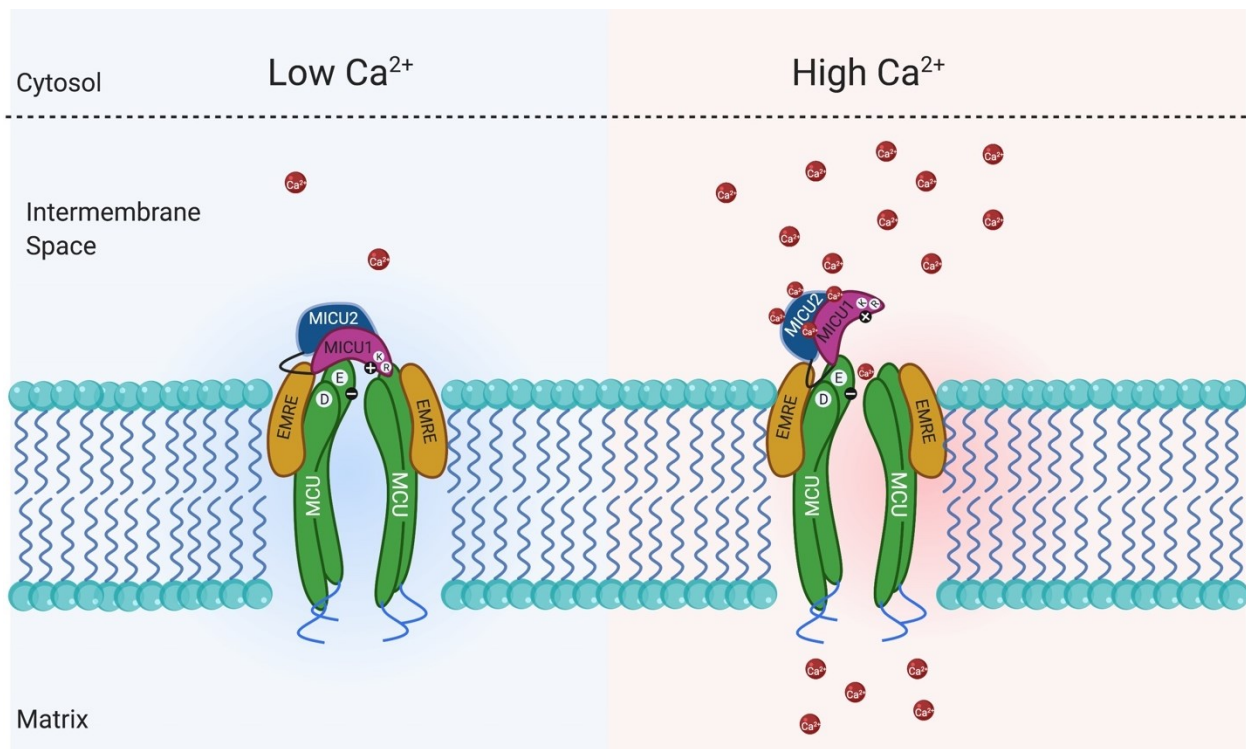


**Figure 1.3: Multisubunit Mitochondrial Calcium Uniporter Complex**

MCU is a tetramer associated with two copies of EMRE. MICU1 and MICU2 are two EF hand containing proteins which heterodimerize. EMRE helps to stabilize MICU1 and 2 and their interaction with MCU. The MCU pore regions also indicate a few important negatively charged amino acid residues (Aspartic Acid and Glutamic acid). MICU1 has positively charged groups (Lysine and Arginine). Under low  $\text{Ca}^{2+}$  conditions, MICU1 occludes the MCU pore. Under high  $\text{Ca}^{2+}$  conditions,  $\text{Ca}^{2+}$  induces a conformational change in MICU1 and allows the pore in an open state, allowing  $\text{Ca}^{2+}$  into the mitochondrial matrix. (Adapted from (73))

### Factors affecting $[\text{Ca}^{2+}]$ in mitochondria

Some of the studies described above with different models of MCU-KO (global vs cardiac-specific)(55) (58) contrasted in conferring protection against I/R injury. Nevertheless, in both

these models, basal  $mCa^{2+}$  levels were not close to 0 in MCU-KO. This suggests that there could be other regulatory mechanisms that overrule MCU's role in  $mCa^{2+}$  influx. MCU in cardiac mitochondria is seen to have a lower current density than mitochondria from other tissues (74). The ratio of MCU:MCUb is varied among different tissues – e.g., in the heart it is 3:1 (MCU:MCUb) and in skeletal muscle it is 40:1 (75), thus resulting in differential regulation of  $Ca^{2+}$ . In addition, other modes of  $Ca^{2+}$  entry into the mitochondria have also been observed: the mitochondrial ryanodine receptor (76), (77) and the LETM1-  $Ca^{2+}/H^+$  exchanger (78), (79) and the mitochondrial  $Na^+/Ca^{2+}/Li^+$  exchanger that is responsible for  $Ca^{2+}$  efflux may work in reverse under Ischemic conditions (80) (Figure 1.4). These factors and modes of  $Ca^{2+}$  entry could come into play when MCU is compromised.

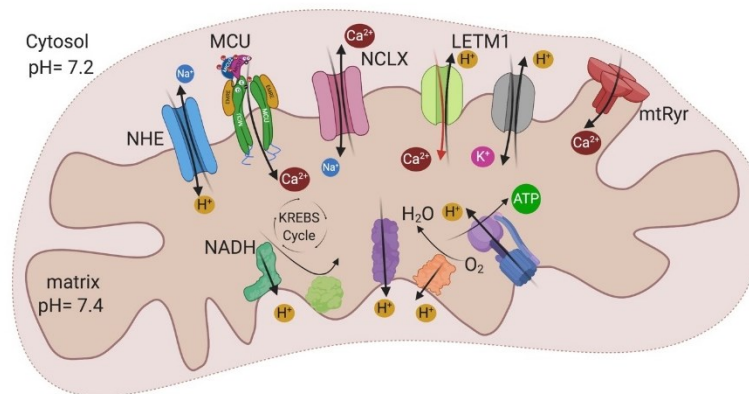


**Figure 1.4: Mitochondrial  $Ca^{2+}$  Influx/Efflux pathways**

The primary mode of  $Ca^{2+}$  import into mitochondria is the MCU. Other pathways such as mitochondrial Ryanodine Receptor (mtRyr) and leucine zipper-EF-hand-containing transmembrane protein 1 (LETM1) have been suggested (81) (79). However, LETM1 was first proposed as a  $K^+/H^+$  exchanger. The  $Na^+/Li^+/Ca^{2+}$  exchanger (NCLX) drives  $Ca^{2+}$  efflux under normal conditions, while importing  $Na^+$ . Under pathological conditions, it is proposed that the NCLX may work in reverse. The  $Na^+/H^+$  exchanger (NHE) uses the energy

of the proton gradient to extrude  $\text{Na}^+$  and maintains matrix  $[\text{Na}^+]$  below cytosolic  $[\text{Na}^+]$ . (Adapted from (82))

### **$\Delta\Psi_m$ oscillatory behavior in cardiomyocyte: Spatial characteristics and Implications**

The first report of oscillatory  $\Delta\Psi_m$  was by Berns et. al in the 1980s (83),(84), who discovered that, in cardiomyocytes, mitochondria excited by a laser flash exhibited  $\Delta\Psi_m$  oscillations. Since then, numerous studies have reported oscillatory phenomena in single mitochondria (85) and intact neonatal or adult cardiac cells and skeletal muscle, using a variety of techniques to trigger them(14) , (28), (16). Studying mitochondrial network properties of synchronization, clustering, contiguity helps one to understand the dynamic relationships between elements in an intracellular network. Much of the information on mitochondrial dynamic network properties were obtained from adult cardiac myocytes, with well-developed mitochondrial network and sarcomeric proteins.

Adult cardiomyocytes display cell-wide synchronization of  $\Delta\Psi_m$  oscillations (indicated by TMRM signal fluctuations) when subjected to metabolic or oxidative stress. However, individual mitochondria within a myocyte may behave differently in terms of their  $\Delta\Psi_m$  frequency and amplitude from the majority (16)(86). This varied behavior was shown to be a function of ROS release and ROS scavenging capacity at the local individual mitochondrial level. Synchronization of mitochondrial clusters occurs when there is a critical number of synchronized oscillators in an organized network: a phenomenon termed 'mitochondrial criticality'. In lattice-like networks, this concept of synchronization is understood by application of 'percolation theory'; i.e., stress in a sufficient number of network elements, the percolation threshold, results in synchronization of the components in the entire network. This value was experimentally observed in the 'lattice-

like' cardiac mitochondria as well. When 60% of mitochondria had significantly increased ROS levels, there was a transition to myocyte-level synchronized oscillations (31).

The size of mitochondrial clusters negatively correlated with the frequency of the clusters, indicating that large clusters had slower oscillation frequencies (16). Kurz et. al (2015) showed that cluster size- frequency relationship changed according to cardiac myocyte metabolism or redox balance, revealing dynamic coupling behavior between mitochondria. For example, substrates that produce more reducing equivalents such as pyruvate and  $\beta$ -hydroxybutyrate had higher rate of change of cluster size per mHz frequency ( $\sim -4\%/mHz$ ) compared to substrates like glucose and lactate ( $\sim -2\%/mHz$ ). In addition, a wider range of cluster sizes, which occurred when pyruvate and  $\beta$ -hydroxybutyrate were the substrates, indicated a fragmented, less well-coupled mitochondrial network. A wide range of frequency distribution (that occurred with pyruvate) indicated dyssynchronous clusters. Under oxidative stress conditions, the frequency distribution narrows and coalesces around slower, larger clusters. Rapid synchronization of mitochondrial clusters depends on the organization of mitochondria in the network and neighbor-neighbor interaction through ROS-induced ROS release, which recruits mitochondrial oscillators into a spanning cluster when they reach the percolation threshold (16), (87). Thus, information about the frequency, cluster size and sensitivity to oscillation can provide clues to the myocyte's susceptibility to death.

## Hypothesis

Under pathological conditions such as Ischemia/ Reperfusion injury, excess  $\text{Ca}^{2+}$  influx into the mitochondria (presumably through the MCU) and excess ROS production due to dysfunction of the mitochondrial oxidative phosphorylation system leads to mitochondrial instability. ROS released from unstable mitochondria, mediates damage and propagation of dysfunction through the ROS-Induced-ROS-Release mechanism.

Based on previous evidence that  $\Delta\Psi_m$  loss/oscillation might occur through either the  $\text{Ca}^{2+}$ -dependent mPTP opening or the ROS-mediated,  $\text{Ca}^{2+}$ -independent mechanism (IMAC), we sought to determine which mechanism predominantly underlies  $\Delta\Psi_m$  instability during reperfusion by knocking out MCU or by boosting the antioxidant capacity, with the ultimate goal of determining how to stop the cascading pathology of reperfusion injury.

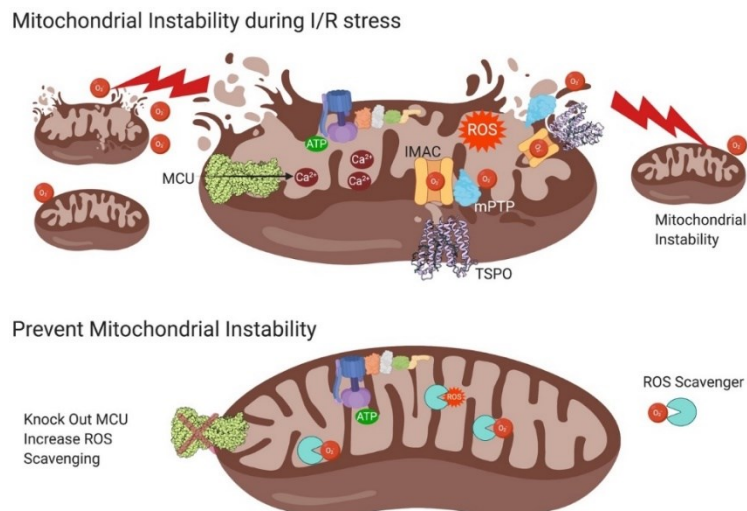


**Figure 1.5: Hypothesis**

Knocking out MCU to prevent excess  $\text{mCa}^{2+}$  accumulation or preventing Reactive Oxygen Species formation by scavenging excess ROS could prevent mitochondrial membrane potential instability during Reperfusion after Ischemic injury.



## **CHAPTER II: Spatio-temporal analysis of mitochondrial membrane potential fluctuations during ischemia-reperfusion**

**Modified from:** Deepthi Ashok & Brian O'Rourke. MitoWave: Spatio-temporal analysis of mitochondrial membrane potential fluctuations during ischemia-reperfusion. Submitted to Biophysical Journal in May 2020

### **Introduction**

Spatio-temporal oscillations (electrical and contractile) are fundamental to normal cardiac function but are also a potential source of pathological instability and chaos (88). A stable supply of energy is required to prevent maladaptive emergent phenomena, and mitochondria are well-suited to dynamically adapt to the varying workloads of the organism. Nevertheless, both under physiological conditions (89) or after metabolic stress, mitochondrial oscillations (84), flickers(90),(91), transients(25), or fluctuations(92)(93) have been observed, when parameters such as  $\Delta\Psi_m$ , flavin or NADH redox potential, pH, or Reactive Oxygen Species (ROS) have been measured. For example,  $\Delta\Psi_m$ , ROS and NADH were shown to oscillate in a self-sustaining manner in adult cardiomyocytes subjected to substrate deprivation (24) or oxidative stress (14) in a frequency range spanning from ~1-40 mHz (16). Similarly, local mitochondrial superoxide oscillations (“mitoflashes”) in cardiomyocytes had a frequency of ~40mHz (32). As we have previously reported,  $\Delta\Psi_m$  oscillation also reproducibly occurs upon reperfusion after ischemia in

neonatal rat ventricular myocyte monolayers (94). Importantly, interventions that suppressed mitochondrial  $\Delta\Psi_m$  instability on reperfusion also abrogated cardiac arrhythmias, both in neonatal myocytes (94) and isolated perfused hearts(17),(95). Hence, understanding the mechanism of mitochondrial destabilization during oxidative stress or ischemia/reperfusion (I/R) injury is essential to develop novel therapeutic strategies to prevent cardiac arrhythmias and contractile dysfunction associated with metabolic stress.

Determining the efficacy of interventions targeting spatiotemporal changes in mitochondria requires a robust, unbiased analytical approach, yet there are few reports describing methods for the automated analysis of non-stationary fluctuations observed in image time series. We have previously employed wavelet transform as a tool for characterizing  $\Delta\Psi_m$  oscillations and to describe dynamic mitochondrial clustering in adult cardiac myocytes by employing a mesh grid to outline individual mitochondrial clusters (86),(96). Here, we describe a workflow for characterizing spatially distributed  $\Delta\Psi_m$  loss and oscillation during I/R in terms of time-resolved frequency components, area of mitochondrial clusters, and times of reversible (ischemia) or irreversible (reperfusion)  $\Delta\Psi_m$  loss in neonatal cardiac cell monolayers. We apply discrete or continuous wavelet transform methods, followed by feature extraction, to analyze reperfusion-induced unsynchronized  $\Delta\Psi_m$  oscillations in neonatal ventricular myocytes. The method accurately identifies key transitions in mitochondrial behavior during I/R and quantifies the principal frequency components of mitochondrial instability and how they evolve over time. Moreover, the method is generalizable to the analysis of spatiotemporal variation of any parameter recorded during image time series. The method provides a workflow to automate

microscopy analysis and allows for unbiased, reproducible quantitation of complex nonstationary cellular phenomena.

## **Methods:**

### **Neonatal cardiomyocyte isolation and cell culture**

Neonatal mouse cardiac myocytes (NMVMs) were isolated using the MACS cell separation kit (Miltenyi Biotec: Catalog #130-100-825 and #130-098-373). Briefly, hearts from 0-2 day old mice were excised, chopped into small pieces and digested using reagents supplied by the kit. A cardiomyocyte-rich cell suspension was obtained by separation of magnetically labelled non-cardiac cells from total cell suspension upon application of a magnetic field.  $1 \times 10^6$  NMVMs were plated on fibronectin-coated (10 $\mu$ g/ml) 35mm (D=20mm) glass coverslip dishes (NEST<sup>®</sup> catalog # 801001) in Medium-199 supplemented with 25mM HEPES, 2 $\mu$ g/ml Vitamin B12, 50U/ml Pen-strep, 1X non-essential 286 Amino acids and 10% FBS. The next day, the medium was changed to 2% FBS medium. Ischemia/Reperfusion experiments and imaging were performed on the 5th-6th day of culture.

### **Inducing Ischemia and Reperfusion and $\Delta\Psi_m$ Imaging**

To monitor mitochondrial inner membrane potential ( $\Delta\Psi_m$ ), 50nM Tetramethylrhodamine methylester (TMRM) was loaded for 30 min at 37°C prior to the start of the experiment and the media was then replaced with fresh Tyrode's buffer (130mM NaCl, 5mM KCl, 1mM MgCl<sub>2</sub>, 10mM NaHEPES, 1mM CaCl<sub>2</sub> and 5mM Glucose). Experiment was performed at 37°C. A typical protocol included a baseline reading for 10 minutes followed by 60 minutes of regional ischemia induced

by placing a glass coverslip and followed by 60 minutes of reperfusion upon removal of the coverslip, as previously described in neonatal rat ventricular myocytes (94),(97) . During this 130-minute period, images were obtained every 15 sec on a laser-scanning confocal microscope (Olympus FV3000RS). TMRM fluorescence was imaged using a 40X silicone-immersion objective (Olympus UPLSAPO40XS) with 561nm excitation/ 570-620nm emission. Cells were imaged in Galvano scanning mode without averaging. Each image was 16-bit with a size of 318.2X319.2 microns (512X512 pixels). To minimize laser-induced damage during the long protocol, a neutral density filter of 10% was applied in the excitation path and the laser intensity was set by the software to 0.06% power (20 mW 561 nm LED laser). At the 15 sec image acquisition interval, only frequencies below 66.67mHz are resolvable based on Nyquist–Shannon sampling theorem (98).

### **Image Analysis**

Image series of the time-course of Ischemia/Reperfusion experiments were analyzed using Fiji (<https://imagej.net/Fiji/Downloads>). A custom-built segmentation-analysis macro was generated to track each cell's  $\Delta\Psi_m$  during the in-vitro I/R injury.  $\Delta\Psi_m$  response to I/R was analyzed at the cellular level by segmentation analysis (ImageJ). Steps for segmentation analysis included a pre-processing step to align the images in the stack using a 'StackReg' plugin (99). Segmentation of each cell was done by applying a median filter (radius=2) to the first image of the stack and then applying an auto local threshold (Niblack). All particles above the radius of 60 were included in the analysis. TMRM fluorescence intensity for each cell over Ischemia and Reperfusion were obtained. Macros included in appendix.

## **Discrete and Continuous wavelet transform**

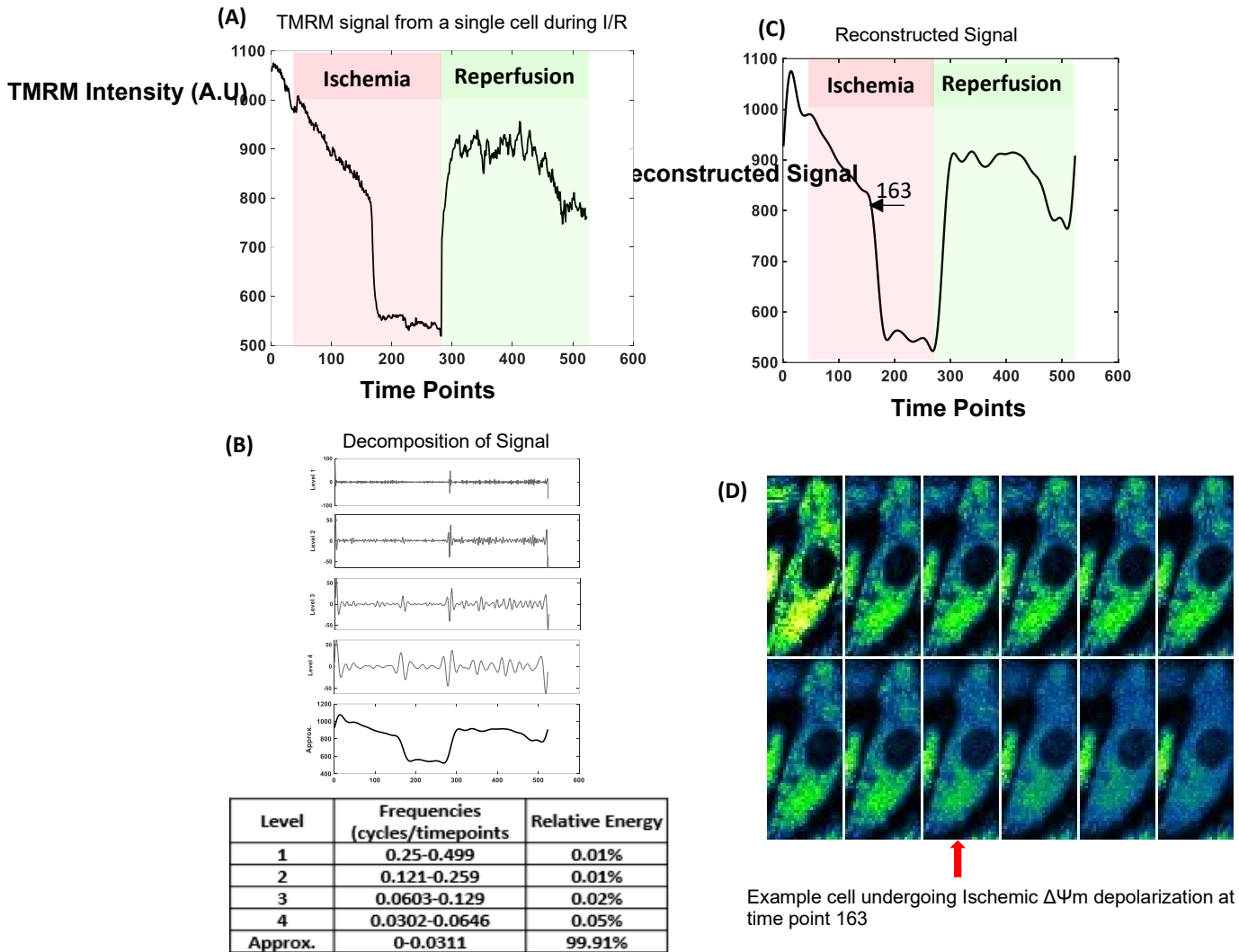
Limited information can be obtained through the use of frequency domain methods such as Fourier transform when analyzing complex biological signals that are non-stationary and time varying. Wavelet transform methods, on the other hand, permit resolution of the time of event occurrences and changes in the frequency relationship over time. Signal processing by wavelet transform generates coefficients that represent the best-fit as a selected “mother wavelet” function is scaled and shifted along the source signal(100). There are two kinds of wavelet transforms, Discrete and Continuous wavelet transforms. With Discrete Wavelet Transform (DWT), the signal is decomposed into discrete frequency bands, without overlap of the time-frequency windows of the wavelet function. To detect major transitions that may be hidden in the noise of a physiological signal, the Maximal Overlap Discrete Wavelet Transform (MODWT)(100) can be employed. MODWT decomposes the signal into finer and finer frequency levels. As the level increases, large-scale approximations of the signal are obtained, and lower frequency components of the signal are well-resolved. MODWT of a signal allows for multi-resolution analysis (MRA) that reconstructs the decomposed time series as a sum of several new series that are aligned in time with the original signal. MODWT-MRA effects a zero-phase filtering of the signal. Features are time-aligned, unlike MODWT alone. Continuous Wavelet Transform (CWT) involves transformation of the signal by continuously changing the scaling and shifting factors. Although this introduces some information redundancy, it presents a more detailed, high resolution view of the characteristics of the signal. Coefficients generated by CWT are represented by a scalogram that is a visual representation of the frequency components of the signal as they change over time. In our experiments on cardiomyocytes loaded with the

potentiometric fluorophore tetramethylrhodamine methyl ester (TMRM) and subjected to an in vitro I/R protocol, we used MODWT-MRA to identify the timing of the major  $\Delta\Psi_m$  depolarization during ischemia for each cell. CWT was utilized to analyze the more complex time varying frequency components of the  $\Delta\Psi_m$  oscillations observed in individual clusters of mitochondria during reperfusion. The image-processing and wavelet transform workflow, along with feature extraction from the images and scalograms obtained, allowed us to precisely determine the following: 1) the time point of  $\Delta\Psi_m$  loss for each cell during Ischemia, 2) the incidence of  $\Delta\Psi_m$  oscillation for each mitochondrial cluster and its frequency throughout the reperfusion period, 3) whether  $\Delta\Psi_m$  stabilized or irreversibly collapsed during reperfusion, and 4) the size distribution of the oscillating mitochondrial clusters.

**(i) Identification of transition time-points of inner mitochondrial membrane potentials during Ischemia**

To analyze a time-series of the mitochondrial inner membrane potential, we used MODWT-MRA to identify time-localized changes in the TMRM signal (using MATLAB's signal processing toolbox). The TMRM signal from each cell during the Ischemic period was transformed with a sym4 wavelet with four levels of decomposition. Lower level decompositions involve higher frequencies and higher-level decompositions involve slower frequencies. For example, Fig.2.1 shows a raw TMRM signal from a single cell (A) decomposed into 4 levels using a sym4 wavelet transform (Fig. 2.1B). Level 1 has the frequency components between 0.033-0.017Hz, level 2 has 0.017- 0.008 Hz, level 3 has 0.008-0.004 and level 4 has 0.004-0.002. All levels of decompositions have associated relative energies. For our purpose of estimating the  $\Delta\Psi_m$  depolarization time, we removed all higher frequency components with lower relative energy and reconstructed the

signal by retaining the highest relative energy (of more than 99%) (Fig. 2.1C). We essentially filter out the ‘noise’ by this process. With this time-aligned reconstructed signal, we used the MATLAB function ‘findchangepoints’ to obtain the time point at which the reconstructed signal changed significantly (Fig. 2.1C). Time point of Ischemia depolarization can thus be automatically determined for several cells (Fig. 2. 1E).



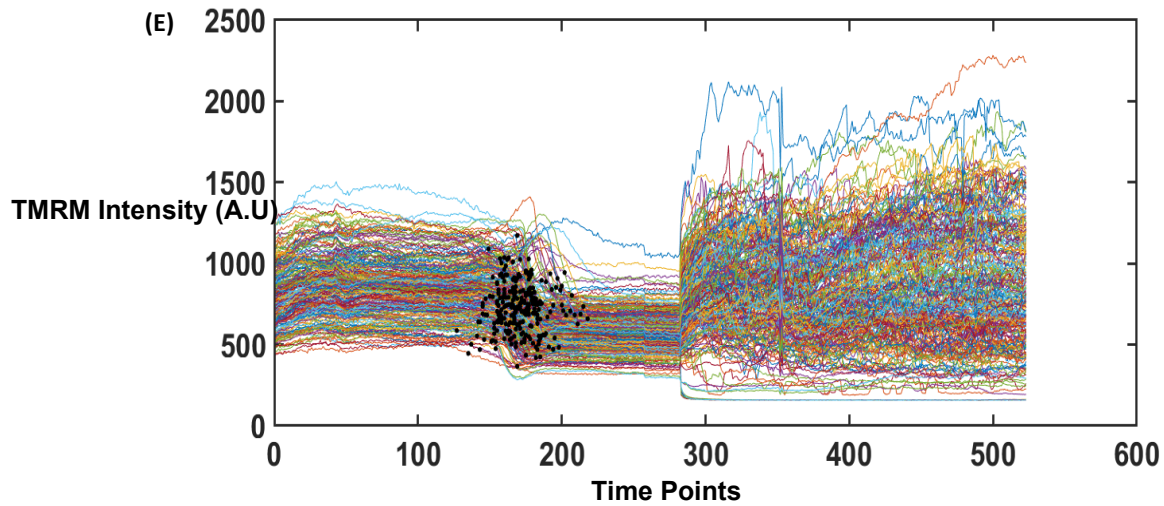


**Figure 2.1: Identification of Ischemic depolarization time.**

Raw TMRM signals during Ischemic period (A) are decomposed using Maximal Overlap Discrete Wavelet Transform (B) and reconstructed by retaining the signal with the highest relative energy (C). MATLAB's 'findchangepts' function identifies the time point at which the signal changed significantly during Ischemia. Here, it is at time point 163. D) Example of a cell with the first image at baseline and subsequent images in the last phases of depolarization. Images are 15 seconds apart. TMRM intensity is abruptly diminished at time point 163. E) Example of Ischemia/ Reperfusion experiment with >100 cells where the black dots represent Ischemic depolarization time points.



**(ii) Obtaining features and frequency components of  $\Delta\Psi_m$  oscillations during reperfusion**

Mitochondria exhibited non-stationary oscillatory behavior throughout reperfusion (Fig 2.2). We categorized  $\Delta\Psi_m$  oscillatory behavior based on our visual observations of 10 experiments. There were five outcomes that were observed based on the oscillatory state of  $\Delta\Psi_m$  throughout the reperfusion time period, i.e., (i)  $\Delta\Psi_m$  oscillations persisting throughout, (ii) No or very few  $\Delta\Psi_m$  oscillations, (iii)  $\Delta\Psi_m$  oscillations that stabilized after oscillating initially, (iv)  $\Delta\Psi_m$  oscillations that occurred, but there was early  $\Delta\Psi_m$  loss, and (v) No  $\Delta\Psi_m$  oscillations occurred, and there was early  $\Delta\Psi_m$  loss (Fig. 2.2). We used a continuous wavelet transform (sym8) (in MATLAB's signal processing toolbox), to process the TMRM signal and observed that the signal processing tool readily detected transitions and frequencies depicting the behavior of mitochondrial  $\Delta\Psi_m$  changes. Figure 2, right panel, shows the scalograms obtained after performing a wavelet transform of the TMRM signal. We observed that an oscillating cluster has high coefficients concentrated in the scale of  $\sim 3$  to 10, corresponding to a frequency of 4.3-45mHz, which does not exist in the scalogram of the non-oscillating cluster or during Ischemia.

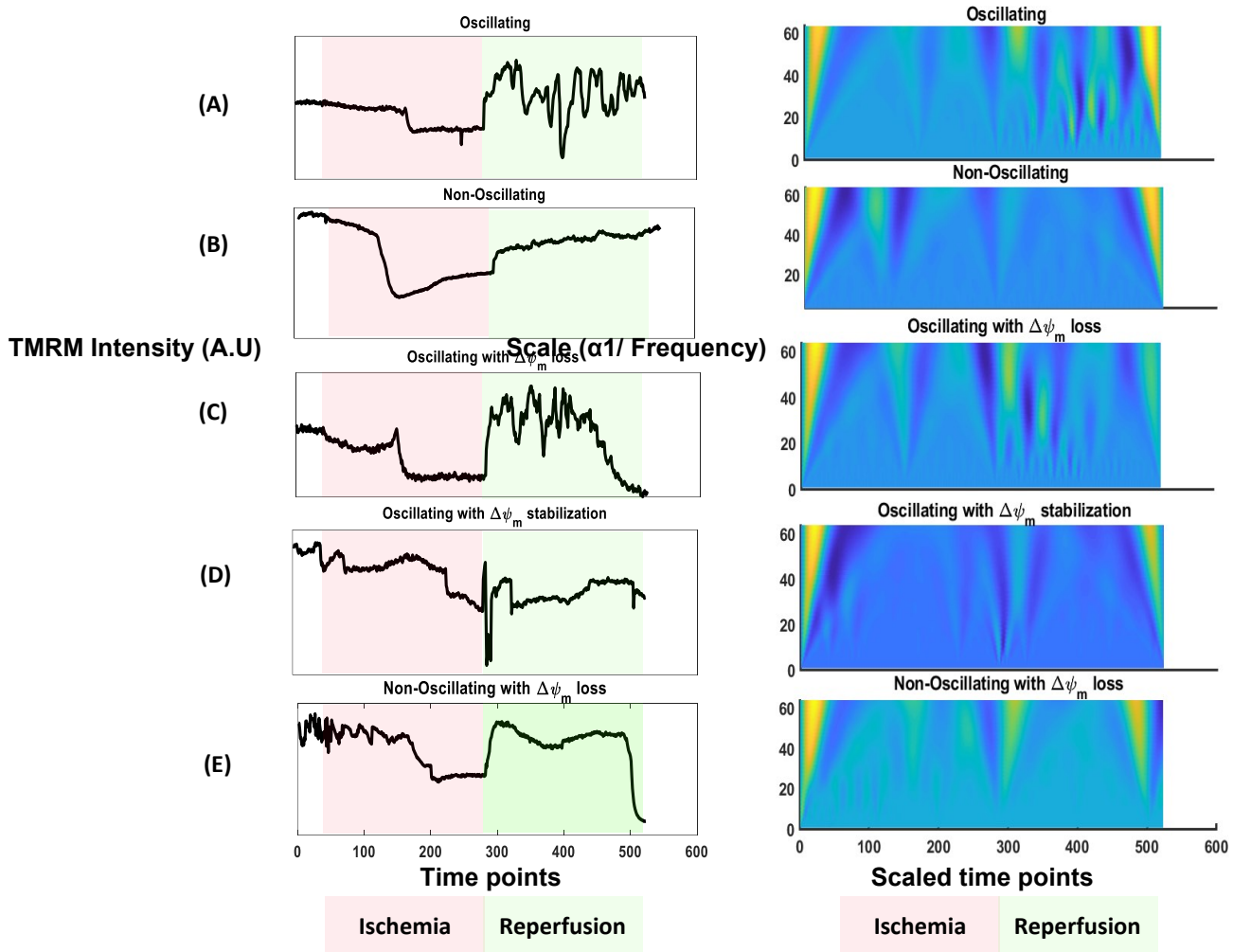


**Figure 2.2: Mitochondria exhibit different  $\Delta\Psi_m$  oscillatory behaviors upon reperfusion.**

$\Delta\Psi_m$  signals (TMRM fluorescence) for representative mitochondrial clusters during ischemia and reperfusion are shown in the left panels and corresponding continuous wavelet transforms are shown in the righthand panels as scalograms. Frequencies and corresponding transition time points can be extracted from the scalograms. Mean TMRM Fluorescence intensities of an oscillating cluster (A), a non-oscillating cluster (B), an oscillating cluster exhibiting  $\Delta\Psi_m$  loss (C), a cluster that oscillates before stabilizing (D), and a non-oscillating cluster exhibiting  $\Delta\Psi_m$  loss (E). The oscillating cluster (A) has high coefficients concentrated in the scale of  $\sim 1$  to 10, corresponding to a frequency of 4.3-45mHz, which is absent in the scalogram of a non-oscillating cluster or during Ischemia.

This wavelet tool was then applied to detect transitions, frequencies and times associated with these changes automatically for a large number of cells (>100 per experiment) and mitochondrial clusters (> 400 per experiment). MATLAB/ FIJI platform was used to perform feature extraction for  $\Delta\Psi_m$  changes throughout the reperfusion time period (Figure 2.3). The procedure involved the following steps: (A) *image acquisition* with a confocal microscope using TMRM to monitor  $\Delta\Psi_m$  changes; (B) *cellular segmentation* using custom-made FIJI macros to separate each cell. The same thresholding method was applied to every image to outline each cell in the field of view; (C) By applying the threshold, each cell was separated into an image series; (D) *creation of an image Differential Stack* of the reperfusion phase of the image series by subtracting the  $n^{\text{th}}$  image from the  $(n-1)^{\text{th}}$  image. The sum of differentials in this stack could then be used to highlight the mitochondrial clusters that oscillate during the reperfusion period; (E) thresholding the z-projection of this differential image stack to obtain Regions of Interest (ROI) *outlining oscillating mitochondrial clusters*; (F) application of the ROIs to the reperfusion phase to *obtain TMRM signals for each cluster* through this time period; (G) *continuous wavelet transform of the TMRM signal* (with a sym 8 wavelet) to generate a coefficient matrix, visualized as a scalogram. The regions on the scalogram with large coefficients indicate where the mother wavelet fits the signal well. The x-axis represents the scaled time points and y-axis represents the scale (scale  $\propto 1/\text{frequency}$ ). Usually an oscillating mitochondrion shows high coefficient peaks corresponding to the scale range from 3-10.  $\Delta\Psi_m$  can also undergo larger transitions throughout reperfusion and these changes are reflected in the scalograms as high coefficient peaks; (H) importation of the resulting coefficient matrix as a scalogram-image and *extraction of predominant frequency features* as a function of reperfusion time. X and Y co-ordinates of the

outlined maximum coefficients were obtained. The X-axis of the scalogram represents the time and the Y-axis, the scale (scale  $\propto 1/\text{frequency}$ ); (I) Mitochondrial oscillators associated with time are *classified into high/low frequency bands*. If a mitochondrial cluster oscillates in a particular frequency band at multiple times during reperfusion phase, then, an average of the frequency and the time is obtained. Thus, patterns of oscillatory behavior are obtained. We will henceforth refer to this routine as the MitoWave Analysis. (ImageJ macros and MATLAB codes are included in appendix and on GitHub <https://github.com/dashok1/MitoWave/releases/tag/v1.0.2>).

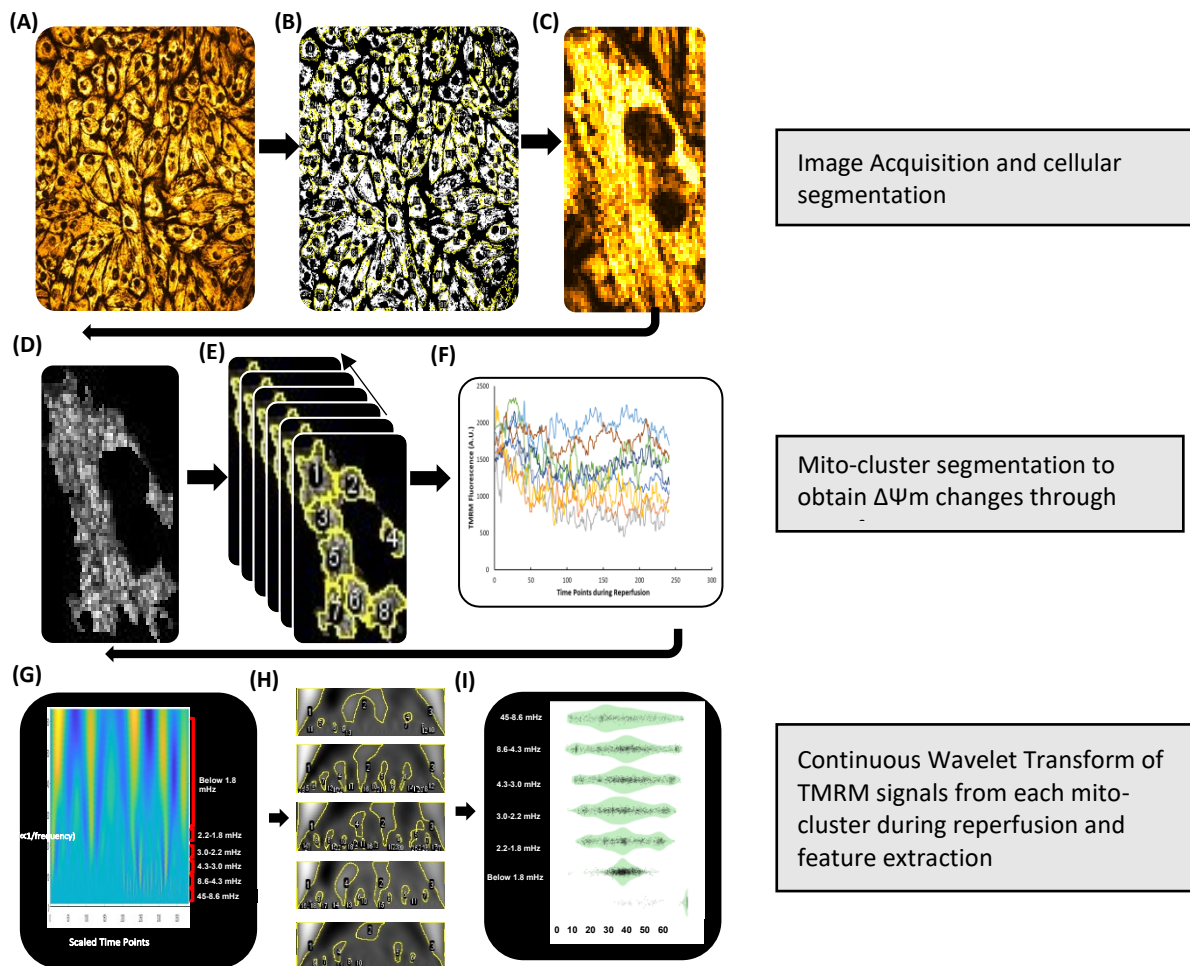


Figure 2.3: Schematic of Mito-wave analysis for  $\Delta\Psi_m$  feature extraction.

It involves the following steps: A) Image Acquisition with a Confocal microscope using TMRM to monitor  $\Delta\Psi_m$  changes, B-C) Cellular Segmentation using custom-made FIJI macros to separate each cell, D) Differential stack Z-projection image for each cell is used to identify mitochondrial clusters that oscillate (MATLAB/FIJI Routine), E-F) TMRM fluorescence time course for each cluster is obtained, G) Scalograms are generated by continuous wavelet transform of the TMRM signal, H) Features and frequency components are extracted from the scalograms, and I) Mitochondrial oscillators are classified into high/low frequency bands to obtain patterns of oscillatory behavior as a function of reperfusion time.

## Results

### Defining oscillatory behavior patterns during Reperfusion

The behavior of each mitochondrial cluster was plotted into its corresponding frequency band, which varied over the reperfusion time period, represented as violin plots (Fig. 2.4). Frequencies were categorized as high frequency, ranging from 45 to 4.3 mHz (~22 seconds to 230 seconds), moderately fast frequencies ranging from 4.3-2.2 mHz (~ 230 seconds to 450 seconds), slow frequencies ranging from 2.2mHz to 1.8 mHz (~ 450 seconds to ~ 550 seconds) and below 1.8 mHz. Mitochondrial oscillators typically were present in the 45-4.3 mHz band. We also plotted the time at which there was complete  $\Delta\Psi_m$  loss during the reperfusion period. Applying Mito-Wave Analysis on ten in-vitro Ischemia/ Reperfusion experiments, we verified that our visual observations matched the quantitative analysis. In experiments where the mitochondrial oscillations persisted throughout the reperfusion period, high-frequency oscillators appeared at all time periods in the violin plots (Fig 2.4 A) and when mitochondria had few/ no oscillations, the presence of high-frequency oscillators tapered off near 20 minutes of reperfusion (Fig 2.4B). We also observed, in some experiments, that mitochondrial oscillations occurred in the beginning of reperfusion, but started losing their  $\Delta\Psi_m$  during mid-late reperfusion, so the high-frequency oscillations tapered off, but shows up in the band where there is  $\Delta\Psi_m$  loss (Fig 2.4C). We also observed in some experiments (Fig 2.4D), mitochondria exhibited few low amplitude or no oscillations at the beginning of reperfusion, so the number of high-frequency oscillators taper off around 20 minutes (similar to the distribution pattern of high frequency oscillators in Fig 2.4B), but they begin to lose their  $\Delta\Psi_m$  around 25 minutes of reperfusion. Finally, in some experiments we observed that mitochondria stabilize their  $\Delta\Psi_m$  oscillations throughout the reperfusion time

period (Fig 2.4E) where the presence of high-frequency oscillators taper off while  $\Delta\Psi_m$  is maintained during reperfusion. We then classified these experiments into the 5 different oscillation categories: Oscillating (2.4A), Non-Oscillating (2.4B), Oscillating with early  $\Delta\Psi_m$  loss(2.4C), Oscillating with early  $\Delta\Psi_m$  stabilization (2.4D) and Non-Oscillating with early  $\Delta\Psi_m$  loss (2.4E).

<b>Table 1</b>	<b>Visual Observations during reperfusion</b>
<b>1</b>	Oscillating mitochondrial clusters
<b>2</b>	No Oscillations during reperfusion
<b>3</b>	Oscillations with early $\Delta\Psi_m$ loss
<b>4</b>	Yes Oscillations, then stabilization
<b>5</b>	No fast Oscillations, but show early $\Delta\Psi_m$ loss

Table 1. Visual Observations during reperfusion

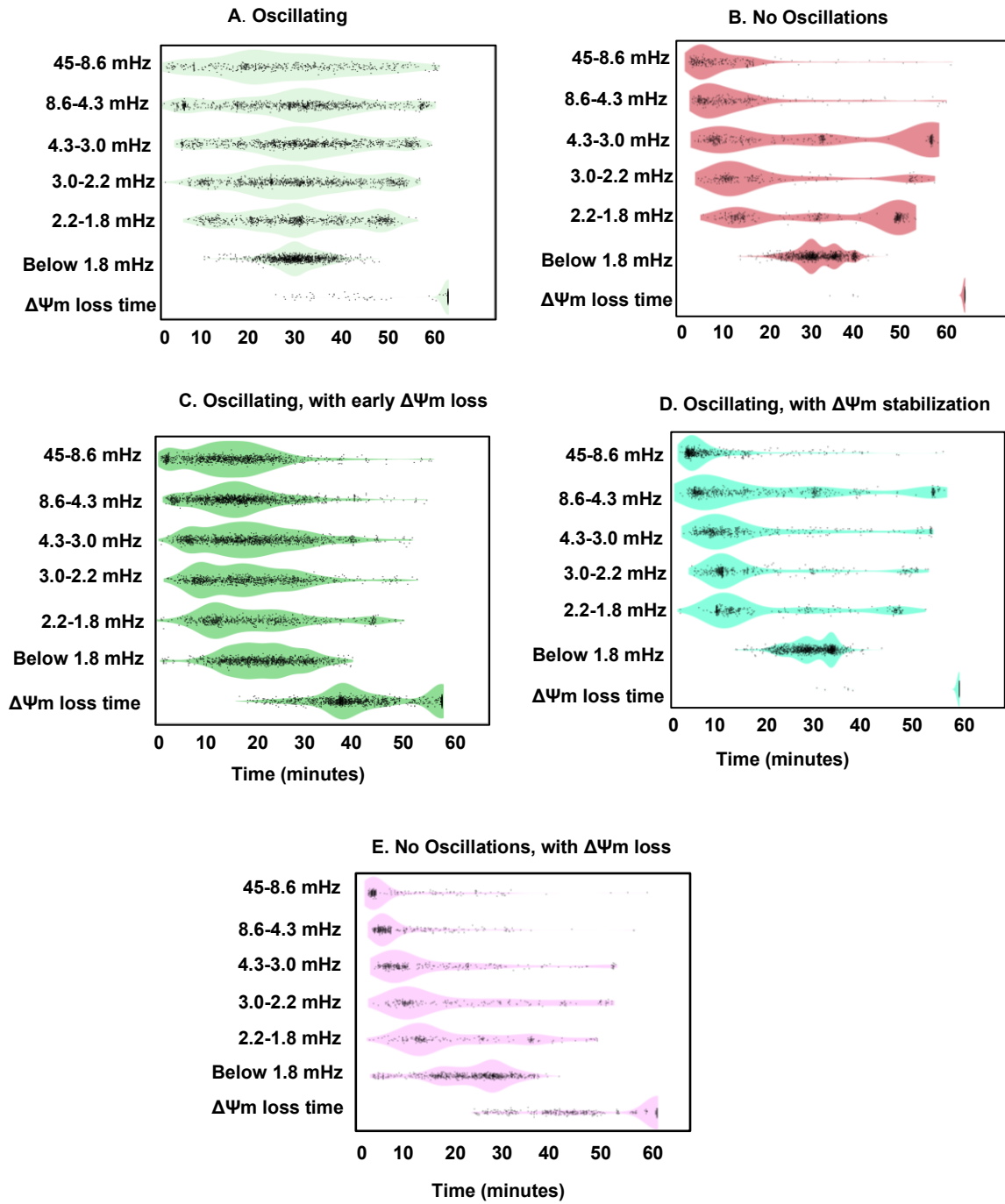


**Figure 2.4: Defining  $\Delta\Psi_m$  Oscillatory patterns during reperfusion qualitatively and quantitatively:**

Visual observations of the Ischemia/Reperfusion image stack can qualitatively classify oscillatory behavior patterns of mitochondrial clusters during reperfusion. We classified oscillatory patterns from 10



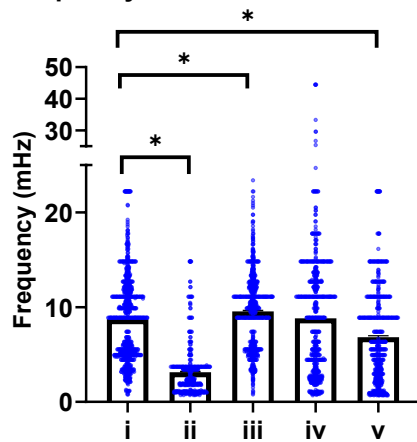
experiments into 5 groups: Oscillating, Not Oscillating, Oscillating with early  $\Delta\Psi_m$  loss, Oscillating with  $\Delta\Psi_m$  stabilization, and Non-Oscillating clusters with Early  $\Delta\Psi_m$  loss (Table 1). By subjecting the TMRM signal from each mitochondrial cluster to MitoWave Analysis, we characterize oscillatory behavior quantitatively with violin plots (Fig. 2.4A-E). Each dot represents a mitochondrial cluster oscillating at a certain frequency corresponding to a certain time point. Visual observations (Table 1) are corroborated by results from the quantitative MitoWave analysis routine (Fig 2.4A-E). We see that a mitochondrial cluster can change its oscillatory pattern throughout the reperfusion period, i.e., its frequency may change from one frequency band to another. Y-axis shows six frequency bands, as well as the time at which a mitochondrial cluster completely loses  $\Delta\Psi_m$  during reperfusion. X-axis represents the time of reperfusion.

### **Predominant frequencies of mitochondrial clusters**

We obtained the predominant frequencies of mitochondrial clusters by considering the first, fast frequency band (8.6- 45mHz). If the mitochondrial cluster did not have a frequency in that band, the next frequency band was considered, and so on till the slowest frequency band. This way we could extract the frequencies that most closely represented mitochondrial oscillating frequencies. An average or a weighted average could be used since most mitochondrial clusters also have slow frequency components, but not all mitochondria have fast frequency components. Oscillating clusters have a frequency of  $8.73\pm 4.35\text{mHz}$  (1081 clusters), Non-Oscillating Clusters have  $3.13\pm 2.61\text{mHz}$  (732 clusters), Oscillating clusters with early  $\Delta\Psi$  loss have  $9.56\pm 3.66\text{mHz}$  (1402 clusters), Oscillating clusters with  $\Delta\Psi_m$  stabilization have  $8.81\pm 6.03\text{mHz}$  (1009 clusters) and Non-Oscillating clusters with Early  $\Delta\Psi_m$  loss have  $6.82\pm 4.63\text{mHz}$  (880 clusters) (Fig 2.5A).

Further, we analyzed the distribution of high frequency oscillators (in the 8.6-45mHz frequency band) to see how they vary throughout reperfusion time among the different categories. Clusters that didn't have a frequency in this band (of 8.6-45mHz) were given a value of 0. We plotted the percentage of the different categories of oscillating clusters against time (Fig.2.5B). We observed that among the Oscillating category (blue line), 8-12% of mitochondria exhibited this high-frequency oscillations from 15-40 minutes of reperfusion. This was absent in the Non-Oscillating (orange line), in the Oscillating with early  $\Delta\Psi_m$  stabilization (Violet line) and the Non-Oscillating with  $\Delta\Psi_m$  loss (green line) categories. The Oscillating with early  $\Delta\Psi_m$  loss (pink line) shows  $\sim$  7-15% of mitochondria exhibit high frequency only in the early reperfusion phase, till about 25 minutes, after which they do not. Further, we also statistically analyzed the distribution of these high frequency oscillators. A Kolmogorov-Smirnov non-parametric two sample test (kstest2 on MATLAB) was performed to test the null hypothesis that distribution of various oscillation behaviors were not different during the reperfusion time period. KS-test show significant differences between the different categories, comparing Oscillating and Non-Oscillating clusters, Oscillating and Oscillating with early  $\Delta\Psi_m$  loss, Oscillating and  $\Delta\Psi_m$  stabilizing clusters, and Oscillating and Non-Oscillating with early  $\Delta\Psi_m$  loss ( $p < 0.0001$ ). Thus, we quantitatively confirm our visual observations that the distribution of oscillating mitochondrial clusters that change dynamically over time are different between different categories of oscillating experiments.

### A. Frequency of Mitochondrial Clusters



### B. Percentage of fast oscillating mitochondrial clusters existing in 4-minute time intervals during reperfusion

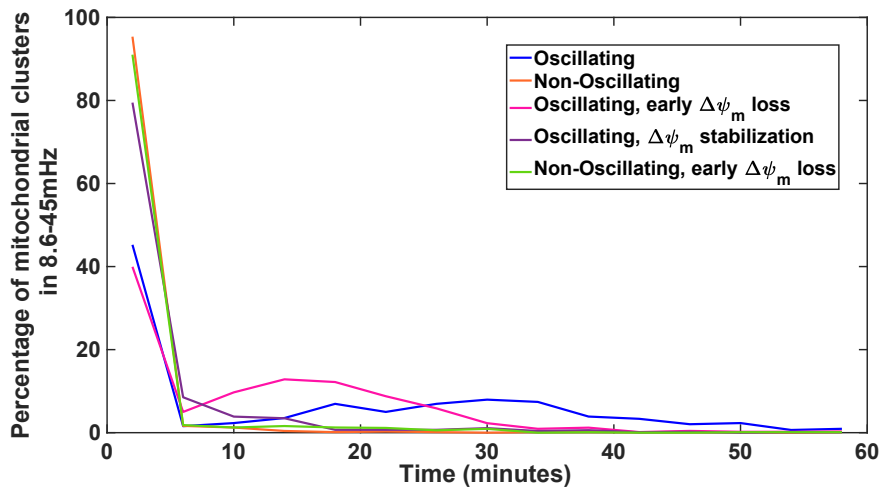


**Figure 2.5: Predominant frequencies exhibited by mitochondrial clusters during reperfusion.**

The predominant frequencies exhibited by mitochondrial clusters fell within the 8.6 to 45mHz band. A)

The mean predominant frequency  $\pm$  SEM for i) Oscillating clusters,  $8.73 \pm 4.35$  mHz (1081 clusters); ii) Non-Oscillating Clusters,  $3.13 \pm 2.61$  mHz (732 clusters); iii) Oscillating cluster with early  $\Delta\Psi_m$  loss,  $9.56 \pm 3.66$  mHz (1402 clusters); iv) Oscillating cluster with  $\Delta\Psi_m$  stabilization,  $8.81 \pm 6.03$  mHz (1009 clusters); and v) Non-Oscillating clusters with early  $\Delta\Psi_m$  loss,  $6.82 \pm 4.63$  mHz (880 clusters). One-way ANOVA was performed to

determine statistical significance, \*  $p < 0.0001$ . B) Percentage of mitochondrial clusters oscillating in the 8.6-45mHz frequency band binned at 4-minute intervals during the reperfusion period.

### **Frequency and mitochondrial cluster size are negatively correlated**

We observed that in experiments where there were no/ few oscillations, mitochondrial clusters seem larger than in experiments where mitochondria had persistent oscillations. Previous reports in adult cardiac myocytes also showed that larger clusters have slower oscillations (16). Therefore, we wanted to check if this was true in Neonatal Cardiac myocytes as well. The Mito-Wave analysis of NMVMs subjected to I/R agreed with our visual observations. Oscillating mitochondria had the lowest area of  $49.3\mu\text{m}^2$  vs a larger area of  $65.92\mu\text{m}^2$  for non-oscillating mitochondria (Fig 2.6A). We performed non-parametric correlation coefficient analysis to understand the relationship between the size of mitochondrial clusters and its frequency. We found that there is a negative correlation between oscillating frequency and the size of the mitochondrial cluster, with a correlation coefficient of  $r = -0.58$  (Fig. 2.6B). Mitochondrial cluster size decreased by  $\sim 4.56\mu\text{m}^2$  for every millihertz increase. This suggests that if mitochondria are organized in larger clusters, they undergo slower oscillations and may eventually stabilize  $\Delta\Psi_m$  and be protected against  $\Delta\Psi_m$  loss during reperfusion after Ischemia.

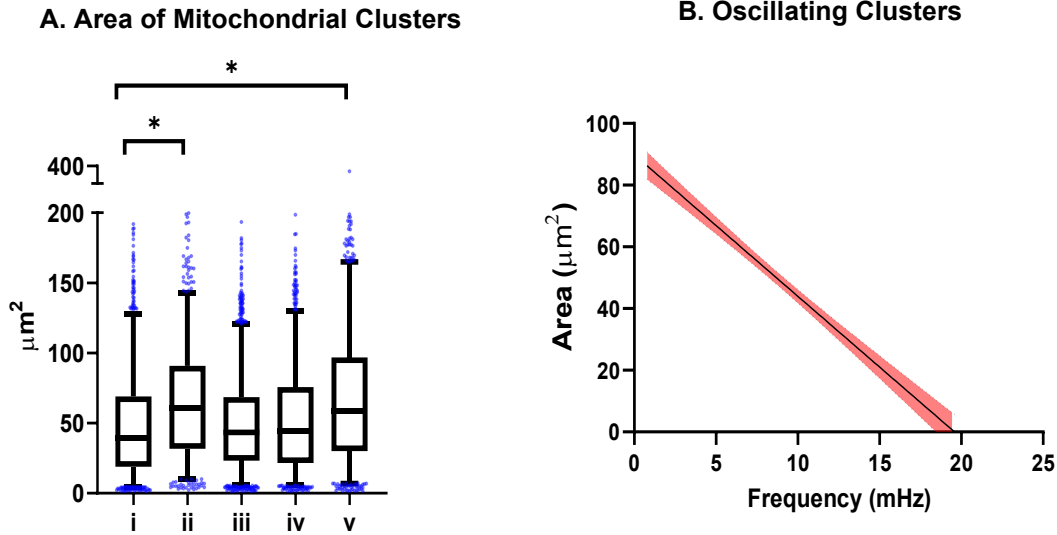


**Figure 2.6: Mitochondrial Cluster size and Frequency relationship.**

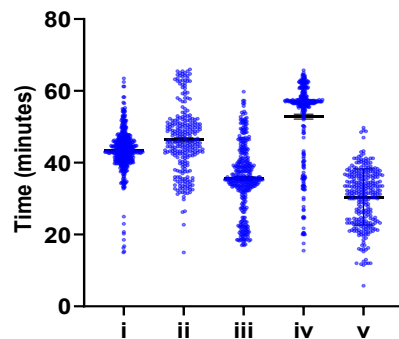
A) Mitochondrial Cluster size and Frequency relationship. Areas of mitochondrial clusters were compared for clusters exhibiting different oscillatory behaviors (across several experiments). (i) Oscillating clusters had an area of  $49.78 \pm 40.64 \mu\text{m}^2$  (1081 clusters); (ii) Non-Oscillating Clusters,  $65.97 \pm 42.07 \mu\text{m}^2$  (732 clusters); (iii) Oscillating cluster with early  $\Delta\Psi$  loss,  $49.65 \pm 34.35 \mu\text{m}^2$  (1402 clusters); (iv) Oscillating cluster with  $\Delta\Psi$  stabilization,  $53.15 \pm 39.38 \mu\text{m}^2$  (1009 clusters); and (v) Non-Oscillating clusters with Early  $\Delta\Psi$  loss,  $67.92 \pm 49.12 \mu\text{m}^2$  (880 clusters). One-way ANOVA was performed to determine statistical significance, \*  $p < 0.0001$ . B) Frequency and cluster size show an inverse relationship. In Oscillating clusters, the area of the cluster decreases by  $\sim 4.56 \mu\text{m}^2$  for every millihertz increase. 95% confidence intervals are plotted (red) with linear regression line (black).

### **Time taken for $\Delta\Psi_m$ loss during Ischemia and Reperfusion**

Time to  $\Delta\Psi_m$  loss (reversible during Ischemia and irreversible during reperfusion) is an important indicator for mitochondrial resistance to instability during reperfusion after ischemia. It helps to understand if interventions to prevent mitochondrial instability and hence reperfusion injury are

effective. We quantified the time to  $\Delta\Psi_m$  loss during Ischemia per cell (2.7A). The Oscillating category had a mean of  $43.52\pm 5.87$  minutes to  $\Delta\Psi_m$  loss (i), Non-Oscillating took  $46.36\pm 9.17$  minutes(ii), Oscillating with early  $\Delta\Psi_m$  loss took  $35.62\pm 9.25$  minutes(iii), Oscillating with  $\Delta\Psi_m$  stabilization took  $52.84\pm 11.17$  minutes (iv) and Non-Oscillating clusters with Early  $\Delta\Psi_m$  loss took  $30.46\pm 7.81$  minutes(v). We also quantified the time to  $\Delta\Psi_m$  loss per mitochondrion during reperfusion (2.7B). We plotted the time against the percentage of mitochondria. Oscillating clusters take  $58.71\pm 4.75$  minutes to lose  $\Delta\Psi_m$ ; Non-Oscillating clusters did not lose their  $\Delta\Psi_m$  till the end of reperfusion at 60.25 minutes; Oscillating clusters with early  $\Delta\Psi_m$  loss take  $45.8\pm 11.05$  minutes; Oscillating clusters with  $\Delta\Psi_m$  stabilization take  $59.66\pm 3.96$  minutes and Non-Oscillating clusters with early  $\Delta\Psi_m$  loss take  $53.38\pm 10.99$  minutes.

**A. Ischemia  $\Delta\Psi_m$  depolarization**



**B. Percent of mitochondrial clusters exhibiting irreversible  $\Delta\Psi_m$  loss during reperfusion**

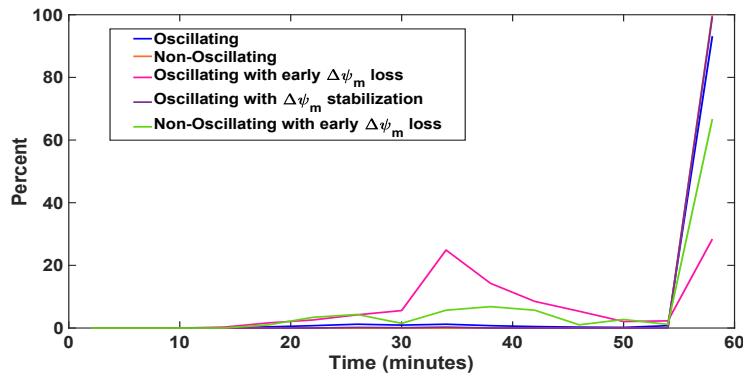


**Figure 2.7: Time taken for  $\Delta\Psi_m$  loss during Ischemia and Reperfusion**

A) Time taken for  $\Delta\Psi_m$  loss during Ischemia versus the ensuing oscillatory behavior on reperfusion. (i) Oscillating clusters maintained  $\Delta\Psi_m$  until  $43.52 \pm 5.87$  minutes; (ii) Non-Oscillating clusters,  $46.36 \pm 9.17$  minutes; (iii) Oscillating with early  $\Delta\Psi_m$  loss,  $35.62 \pm 9.25$  minutes (iv) Oscillating with early  $\Delta\Psi_m$  stabilization,  $52.84 \pm 11.17$  minutes and (v) Non-Oscillating clusters with Early  $\Delta\Psi_m$  loss,  $30.46 \pm 7.81$  minutes. B) Percentage of mitochondrial clusters exhibiting irreversible  $\Delta\Psi_m$  loss during reperfusion. Oscillating clusters lost  $\Delta\Psi_m$  on average at  $58.71 \pm 4.75$  minutes of reperfusion; Non-Oscillating clusters maintained stable  $\Delta\Psi_m$  to the end of 60.25 minutes of reperfusion; Oscillating clusters with early  $\Delta\Psi_m$  loss depolarized at  $45.8 \pm 11.05$  minutes; Oscillating clusters with  $\Delta\Psi_m$  stabilization lasted  $59.66 \pm 3.96$  minutes, and Non-Oscillating clusters with early  $\Delta\Psi_m$  loss depolarized at  $53.38 \pm 10.99$  minutes

### **Correlation between Ischemic depolarization time point and $\Delta\Psi_m$ oscillation frequency**

We wanted to understand if there was any link between mitochondrial recovery during reperfusion and the time to  $\Delta\Psi_m$  loss during Ischemia. We compared the empirical cumulative distribution functions between different oscillation categories during Ischemia (2.8A) and reperfusion (2.8B). We found that late  $\Delta\Psi_m$  loss during Ischemia correlated with mitochondrial  $\Delta\Psi_m$  stabilization during reperfusion.

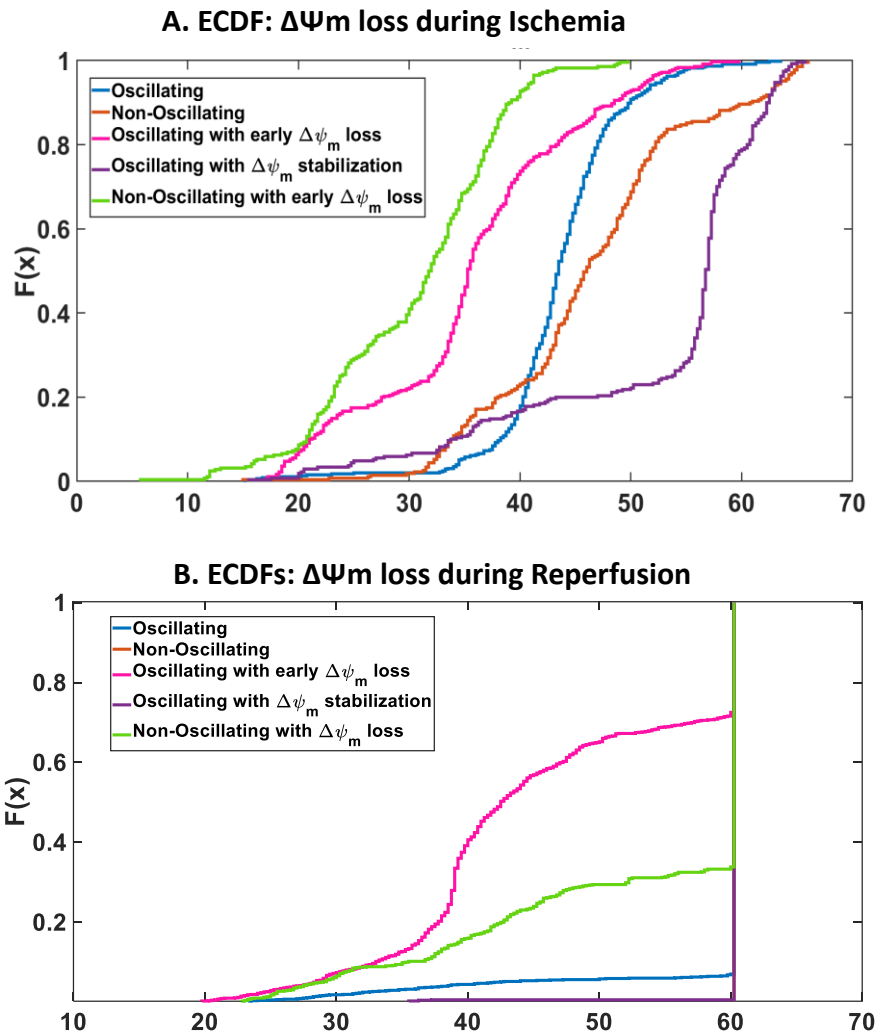


**Figure 2.8: Relationship between Ischemic  $\Delta\Psi_m$  depolarization time and Oscillatory behavior during Reperfusion**

A) Empirical Cumulative Distribution functions showing the probability of depolarization ( $F(x)$ ) as a function of time ( $x$ ) during Ischemia. B) Empirical Cumulative Distribution functions showing the probability of depolarization ( $F(x)$ ) as a function of time ( $x$ ) during Reperfusion. Mitochondrial stabilization during reperfusion correlated with late  $\Delta\Psi_m$  loss during Ischemia (purple line).



## Discussion

Over the course of ischemia-reperfusion, the mitochondrial networks of cultured neonatal mouse cardiomyocytes displayed complex spatiotemporal patterns, including bistability and time-varying oscillatory behavior, presenting significant challenges to analysis. The present work combined image segmentation with the versatility of wavelet transforms to quantify key transitions associated with the pathophysiology of I/R injury in an unbiased manner. Essential information could be captured in a semi-automated workflow, including the time-to-mitochondrial depolarization during ischemia, frequency of  $\Delta\Psi_m$  oscillation of individual mitochondrial clusters upon reperfusion, and time to catastrophic loss of  $\Delta\Psi_m$  with prolonged reperfusion. Subsequent data reduction permits one to make statistical comparisons between different experiments to determine if a given treatment or intervention has significant effect on mitochondrial function (Fig 2.3).

We have previously reported that adult cardiomyocytes subjected to metabolic or oxidative stress undergo spontaneous oscillations in  $\Delta\Psi_m$  that occur either in small clusters or are synchronized across the whole cell (16). Cell wide  $\Delta\Psi_m$  synchronization is observed after a critical number of mitochondria in the network show oxidative stress, a phenomenon we termed “mitochondrial criticality”(101). Synchronization of mitochondria in the organized array of the adult myocyte depends on ROS-dependent neighbor-neighbor interactions between organelles, with long range cluster interactions following the behavior of a percolation lattice(31). In neonatal myocytes, the mitochondrial network is less ordered and reperfusion-induced oscillations are less likely to be synchronized throughout the entire network (94), consistent with a short effective diffusion distance for ROS-induced ROS release(14). In contrast, when the

system is forced by a uniform environmental stress, such as ischemia, mitochondrial network depolarization occurs on a cell-by-cell basis, likely determined by the anaerobic ATP-generating capacity and glycogen store of the individual cells. The average time to ischemic  $\Delta\Psi_m$  depolarization for a given coverslip was compared to the oscillatory behavior of mitochondrial clusters on reperfusion (Fig. 2.7 & 2.8). Interestingly, early  $\Delta\Psi_m$  loss during ischemia correlated with early  $\Delta\Psi_m$  loss during reperfusion; however, this was equally true for both oscillating and non-oscillating clusters, suggesting that there is no specific protective advantage of the oscillatory behavior. In fact, there was a trend towards earlier depolarization during reperfusion for oscillating versus non-oscillating mitochondrial clusters. At least concerning mitochondrial recovery after reperfusion, these findings argue against the idea that oscillations in metabolism might preserve a higher average ATP/ADP ratio while decreasing free energy dissipation compared to steady state operation (102). Instead, mitochondrial  $\Delta\Psi_m$  oscillation could simply be an inevitable consequence of the nonlinear control properties of the nonlinear bioenergetic system. In addition, late  $\Delta\Psi_m$  loss during ischemia correlated with  $\Delta\Psi_m$  stabilization after oscillation on reperfusion. Together these data indicate that mitochondrial energetic recovery strongly depends on resistance to initial ischemic depolarization, consistent with data from intact perfused hearts(103).

The present findings show that in NMVMs subjected to I/R,  $\Delta\Psi_m$  oscillation frequency is inversely correlated with cluster size (Fig. 2.6). This is in agreement with the negative correlation obtained by wavelet transform analysis of adult myocytes under oxidative stress, with large mitochondrial clusters showing slow  $\Delta\Psi_m$  oscillations that could span the entire cell with a stereotypical frequency of 1 - 10 mHz(16). Synchronization of a network of dynamically coupled

oscillators spanning a broad frequency range to a single dominant frequency is common to physical, chemical and biological systems. The lack of synchronization in NMVMs and the broader frequency distribution (Fig. 2.5) may be the result of the more disorganized arrangement of mitochondria in neonatal myocytes or weaker coupling between mitochondria in the immature cells.

The method described here provides a way to uncover and quantify different mitochondrial responses to I/R stress that might otherwise be overlooked if one were to only examine the average behavior of a monolayer, of individual cells, or at single time points during a protocol (e.g., measuring lactate dehydrogenase release as an index of damage after reperfusion). A current limitation of the method is that it would be affected by significant movement of the objects being analyzed in the optical field, which was minimal in our experiments. In the future, it might be possible to further develop the approach by incorporating object tracking methods. Nevertheless, the approach is applicable to any spatially-distributed system of time varying oscillatory signals. Unlike Fourier transform analysis, the underlying oscillator frequencies and phases do not have to be time invariant and the method is largely immune to changes in signal offset (such as photobleaching) or background artifacts. This novel approach, which standardizes the quantitative analysis of complex biological signals, opens the door to in depth screening of the genes, proteins and mechanisms underlying metabolic recovery after ischemia-reperfusion.

# CHAPTER 3: Mitochondrial Membrane Potential instability persists in Ischemia/Reperfusion injury in MCU-KO cardiomyocytes

## Introduction

Physiologic  $\text{Ca}^{2+}$  import into mitochondria is essential for matching energy supply with demand.  $\text{Ca}^{2+}$  import activates three  $\text{Ca}^{2+}$ -regulated dehydrogenases of the Krebs cycle (pyruvate dehydrogenase, 2-oxoglutarate dehydrogenase and isocitrate dehydrogenase)(45) Under pathological conditions, such as I/R injury, an excess of  $\text{Ca}^{2+}$  import damages mitochondria and triggers cell death, notably through mPTP opening and irreversible  $\Delta\Psi_m$  collapse. (9)

The Mitochondrial Calcium uniporter (MCU) is thought to be the primary mechanism of  $\text{Ca}^{2+}$  import into mitochondria (50),(52) (53) (51) (104). The hypothesis that mitochondrial  $\text{Ca}^{2+}$  import via the MCU is detrimental in I/R injury has been tested using genetically engineered mice. In a first study, mice with germline deficiency of MCU did not show any protection or detriment following I/R injury (55), whereas mice with inducible cardiomyocyte-specific deficiency of MCU to I/R injury were protected against I/R injury. (59) (58). In addition, a cardiac-specific overexpression of a dominant negative MCU, that renders the endogenous channel deficient, does not show any protection against I/R injury (60).

While these experiments are highly informative in evaluating the implications of MCU impacting cardiomyocyte death in intact hearts, many mechanistic details regarding the preceding steps remain largely unexplored. Here, we wanted to further evaluate the cellular mechanisms of  $\text{mCa}^{2+}$  import and export using an in-vitro I/R injury model, where  $\text{mCa}^{2+}$  dynamics

and  $\Delta\Psi_m$  instability can be monitored in real time with genetically encoded  $mCa^{2+}$  probe, 4mtd3cpv (MitoCam) and TMRM respectively.

Instability of the mitochondrial membrane potential ( $\Delta\Psi_m$ ) occurs during metabolic or oxidative stress and is capable of triggering ventricular arrhythmias(17) (95) (25) (105), (106). During stress evoked by Ischemia/Reperfusion (I/R) injury, mitochondria undergo substrate and oxygen deprivation, as well as oxidative stress, triggering  $\Delta\Psi_m$  oscillations which lead to  $\Delta\Psi_m$  collapse. Interventions with 4'-chlorodiazepam prevented ventricular arrhythmias on reperfusion (17) and stabilized  $\Delta\Psi_m$  oscillations (94), potentially implicating the benzodiazepine-sensitive Inner Membrane Anion Channel (IMAC) or the outer membrane Translocator Protein (TSPO, a.k.a., the mitochondrial benzodiazepine receptor) in this process. Similarly, interventions that suppress the mitochondrial ROS-Induced-ROS Release (RIRR) amplification mechanism also prevent  $\Delta\Psi_m$  oscillation (107) (14). In this paper, we examine if  $mCa^{2+}$ , and, in particular, MCU, is involved in triggering  $\Delta\Psi_m$  oscillations and irreversible  $\Delta\Psi_m$  collapse in simulated I/R injury.

Interestingly, we find that acutely knocking out MCU in neonatal mouse ventricular myocytes does not alter  $\Delta\Psi_m$  recovery during Reperfusion, instead it shortens the latency to  $\Delta\Psi_m$  depolarization during Ischemia. Moreover, in MCU-KO cardiac monolayers,  $\Delta\Psi_m$  instability after Ischemia persisted. An additional surprising finding was that MCU knockout did not affect  $mCa^{2+}$  import during I/R, although inhibition of the mitochondrial  $Na^+/Ca^{2+}$  exchanger (mNCE) did, indicating that MCU is not the primary mode of  $mCa^{2+}$  import during ischemia.

## **Methods**

### **MCU mice model**

MCU Floxed mice were obtained from Dr. John Elrod's group (59), (58). Briefly, MCU conditional knockout mice were generated by recombinant insertion of a targeting gene containing loxP sites flanking the 5<sup>th</sup> and 6<sup>th</sup> exon of the MCU gene in mouse embryonic stem cells. Breeding pairs were obtained from Dr. John Elrod and neonates were generated in our lab to prepare neonatal mouse ventricular myocytes. All animal procedures were approved by IACUC.

### **Neonatal cardiomyocyte isolation, cell culture and Adenoviral Transfection:**

Neonatal mouse ventricular myocytes (NMVMs) were isolated using MACS Miltenyi Biotec kits (Catalog #130-100-825 and #130-098-373). Briefly, hearts from 0-2-day old mice were excised, chopped into small pieces and digested using reagents supplied by the kit. A cardiomyocyte-rich cell suspension was obtained by separation of magnetically labelled non-cardiac cells from the total cell suspension upon application of a magnetic field.  $1 \times 10^6$  NMVMs were plated on fibronectin-coated (10 $\mu$ g/ml) 35mm (D=20mm) glass coverslip dishes (NEST<sup>®</sup> catalog # 801001) in Medium-199 supplemented with 25mM HEPES, 2 $\mu$ g/ml Vitamin B12, 50U/ml Pen-strep, Non-essential 286 Amino acids and 10% FBS. The next day, the medium was changed to 2% FBS medium. Adenoviruses expressing CRE-Recombinase (to knock-out MCU) or adenoviruses with beta-galactosidase (as a control) were transduced into NMVMs. To monitor mitochondrial Ca<sup>2+</sup>, the cells were also transduced with adenoviruses expressing the mitochondrially-targeted ratiometric Ca<sup>2+</sup> sensor 4mtd3cpv (108). Cells were transduced at a concentration of ~40

infectious particles per cell on the first or second day of isolation. Ischemia/Reperfusion experiments and imaging were performed on the 5th- 6th day of culture.

### **Western blot**

MCU knock-out was confirmed by western-blot (MCU antibody from Cell Signaling #14997), and densitometry analysis using NMVM cell lysates 5-6 days after Ad-Cre transduction. (Figure 3.1)

### **Inducing Ischemia and Reperfusion, $\Delta\Psi_m$ and $Ca^{2+}$ Imaging**

To monitor mitochondrial membrane potential ( $\Delta\Psi_m$ ), 50nM Tetramethyl rhodamine methylester (TMRM) was loaded for 30 min at 37°C prior to the start of the experiment and replaced with fresh Tyrode's buffer (130mM NaCl, 5mM KCl, 1mM  $MgCl_2$ , 10mM NaHEPES, 1mM  $CaCl_2$  and 5mM Glucose). A typical protocol included a baseline reading for 10 minutes followed by 60 minutes of regional ischemia induced by placing a 15mm glass coverslip, followed by 60 minutes of reperfusion upon removal of the coverslip (previously described in NRVMs (97) (109) (94)). During this 130-minute period, images were obtained every 15 seconds on a laser-scanning confocal microscope (Olympus FLUOVIEW 3000), where both mitochondrial membrane potential and mitochondrial  $Ca^{2+}$  were monitored sequentially at 40X magnification using a silicone-immersion objective (Olympus UPLSAPO40XS). A neutral density filter of 10% was applied to the excitation beam and cells were imaged with Galvano scanning mode without any averaging. Laser powers of 0.06% for TMRM and 2% for CFP/YFP FRET were used (Fig. 3.1 A and B)

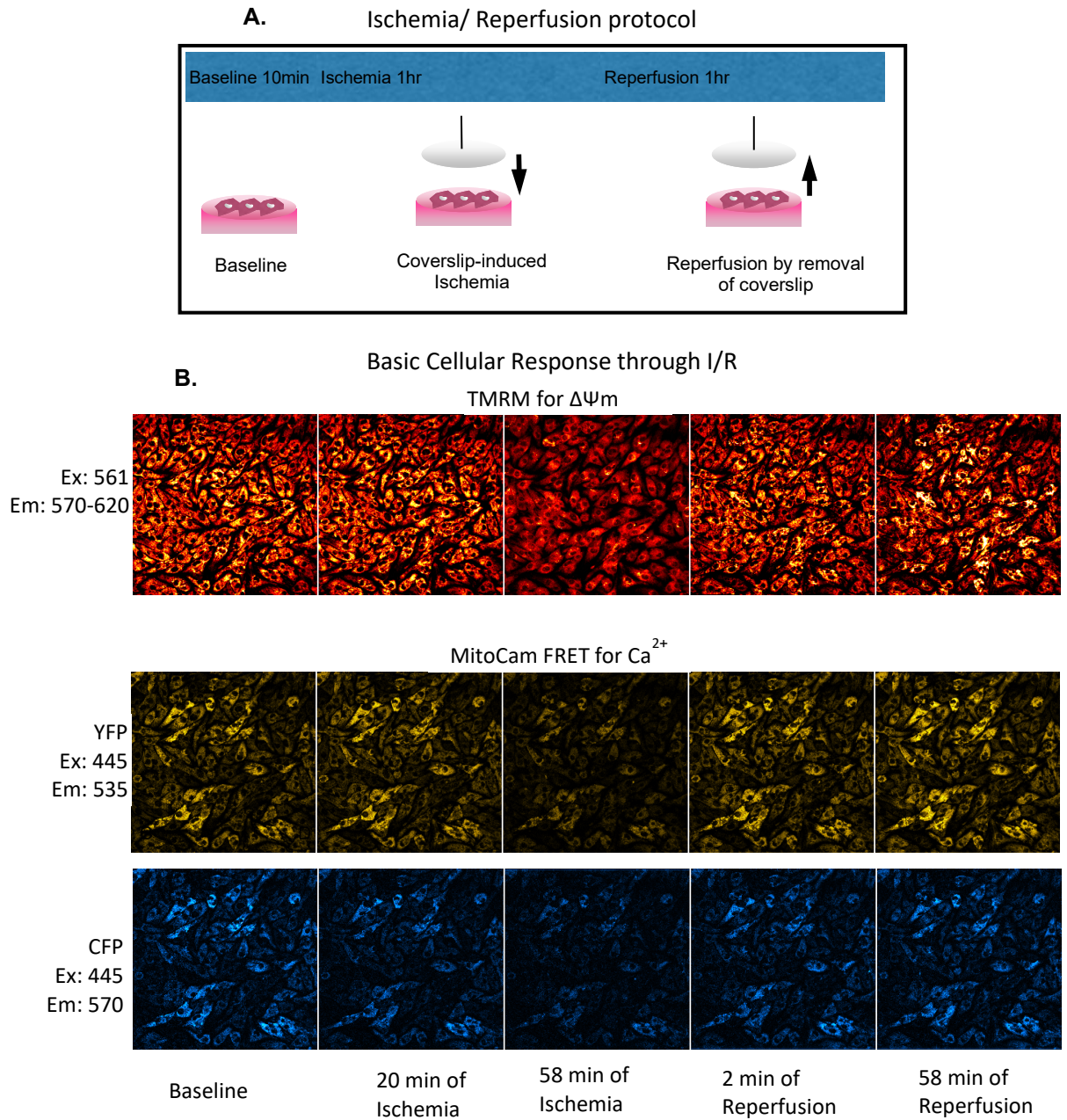


**Figure 3.1: Methods and Protocol**

(A) In vitro Ischemia and Reperfusion protocol on a neonatal ventricular myocyte monolayer.

(B) Basic Cellular Response during baseline, Ischemia and Reperfusion. Mitochondrial Membrane Potential and mitochondrial Calcium were monitored with TMRM and a genetically-encoded MitoCam (4mtd3cpv) FRET probe targeted to the mitochondria, respectively. TMRM was excited at 560nm and



emission collected from 570-620nm. For MitoCam, CFP was excited at 445nm and emission was collected at 535nm. The FRET signal (YFP) was collected at 570nm. The ratio of the FRET signal to CFP after background subtraction indicated  $mCa^{2+}$  levels.

### **Monitoring Mitochondrial Membrane Potential**

Excitation wavelength used for TMRM was 561 nm and the emitted fluorescence between 570-620 nm was collected. Images were collected every 15 seconds. When mitochondria are depolarized, TMRM disperses into the cytoplasm from the mitochondria, causing a more diffuse distribution of TMRM fluorescence in the cell. Therefore we use the Spatial Dispersion of the signal as an indicator of mitochondrial polarization (110). This is a dimensionless value determined by calculating the coefficient of variation of the image fluorescence intensity (ratio of standard deviation to the mean). This measure minimizes potential artifacts related to bleaching, changes in dye load and illumination (94)(111).

### **Monitoring mitochondrial $Ca^{2+}$ and Calibration of the probe**

Mitochondrial  $Ca^{2+}$  was monitored using a genetically encoded FRET-probe, 4mtd3cpv. Originally developed by Palmer and Tsien (108), this probe has been characterized for use in cardiac myocytes by Wüst et.al (112). It contains four mitochondrial targeting sequences and a circularly permuted venus group which makes it less susceptible to changes in pH (since pH changes are often seen during Ischemia/Reperfusion). We incorporated this probe into an adenovirus using Invitrogen's Gateway® system. An excitation light of 445 to excite CFP and emission at 535nm and 570nm (for YFP, FRET signal) were collected.

## Image Analysis

Image series of the time-course of the Ischemia/Reperfusion experiment were analyzed using Fiji (<https://imagej.net/Fiji/Downloads>) (113). A custom-built segmentation-analysis macro was generated to track each cell's  $\Delta\Psi_m$  and  $mCa^{2+}$  during the in-vitro I/R injury. For  $mCa^{2+}$ , the ratio of YFP to CFP was obtained per cell using the 'Ratio-Profiler' plugin on Fiji.

**Depolarization Time estimation:** TMRM signal from each cell was subjected to Multi-resolution wavelet decomposition to separate higher frequencies (noise) from large transitions in signal ( $\Delta\Psi_m$  depolarizations). Decomposed signals were used to find 'transition points' using MATLAB's 'findchangepts' function.

**Oscillation Analysis:** We followed the same protocol as described in Chapter II, called 'MitoWave', currently available as a preprint (114). Briefly, to obtain the frequency of the oscillating clusters of mitochondria during reperfusion, each cell was separated by segmentation and a difference stack was generated to define its oscillating clusters (after a z-projection of the difference stack). A region-of-interest was defined for each oscillating cluster and the raw TMRM intensity was obtained for each cluster. This TMRM signal was subjected to a Continuous wavelet transform to obtain a scalogram using MATLAB's Wavelet Transform toolbox. Each Scalogram was then subjected to ImageJ-based thresholding to obtain the co-ordinates of the highest coefficients. These coefficients provide the frequencies and the associated time of each oscillating cluster. Each oscillating cluster was categorized into different frequency bands throughout the reperfusion period. A violin plot visually represents the behavior of these oscillating clusters. Each cluster may change its frequency band during reperfusion depending on whether it stabilizes or not during reperfusion.

### **LDH Assay**

Supernatants were collected from cells subjected to Ischemia/Reperfusion and a Lactate Dehydrogenase Assay was performed to assess the level of cellular toxicity. CyQUANT™ LDH Cytotoxicity Assay from Thermo Fisher was used (Catalog number: C20300). LDH levels are expressed as a percentage of maximum LDH levels released from lysed cells.

### **Statistical Analysis**

Data were analyzed with GraphPad Software, San Diego (version 8.0) and MATLAB and Statistics Toolbox Release 2019b. Statistical significance between different treatments (genetic knockout or inhibitors) were evaluated with Kruskal-Wallis nonparametric test with Dunn's multiple comparisons test for correction for multiple tests. Summary statistics are presented as mean +/- SEM. Statistical analysis for estimating differences in Oscillation patterns were performed with non-parametric Kolmogorov-Smirnov test using an alpha of 0.001 to reject the null-hypothesis.

## Results

### MCU is required for rapid $\text{Ca}^{2+}$ uptake into mitochondria

$\text{Ca}^{2+}$  uptake into the mitochondria is driven by the electrochemical  $\text{Ca}^{2+}$  gradient and the negative membrane potential inside mitochondria (115) (104). MCU is the primary mode of  $\text{Ca}^{2+}$  entry into the mitochondria and is responsible for the rapid uptake of  $\text{mCa}^{2+}$  (50), (74), (51). Therefore, we wanted to confirm that knocking out ~80% of the MCU acutely (in 5 days) in culture (Figure 3.2A&B) has functional consequences. We first measured  $\text{mCa}^{2+}$  levels in Neonatal Mouse Ventricular Myocytes using the genetically-encoded MitoCam FRET probe (Figure 3.4A). We recorded baseline  $\text{mCa}^{2+}$  levels in unstimulated cells for 10 minutes, acquiring an image every 15 seconds. We found no difference between matrix  $\text{Ca}^{2+}$  levels in MCU-WT and KO cells, similar to observations in several other MCU knockout studies (59), (58), (116). We also wanted to check if blocking the mitochondrial  $\text{Na}^+/\text{Ca}^{2+}$  would alter  $\text{mCa}^{2+}$  levels at baseline and found that addition of the mNCE inhibitor CGP-37157 (10 $\mu\text{M}$ ; CGP) did not alter baseline  $\text{mCa}^{2+}$  levels (Fig. 3.4A). However, when we measured beat-to-beat  $\text{mCa}^{2+}$  transient amplitudes in MCU-WT and MCU-KO myocytes (Fig. 3.3), we observed a 55% decrease in MCU-KO myocytes compared to WT (Fig. 3.4B). To see if there was any difference in  $\text{mCa}^{2+}$  uptake in response to a large rise in cytosolic  $\text{Ca}^{2+}$ , we initiated caffeine-induced SR- $\text{Ca}^{2+}$  release (117). Cells were superfused with  $\text{Na}^+$ - and  $\text{Ca}^{2+}$ -free buffer to prevent  $\text{Ca}^{2+}$  extrusion via the Sarcolemmal  $\text{Na}^+/\text{Ca}^{2+}$  exchanger (NCX). 20mM Caffeine was then added to release the SR- $\text{Ca}^{2+}$  stores. Under these conditions,  $\text{Ca}^{2+}$  accumulation into the mitochondria was measured. We found that  $\text{mCa}^{2+}$  uptake into the mitochondria was significantly reduced by ~80% in MCU-KO cells (Fig. 3.4C). We also calibrated the MitoCam probe in both WT and KO cells to obtain the minimum ( $R_{\text{min}}$ ) and maximum ( $R_{\text{max}}$ ) YFP/CFP FRET ratios

for calibrating the signal in different experiments. The  $R_{\min}$  and  $R_{\max}$  were not significantly different between MCU-WT and KO cells (Fig. 3.4D and 3.4E). Examples of the calibration traces are shown in Fig. 3.5. Further, since the mitochondria contribute to beat-to-beat buffering of systolic  $\text{Ca}^{2+}$  transients (57) via MCU, we also measured cytosolic  $\text{Ca}^{2+}$  transients using Fura-2. MCU-KO monolayers displayed a ~37% increase in cytosolic  $\text{Ca}^{2+}$  transient amplitude compared to WT. Adding 10 $\mu\text{M}$  CGP to WT cells, which should also facilitate redistribution of  $\text{Ca}^{2+}$  from the mitochondrial compartment to the SR, increased cytosolic transient amplitude by ~24% compared to controls (Fig 3.4F). This demonstrates that CGP does not inhibit cytosolic  $\text{Ca}^{2+}$  cycling (important for the subsequent interpretation of its effect on I/R  $\text{Ca}^{2+}$ ).

*These results confirm previous findings that although there is no difference in matrix  $\text{Ca}^{2+}$  levels at baseline between MCU-WT and KO, fast  $\text{mCa}^{2+}$  uptake is significantly reduced in MCU-KO cells.*

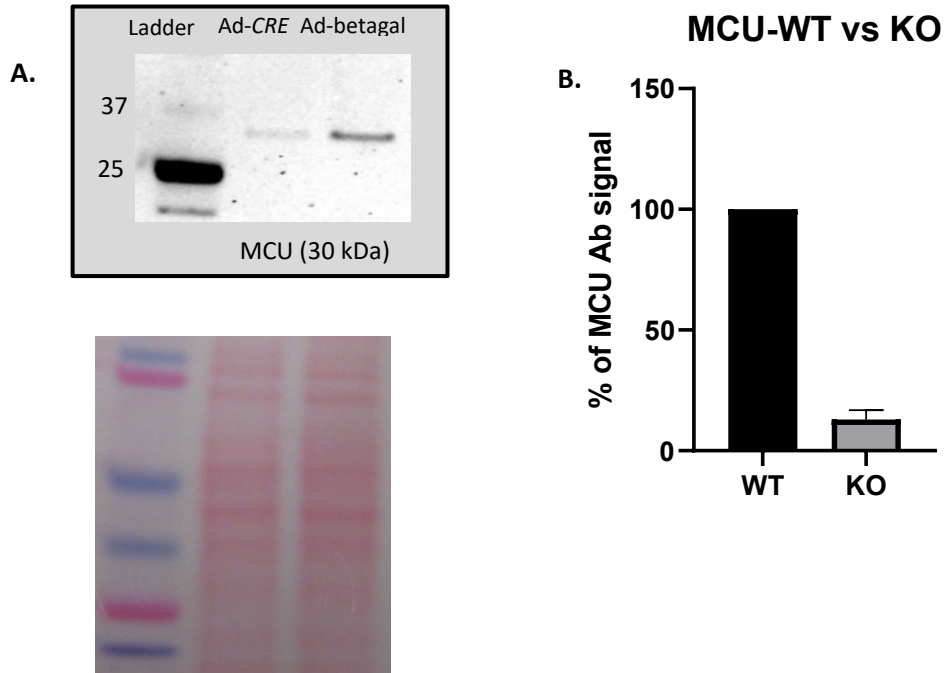


**Figure 3.2: Addition of Ad-Cre results in knockout of MCU in 5 days in NMVMs**

(A) Cardiomyocytes from MCU<sup>fl/fl</sup> neonatal mice (NMVMs) were transduced with adenovirus expressing *Cre*-recombinase (Ad-*Cre*) or  $\beta$ gal (Ad- $\beta$ gal) control virus. An 80% reduction in MCU protein (expected molecular weight of 30kDa) was seen on the 5<sup>th</sup> day of viral transduction in Ad-*Cre* treated cells. Below is the ponceau stain used as loading control.

(B) Quantification of MCU antibody signal from western blots (n=6).

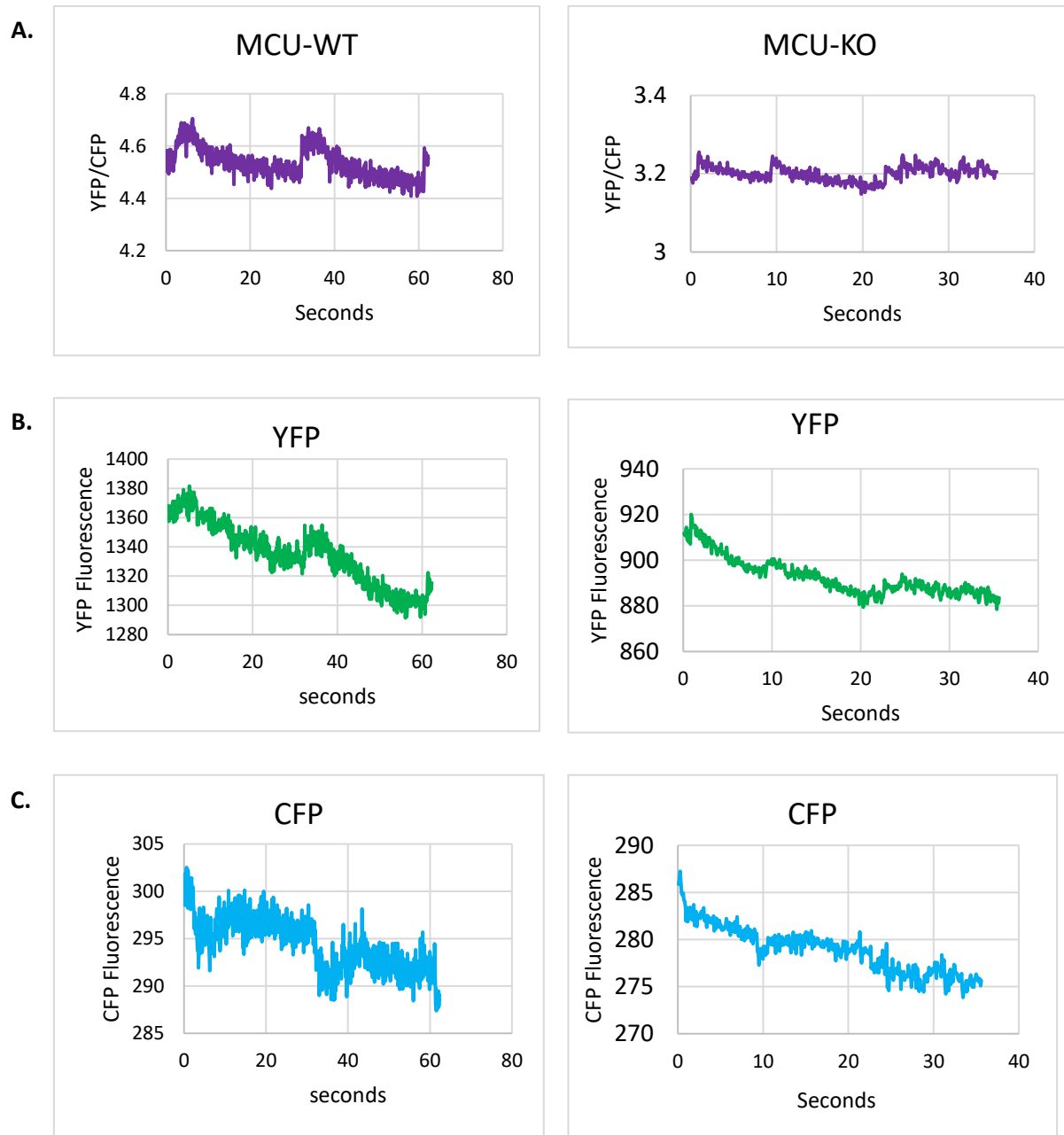


**Figure 3.3: Functional effects of MCU knockout; representative mCa<sup>2+</sup> transients in spontaneously beating MCU-WT and MCU-KO neonatal mouse ventricular myocytes.**

(A) Ratio of YFP/ CFP signal indicating mCa<sup>2+</sup> levels. (B) Raw YFP signals (C) Raw CFP signals.

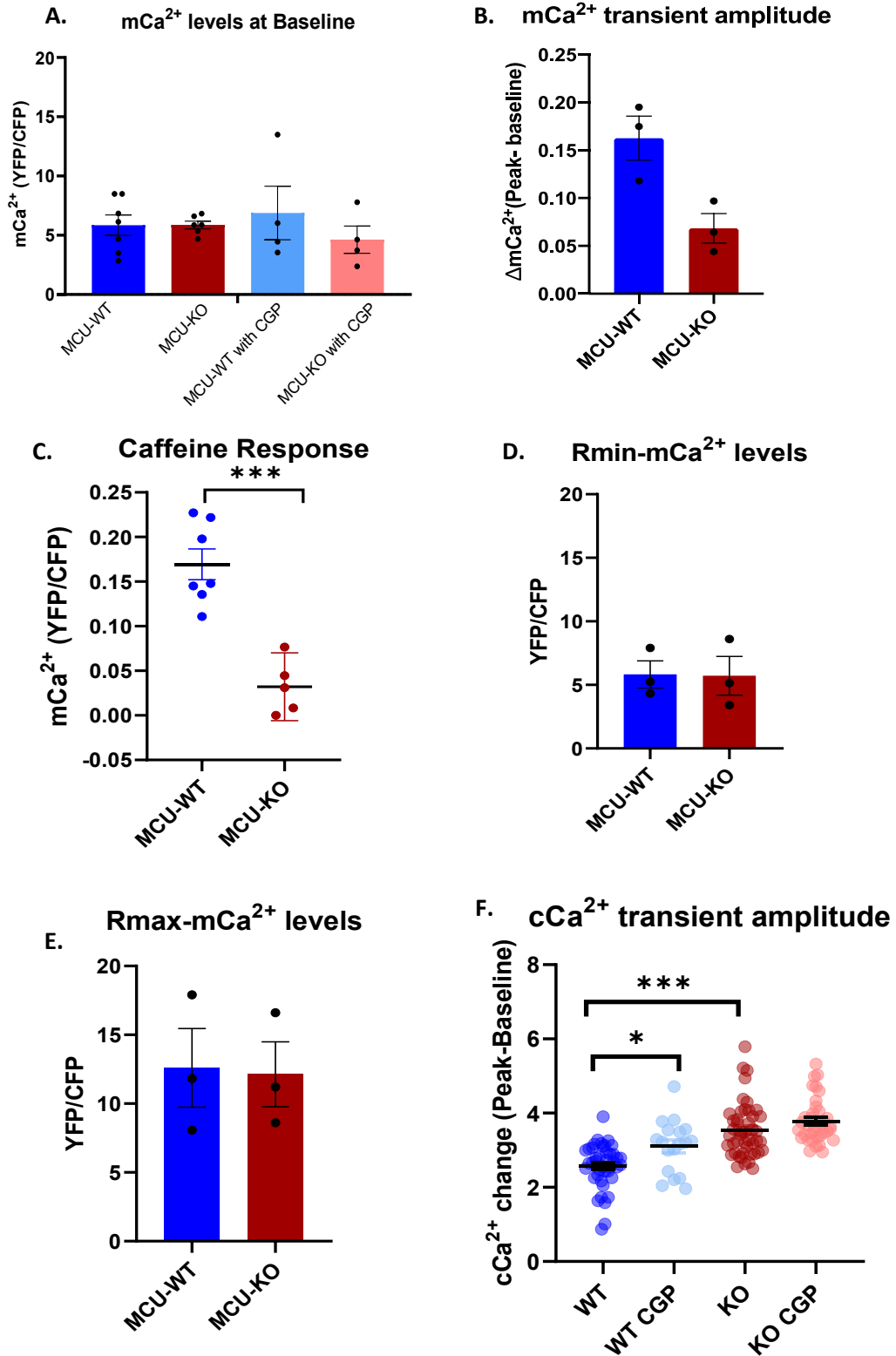
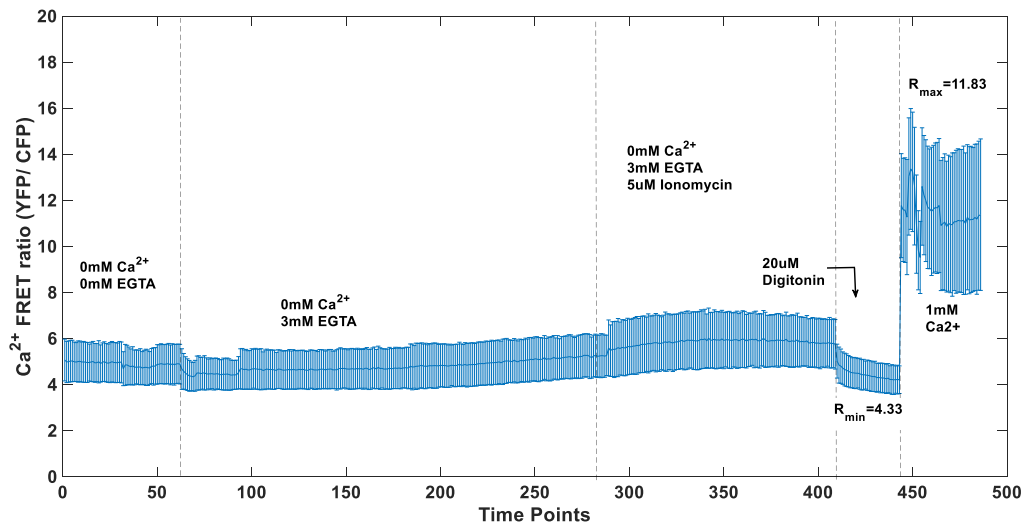


Figure 3.4: MCU is required for rapid Ca<sup>2+</sup> uptake into mitochondria



(A)  $mCa^{2+}$  levels at baseline in Neonatal Mouse Ventricular Myocytes using MitoCam probe.  $mCa^{2+}$  levels are represented as a ratio of the FRET signal (YFP) to CFP. Baseline  $mCa^{2+}$  for MCU-WT, MCU-KO as well as MCU-WT with CGP vs MCU-KO with CGP are shown. (B)  $mCa^{2+}$  transient amplitude in unstimulated cells in MCU-WT and KO. (C)  $mCa^{2+}$  uptake measured when SR- $Ca^{2+}$  is released by caffeine in the presence of 0mM  $Na^+$  (Welch's t test, WT= 7, KO= 5 cells). (D & E)  $R_{min}$  and  $R_{max}$   $mCa^{2+}$  levels after calibrating the MitoCam probe signal. (F) Cytosolic  $Ca^{2+}$  transients measured using Fura-2, with and without CGP. N= more than 18 cells (Kruskal Wallis non-parametric test, with Dunn's Multiple comparison. Experiments (and calibrations) were repeated at least 3 times. SEM is shown.



**Figure 3.5: 4mtd3cpv (MitoCam) FRET probe calibration trace**

NMVMs were incubated in Tyrode's with 0mM  $Ca^{2+}$  and 0mM EGTA to begin with. Then it was switched to medium with 3mM EGTA and 0mM  $Ca^{2+}$ . 5 $\mu$ M Ionomycin was added to release intracellular  $Ca^{2+}$  stores. 20 $\mu$ M Digitonin was added to permeabilize the cells.  $R_{min}$  was noted at this stage. Then 1mM  $Ca^{2+}$  was added to NMVMs,  $R_{max}$  was noted at this stage.

**MCU knockout does not affect mitochondrial Calcium import during Ischemia and Reperfusion, but blocking mNCE with CGP-37157 prevents mCa<sup>2+</sup> increase during Ischemia**

The phenomena of excess Ca<sup>2+</sup> into mitochondria, triggering cell death pathways via mPTP has been well established (118). The hypothesis that preventing or reducing Ca<sup>2+</sup> influx into mitochondria during Ischemia could be beneficial has given rise to multiple studies evaluating this effect. Given the conflicting reports of the role of MCU in *in-vivo* I/R injury(59) (58) (60), we next assessed the impact of genetic knockout of MCU in an in vitro model of I/R injury. Particularly, we wanted to understand the mechanisms of Ca<sup>2+</sup> import into mitochondria during I/R. We tracked Ca<sup>2+</sup> import into mitochondria during Ischemia and reperfusion while simultaneously monitoring  $\Delta\Psi_m$ . To monitor mitochondrial Ca<sup>2+</sup>, an adenovirus expressing MitoCam (4mtd3cpv) was transduced into these cells at least 48hr prior to imaging. mCa<sup>2+</sup> and  $\Delta\Psi_m$  were monitored during 1hr of Ischemia (induced by placing a coverslip) followed by 1hr of Reperfusion (removing the coverslip). We wrote a custom-made macro to monitor signals from each cell in the CFP channel (donor) and the YFP (FRET channel). The ratio of the FRET signal to the donor signal after background subtraction was used as a measure of mCa<sup>2+</sup> levels. The FRET ratio was obtained for about 100 cells per experiment. The overall response of different cells with different levels of expression was considered to check if they behaved similarly, since high expression levels could potentially cause Ca<sup>2+</sup> buffering. (Example traces of mCa<sup>2+</sup> during I/R in MCU-WT and MCU-KO monolayer of cells are represented in Fig 3.6). We observed a rise in Ca<sup>2+</sup> levels during early Ischemia up to ~25 minutes, after which mCa<sup>2+</sup> levels declined in both MCU-WT and MCU-KO cells (Fig. 3.7A and C), in parallel with loss of  $\Delta\Psi_m$ . At the end of Ischemia, mCa<sup>2+</sup>

levels were slightly lower than at baseline. Immediately upon reperfusion, mCa<sup>2+</sup> influx was observed in both MCU-WT and MCU-KO cardiomyocytes. No significant difference was found in mCa<sup>2+</sup> levels between MCU-WT and MCU-KO cells at early, mid, or late Reperfusion phases (Fig.3.7C). We then subjected NMVMs to CGP-37157 to block mNCE, while monitoring mCa<sup>2+</sup> and  $\Delta\Psi_m$  during I/R. We found that CGP-37157 abolished the rise of mCa<sup>2+</sup> in early Ischemia and suppressed mCa<sup>2+</sup> influx during reperfusion (Fig 3.7B and C). Although the ischemia-induced early rise in mCa<sup>2+</sup> levels was suppressed, mCa<sup>2+</sup> at the end of Ischemia was not significantly different in CGP-treated versus untreated cells. We also measured cytosolic Ca<sup>2+</sup> with a genetically-encoded cytoplasmic Ca<sup>2+</sup> probe (d3cpv), with or without CGP to confirm that CGP did not affect cytoplasmic Ca<sup>2+</sup> levels during Ischemia/Reperfusion (Fig 3.8). These results suggest that the mNCE mediates mitochondrial Ca<sup>2+</sup> uptake during Ischemia. Indeed, Griffiths et. al., first proposed mNCE as a possible pathway for mitochondrial Ca<sup>2+</sup> loading in adult cardiomyocytes subjected to hypoxia and re-oxygenation (47) based on inhibition by clonazepam. They hypothesized that, under conditions of reduced  $\Delta\Psi_m$  and changes in  $\Delta pH$ , the mitochondrial mNCE could work in the reverse mode. Therefore, we also monitored  $\Delta\Psi_m$  changes simultaneously during the I/R period and confirmed that the observed changes in mCa<sup>2+</sup> uptake in CGP-treated cells was not due to alterations in the driving force for mCa<sup>2+</sup> uptake.

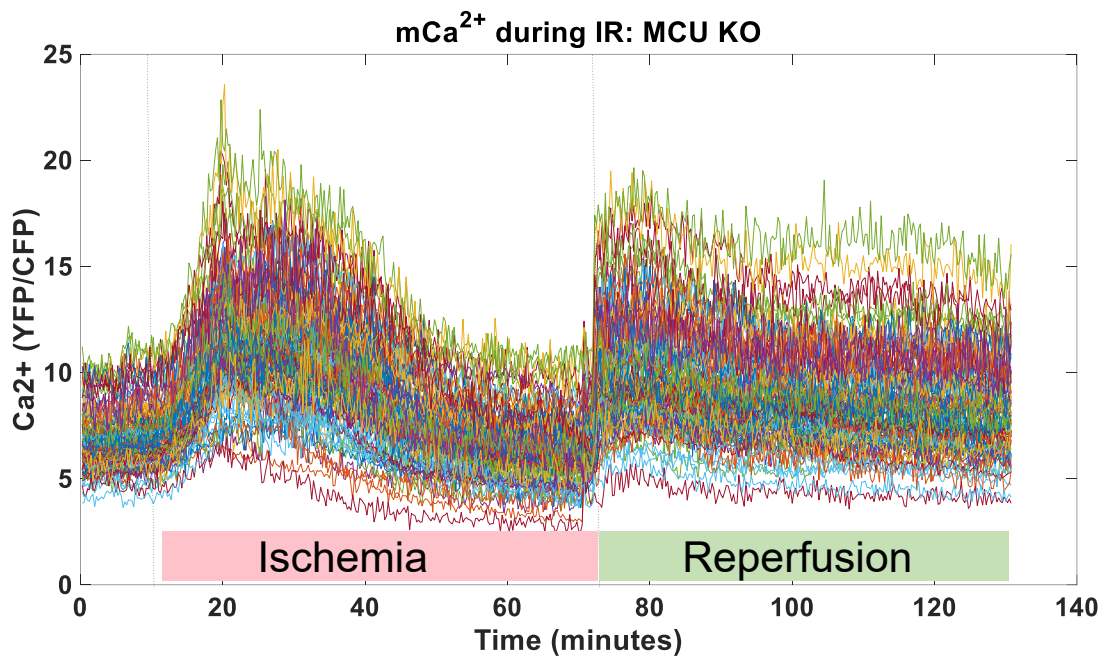
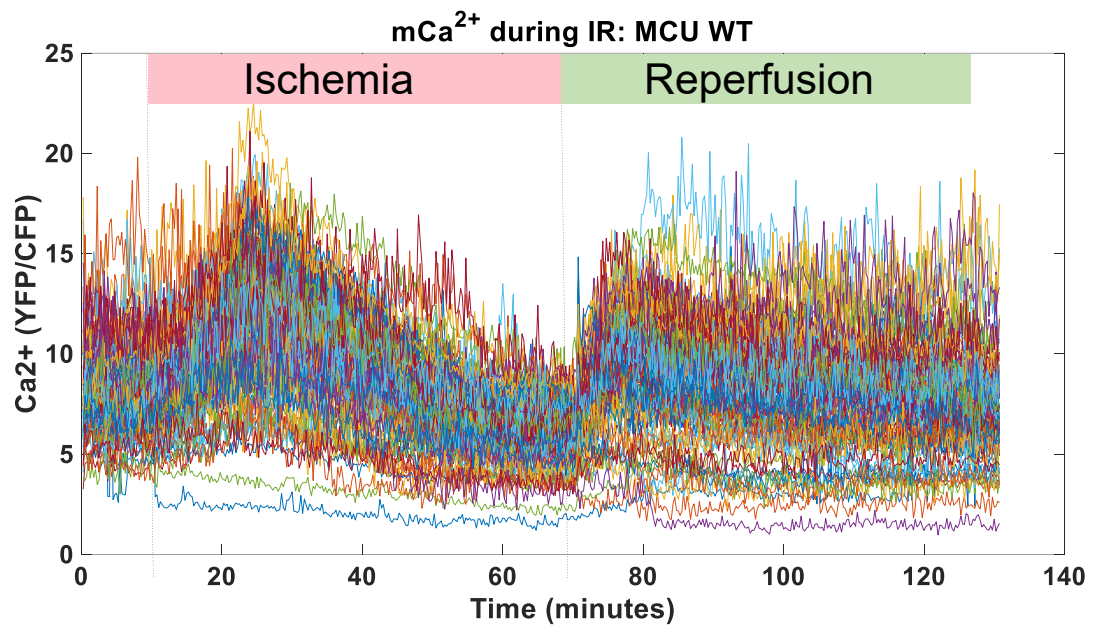
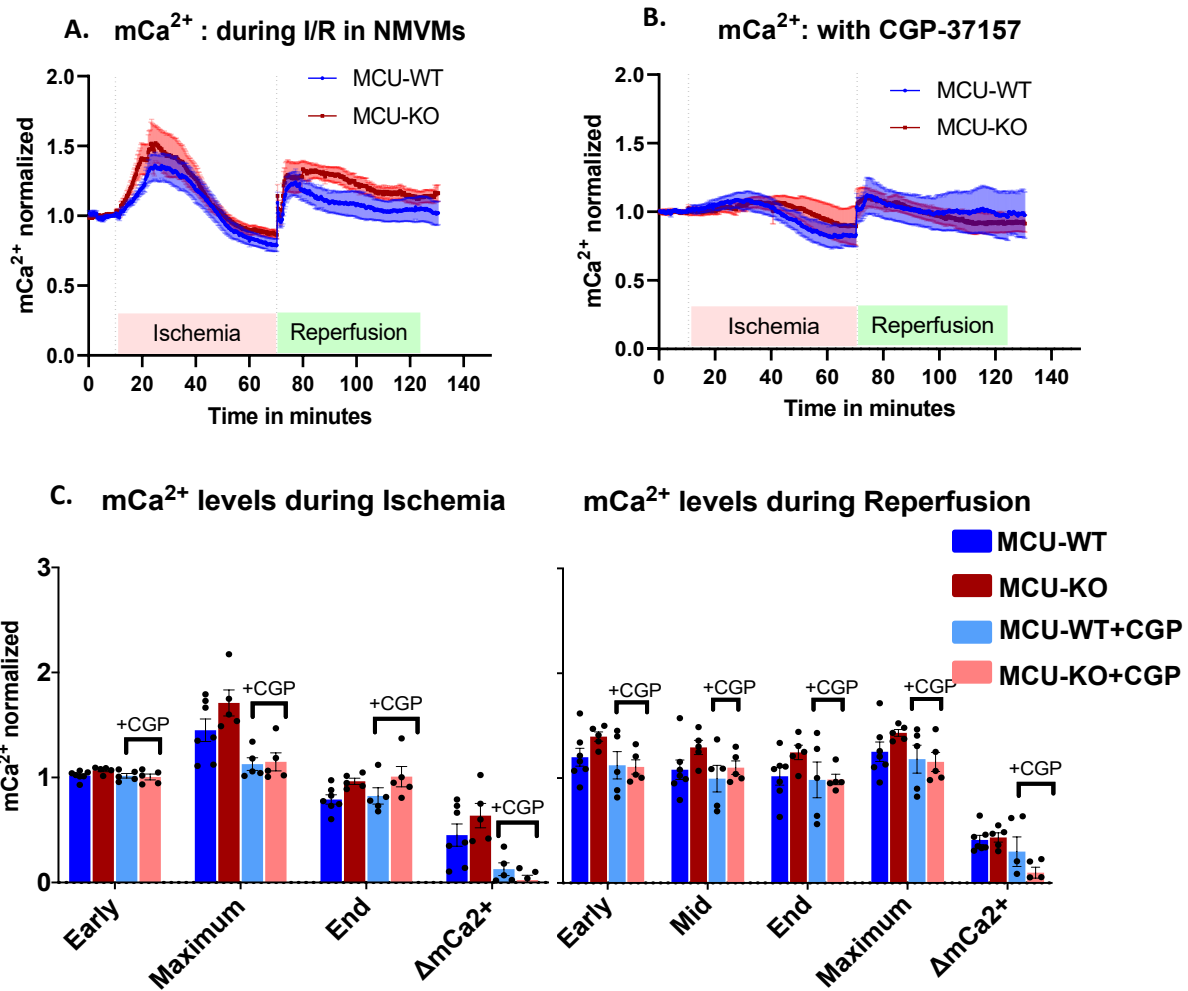
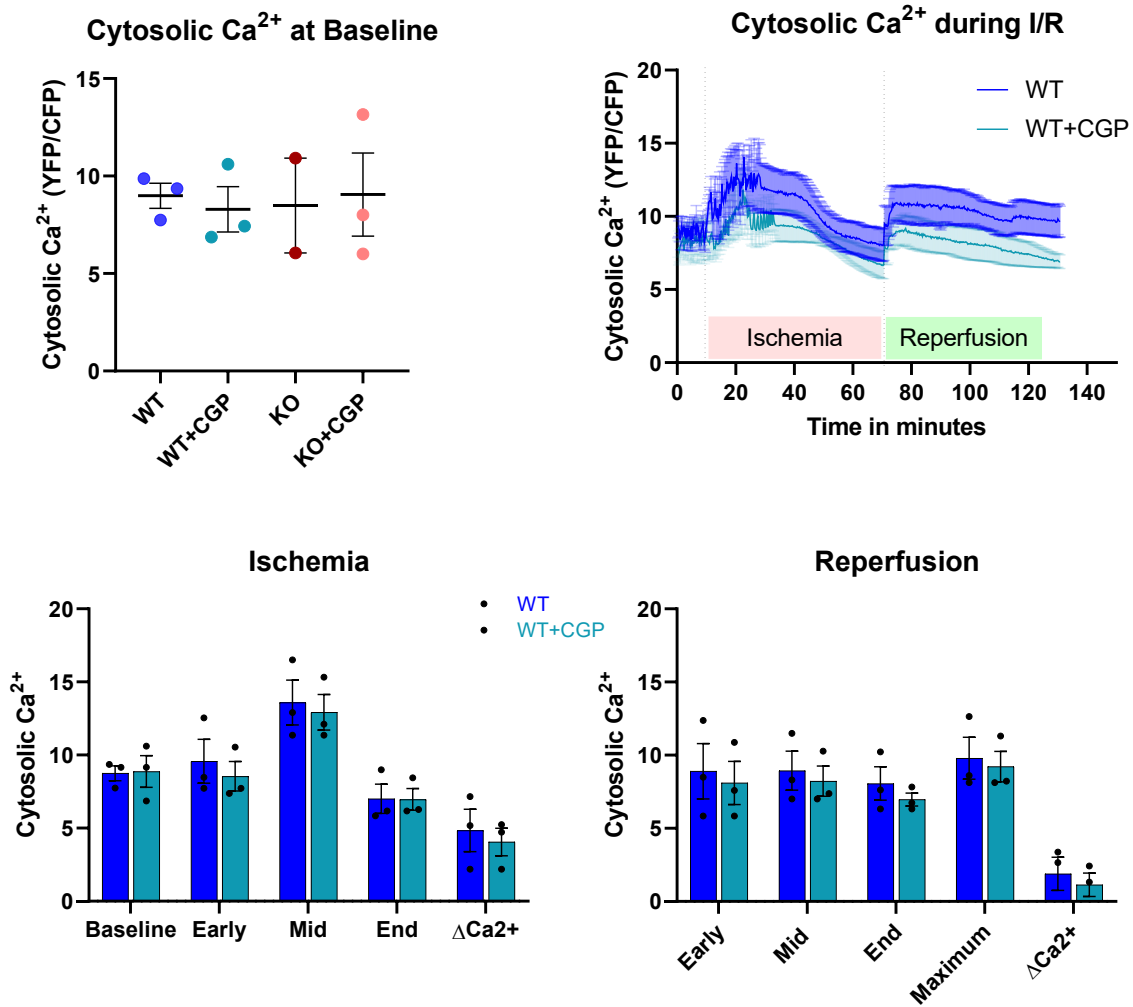


Figure 3.6: Example traces of mCa<sup>2+</sup> during Ischemia/Reperfusion in MCU WT (top) and KO (bottom) monolayers.



**Figure 3.7: MCU knockout does not affect mitochondrial Ca<sup>2+</sup> import during Ischemia and Reperfusion, but blocking mNCE with CGP-37157 prevents mCa<sup>2+</sup> during Ischemia**

(A) Mitochondrial Calcium monitored in Neonatal Mouse Ventricular Myocytes with WT-MCU or MCU-KO during 1hr of Ischemia and 1hr of reperfusion with a genetically encoded probe 4mtDd3cpv. mCa<sup>2+</sup> for each cell was quantified by obtaining the ratio of the YFP signal to CFP and normalized to baseline before Ischemia (B) mCa<sup>2+</sup> in MCU-WT and MCU-KO cells with CGP-37157. (C) Quantification of mCa<sup>2+</sup> levels at different stages during Ischemia and Reperfusion. Number of experiments, WT (7), KO (6), WT+CGP (5), KO+CGP(5).



**Figure 3.8: CGP-37157 effect on Cytoplasmic Ca<sup>2+</sup>**

Using a cytoplasmic genetically-encoded FRET probe (d3cpv), cytoplasmic Ca<sup>2+</sup> (cCa<sup>2+</sup>) levels were monitored during IR in NMVMs treated with CGP. No significant differences in cCa<sup>2+</sup> levels between CGP-treated or untreated NMVMs were observed at baseline or during I/R.

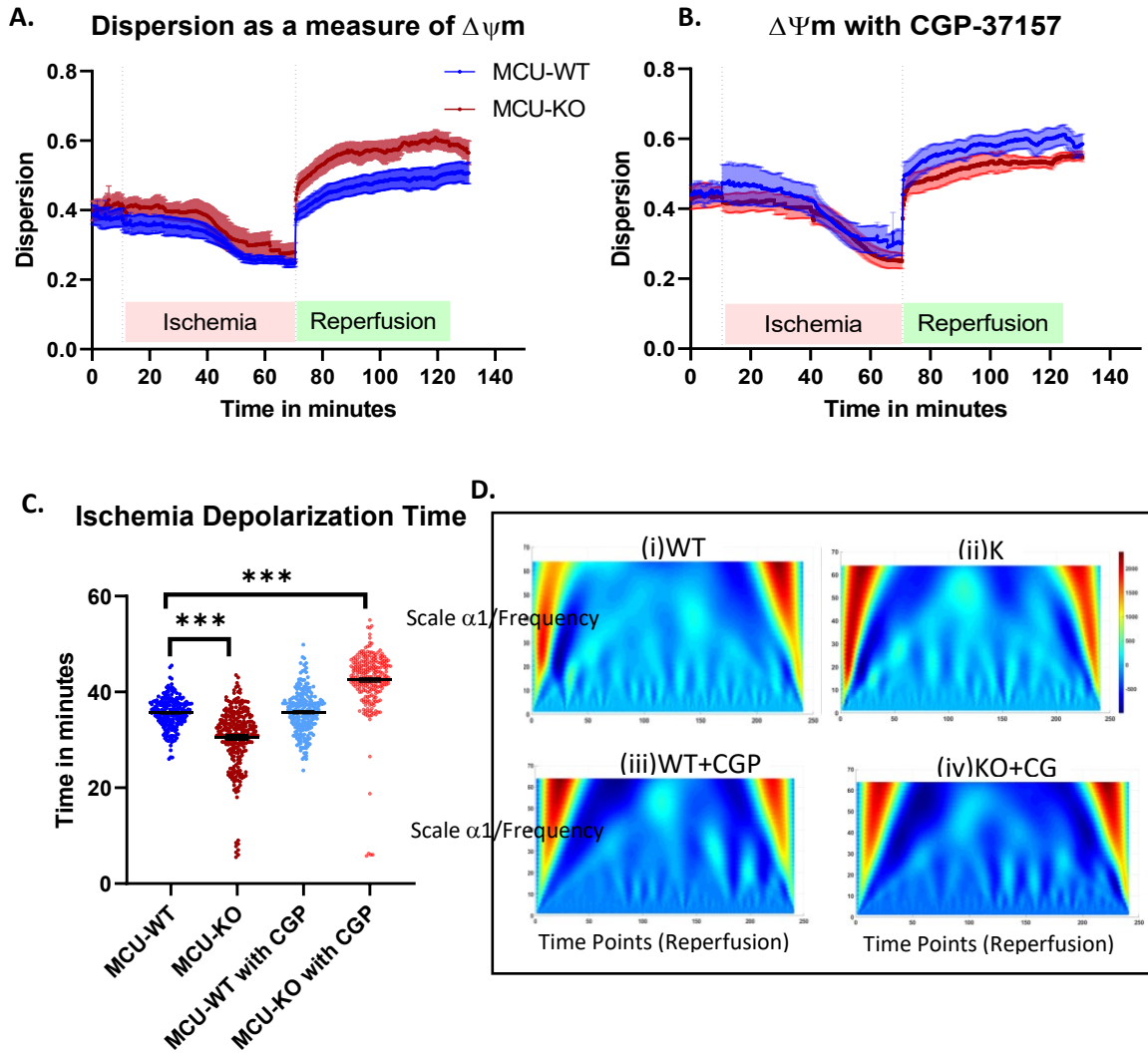
### **MCU-KO does not protect against $\Delta\Psi_m$ loss during I/R, nor does CGP**

$\Delta\Psi_m$  was monitored using TMRM. TMRM fluorescence and spatial standard deviation was obtained per cell by segmentation analysis using custom-made macros on ImageJ. The TMRM Dispersion (the ratio of spatial TMRM standard deviation to the average TMRM fluorescence) per cell is a normalized measure of cellular TMRM distribution and is used to assess  $\Delta\Psi_m$  changes throughout the time-period of Ischemia/Reperfusion (110), (119), (94). This measure minimizes potential artifacts due to dye loading variability and fluorescence decay over the experimental time-course. We obtained the measurements of TMRM fluorescence, Standard Deviation and Dispersion of ~100 cells per experiment. Dispersion decreased over the course of Ischemia indicating loss of  $\Delta\Psi_m$ , consistent with visual observations, and upon Reperfusion, dispersion was restored, indicating  $\Delta\Psi_m$  repolarization. When we compared the  $\Delta\Psi_m$  response in MCU-WT to MCU-KO NMVMs, or to CGP-treated monolayers, we did not find a noticeable difference in the pattern of behavior between the different groups (Figure 3.9A and B). Although MCU-KO showed a higher Dispersion, this we attributed to an increase in the spatial heterogeneity of the mitochondrial network within cells rather than an actual increase in  $\Delta\Psi_m$  in the KO cells. While dispersion may give us a broad representation of  $\Delta\Psi_m$  in all cells and accounts for dye bleaching over time, it does not facilitate identification of the transition states of  $\Delta\Psi_m$  polarization and depolarization in a cell. This prompted us to track each cell's TMRM fluorescence and assess  $\Delta\Psi_m$  changes at the single-cell level during Ischemia and Reperfusion. We adopted a signal processing tool using wavelet transform to automatically detect transition points during Ischemia (114). We found that MCU-KO accelerates the time to  $\Delta\Psi_m$  loss during Ischemia. CGP-37157 delayed the time to Ischemic  $\Delta\Psi_m$  loss in MCU-KO cells but not in MCU-WT cells (Figure 3.9C).

Next, we determined if modulating  $mCa^{2+}$  influx affects  $\Delta\Psi_m$  instability during reperfusion.  $\Delta\Psi_m$  instability during reperfusion is a hallmark of mitochondrial damage that could translate to a higher organ level arrhythmias (17). In addition to our visual observations of  $\Delta\Psi_m$  oscillations, we also developed an unbiased approach to quantitatively analyze and categorize  $\Delta\Psi_m$  oscillatory behavior during reperfusion. Since  $\Delta\Psi_m$  oscillations during reperfusion are non-stationary, a wavelet-transform based approach to characterize frequencies and associated time-periods was employed. Wavelet-transform based analysis to obtain  $\Delta\Psi_m$  oscillator frequencies has been previously used by our group in adult cardiomyocytes by F.Kurz et.al., (16). We adopted this method in a MATLAB-ImageJ based routine called 'MitoWave' (114) to obtain the frequencies during the reperfusion phase. We characterized  $\Delta\Psi_m$  oscillatory behaviors by separating them into frequency bands. High frequency oscillators fall into 45-4.3 mHz (~22 seconds to 230 seconds), moderately fast frequencies range from 4.3-2.2 mHz (~230 seconds to 450 seconds), and low frequency oscillators were any oscillations below the 2.2 mHz frequency band (~ 450 seconds and above). The time at which a mitochondrion undergoes irreversible  $\Delta\Psi_m$  collapse during reperfusion was also included in this characterization. We represent these data in a violin plot where each mitochondrion is classified into these frequency bands during the reperfusion time period. Importantly, knocking out MCU did not prevent high-frequency  $\Delta\Psi_m$  oscillations during reperfusion (Fig. 3.9E and F). Addition of CGP-37157 suppressed  $mCa^{2+}$  uptake during Ischemia as well as reperfusion, but this too did not prevent  $\Delta\Psi_m$  oscillations on reperfusion. There were no significant differences in the patterns of  $\Delta\Psi_m$  oscillatory behavior as well (Fig 3.9 G and H).



Taken together, these results suggest that: 1) knocking out MCU does not affect mitochondrial membrane potential instability during I/R injury. 2) MCU is not the primary mode of  $mCa^{2+}$  influx into mitochondria during Ischemia; instead, it is mediated by reverse-mode mitochondrial  $Na^{+}/Ca^{2+}$  exchange, and 3)  $\Delta\Psi_m$  instability upon reperfusion is independent of  $mCa^{2+}$  influx.



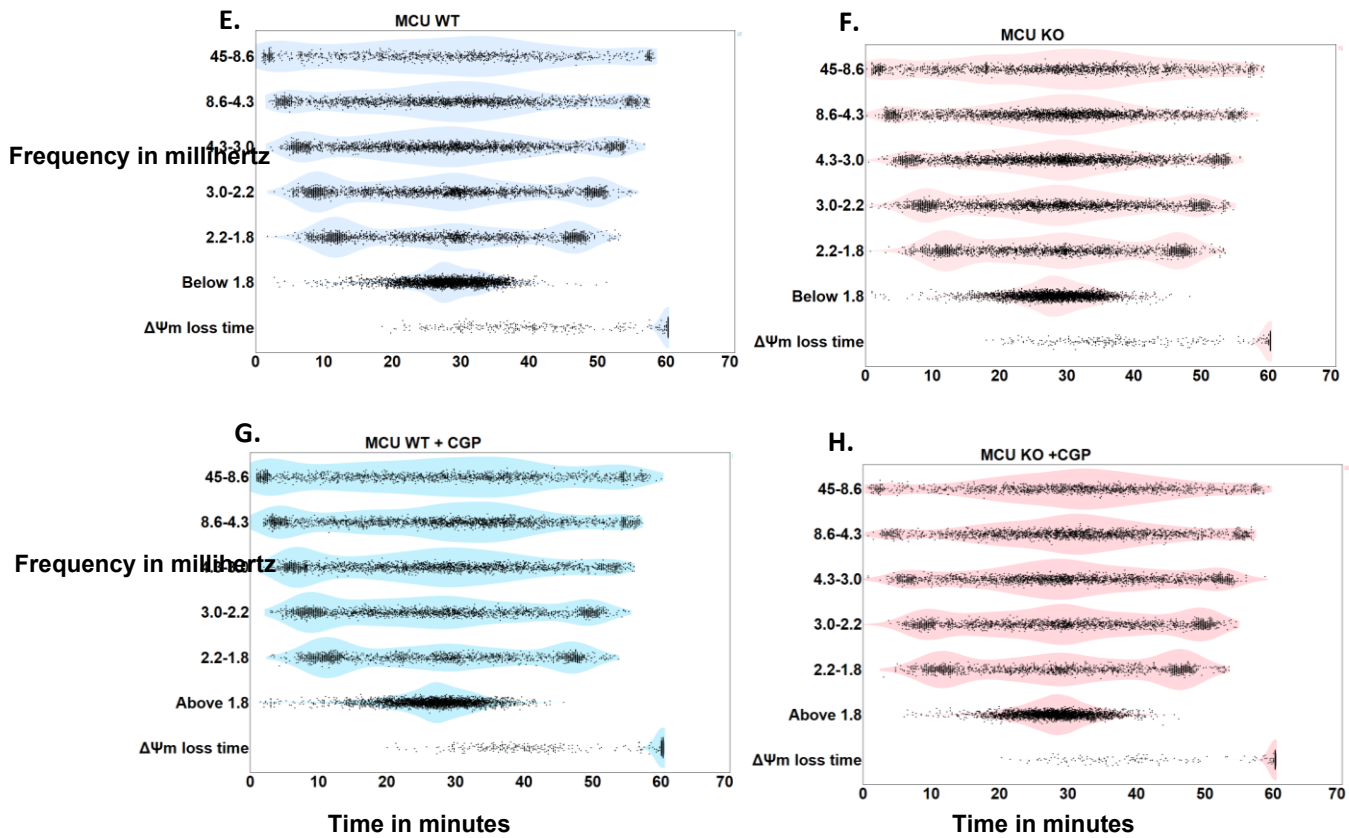


**Figure 3.9: MCU-KO does not protect against  $\Delta\Psi_m$  loss during I/R, nor does CGP**

(A) TMRM dispersion plots show  $\Delta\Psi_m$  changes in MCU-WT and MCU-KO myocytes throughout Ischemia/Reperfusion. (B) Dispersion plot comparing MCU-WT+CGP and MCU-KO+CGP myocytes throughout Ischemia/Reperfusion (C)  $\Delta\Psi_m$  depolarization time during Ischemia in WT, KO and CGP-treated cells. (D) Representative scalograms of oscillating mitochondrial clusters in the 60-minute reperfusion phase showing the presence of peak coefficients in the low scale range of 1-10 (i.e., high-frequency range) corresponding to 4.3-45 mHz. Insets (i), (ii), (iii) and (iv) show scalograms from mitochondrial clusters from WT, KO, WT+ CGP and KO+ CGP treated cells. (E), (F), (G) &(H) are violin plots showing the distribution of oscillating clusters throughout the reperfusion phase between six frequency

bands ranging from the fastest (45-8.6mHz) to the slowest (Below 1.8mHz). The time to irreversible  $\Delta\Psi_m$  depolarization of an oscillating cluster is also indicated as the lowest band. (E) Frequency distribution during reperfusion of oscillating mitochondrial clusters from WT cells (4093 mitochondrial clusters were analyzed from 7 different I/R of monolayers); (F) Frequency distribution from oscillating mitochondrial clusters from MCU-KO cells (3643 clusters from 6 different I/R of monolayers); (G) from MCU-WT cells treated with CGP (3208 clusters from 5 different I/R of monolayers); (H) MCU-KO cells treated with CGP (2977 clusters from 5 different I/R of monolayers were analyzed).

**Blocking mitochondrial electron transport chain component complex I stabilizes  $\Delta\Psi_m$  oscillations during Reperfusion in WT cells.**

Complex-I is the first electron acceptor in the mitochondrial respiratory chain and a potential source of ROS production. During reperfusion after ischemic injury, ROS production from the mitochondrial respiratory chain is a major source of oxidative damage. Previously, we showed that rotenone treatment, as well as other electron transport chain inhibitors (except the Complex III inhibitor antimycin A), stabilized laser-induced  $\Delta\Psi_m$  oscillations in adult guinea pig cardiomyocytes while decreasing ROS (14). Knocking out of *Ndufs4h* of Complex-1 also reduced the number of mitochondrial ‘flashes’ in Langendorff perfused hearts (120). Therefore, we blocked mitochondrial complex I with 1 $\mu$ M rotenone acutely during reperfusion.  $\Delta\Psi_m$  oscillations were inhibited, with stabilization of  $\Delta\Psi_m$ , within the first 10 minutes of reperfusion (Fig. 3.10C and D). At around 20 minutes of reperfusion, mitochondria started to lose  $\Delta\Psi_m$  in the presence of rotenone, presumably because of loss of proton pumping by Complex I and depletion of alternative electron donors to the respiratory chain that may have supported  $\Delta\Psi_m$  (Fig. 3.10A

and D). Figure 4C is a scalogram of a representative mitochondrion during reperfusion. A large spike of scalogram coefficients occurs around the 110<sup>th</sup> time point corresponding to ~25 minutes of reperfusion, when the mitochondrion has undergone complete  $\Delta\Psi_m$  depolarization.  $mCa^{2+}$  import was not affected when rotenone is added to the cells (Fig 3.10 B). We also added cell-permeable dimethyl succinate, a substrate for Complex II, to bypass Complex-I in the presence of rotenone inhibition.  $\Delta\Psi_m$  oscillations still occurred in some mitochondria under these conditions (Fig 3.10 G). We observed a few low coefficient peaks in the scalogram before they undergo complete  $\Delta\Psi_m$  depolarization around 20-30 minutes. This suggests that bypassing Complex I and supplying electrons via Complex II can partially reactivate the oscillatory mechanism, perhaps by restoring ROS emission from complexes of the ETC downstream of Complex I, namely complexes II, III or IV.

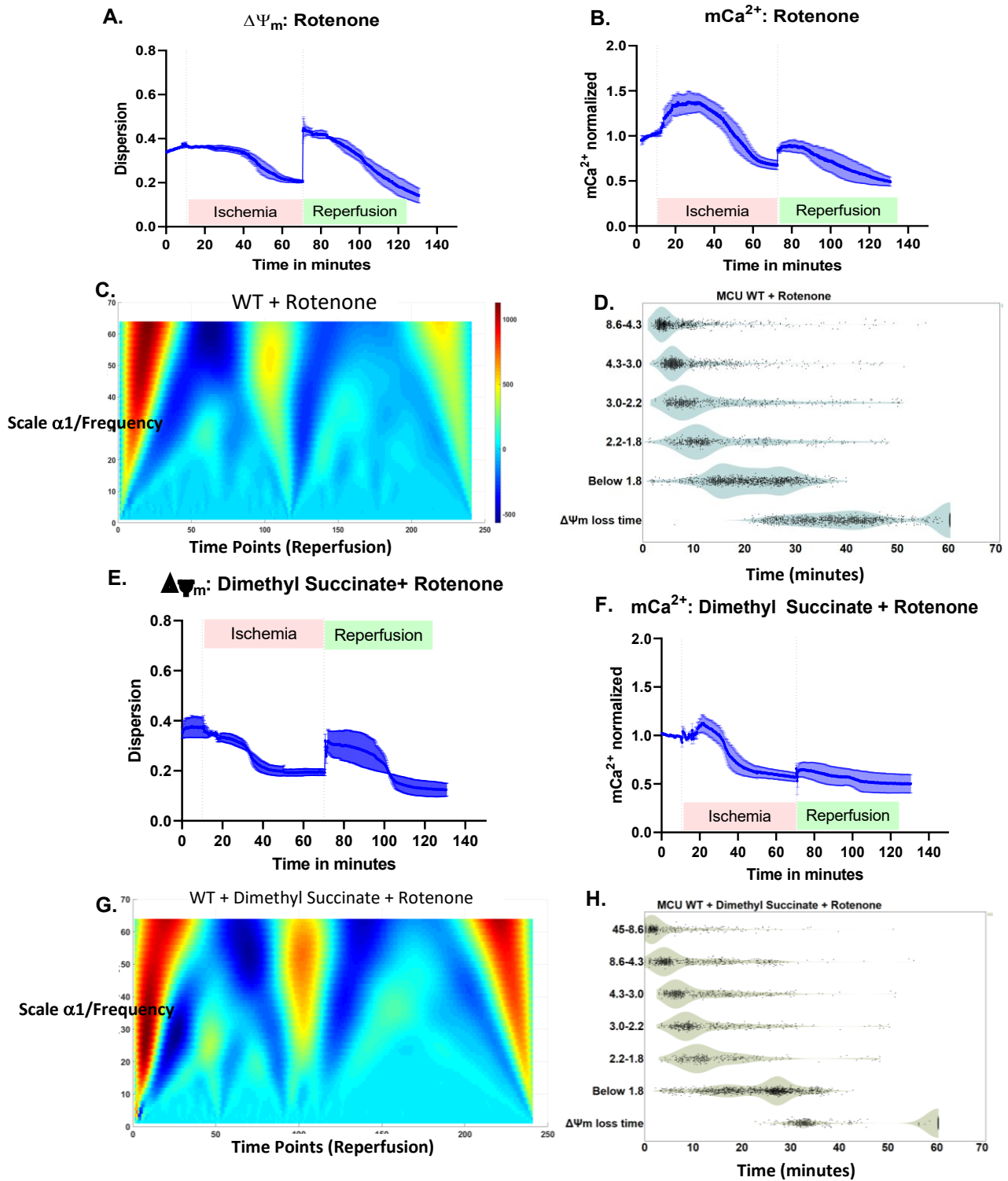


Figure 3.10: Inhibiting mitochondrial electron transport chain component Complex I stabilizes  $\Delta\Psi_m$  oscillations during Reperfusion in MCU-WT cells.

(A)  $\Delta\Psi_m$  was monitored during I/R and 1 $\mu$ M Rotenone was added acutely upon Reperfusion. (B) mCa<sup>2+</sup> uptake is shown and mCa<sup>2+</sup> uptake is reduced during Reperfusion. (C) Scalogram of a representative mitochondrial cluster showing oscillations stopping in 30 minutes of reperfusion. (D) Violin plots representing distribution of frequency of oscillating mitochondrial clusters during reperfusion. The presence of high frequency oscillators (in 4.3-45mHz bands) decreases in 10-15 minutes of reperfusion.  $\Delta\Psi_m$  loss starts to occur around 20-30 minutes of reperfusion. (E)  $\Delta\Psi_m$  response when cells are incubated with 5mM Dimethyl Succinate and subjected to I/R. Rotenone was added acutely upon reperfusion. (F) mCa<sup>2+</sup> uptake is shown and mCa<sup>2+</sup> is reduced during Ischemia and Reperfusion. (G) Scalogram of a representative mitochondrial cluster showing some reduced low amplitude oscillations in the first 15 minutes, followed by  $\Delta\Psi_m$  loss around the 30<sup>th</sup> minute. (H) Violin plots representing distribution of frequency of oscillating mitochondrial clusters during reperfusion.

The I/R with Rotenone experiment was repeated on 3 different coverslips and 1685 clusters were analyzed for their oscillation patterns; I/R with Dimethyl Succinate and Rotenone was done on 3 different experiments and 1319 clusters were analyzed for their oscillation patterns. Mean+SEM are shown on I/R time courses.

### **Supplementing NMVMs with cell-permeable glutathione stabilizes $\Delta\Psi_m$ oscillations during reperfusion**

To test the hypothesis that ROS is the primary trigger for  $\Delta\Psi_m$  oscillations on reperfusion, we examined the effects of the cell-permeable Reduced Glutathione ethyl ester (GSHee) to increase intracellular glutathione reserves. NMVMs were preincubated with 4mM GSHee for 3 hours before replacing the media with normal Tyrode's to perform I/R while monitoring mCa<sup>2+</sup> and

$\Delta\Psi_m$ . We observed the initial rise of  $mCa^{2+}$  during Ischemia as expected and the increase in  $mCa^{2+}$  upon reperfusion as well (Fig 3.11B). The overall  $\Delta\Psi_m$  response throughout the I/R period was not different (Fig 3.11A); however,  $\Delta\Psi_m$  oscillations were stabilized after 20 minutes of reperfusion (Fig 3.11C and D).

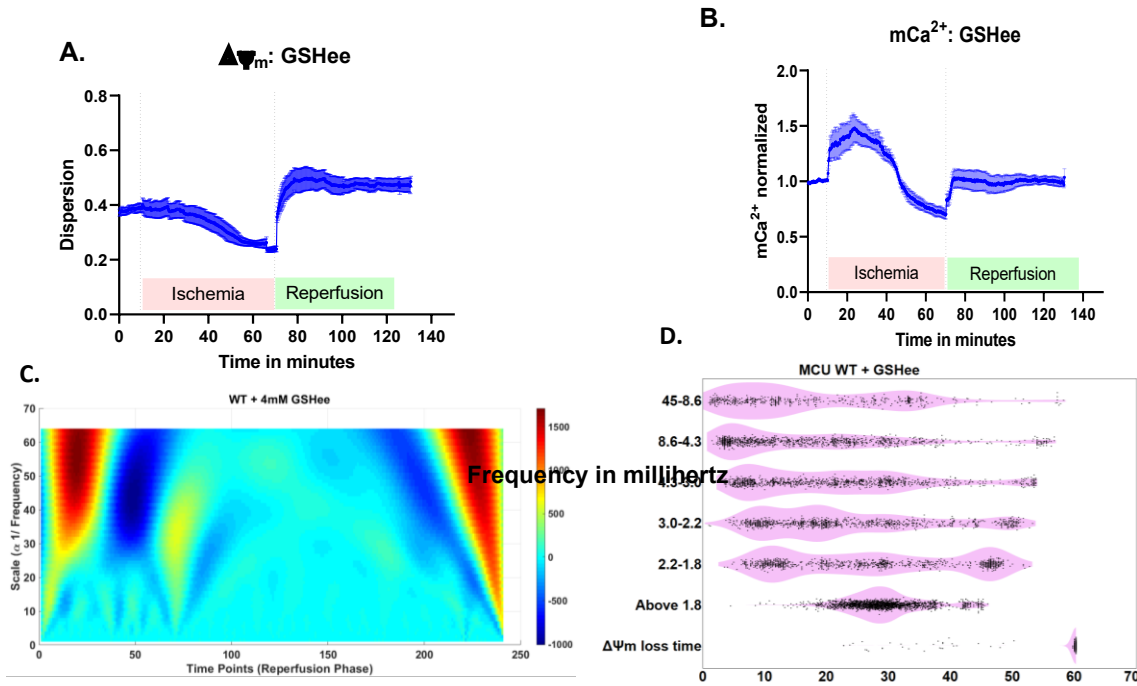


**Figure 3.11: Addition of cell-permeable Glutathione ethyl ester (GSHee) reduces and eventually stops  $\Delta\Psi_m$  oscillations during reperfusion**

(A)  $\Delta\Psi_m$  during I/R. (B) GSHee did not alter  $mCa^{2+}$  during I/R. (C) Scalogram of a representative mitochondrial cluster showing oscillations up to 18 minutes (Time Point ~75) of reperfusion that then stabilized. (D) Violin plots showing all the oscillating mitochondrial clusters. High frequency oscillators (4.3-45 mHz) stabilize around 20 minutes of reperfusion, shown by the decreasing

number of oscillators in those bands. 4 coverslip experiments with 2020 mitochondrial clusters analyzed for oscillatory patterns.

**Addition of Cyclosporine A does not prevent  $\Delta\Psi_m$  oscillations.**

Mitochondrial permeability transition pore (mPTP) opening has been implicated in mitochondrial dysfunction to precipitate cell death during reperfusion. Cyclosporine A is an inhibitor of the mPTP (121), (36). We tested whether Cyclosporine A (CsA) improved  $\Delta\Psi_m$  recovery and  $mCa^{2+}$  changes during I/R and found no salutary effect (Figure 3.12A and B). CsA also did not stop  $\Delta\Psi_m$  oscillations (Figure 3.12C and D).

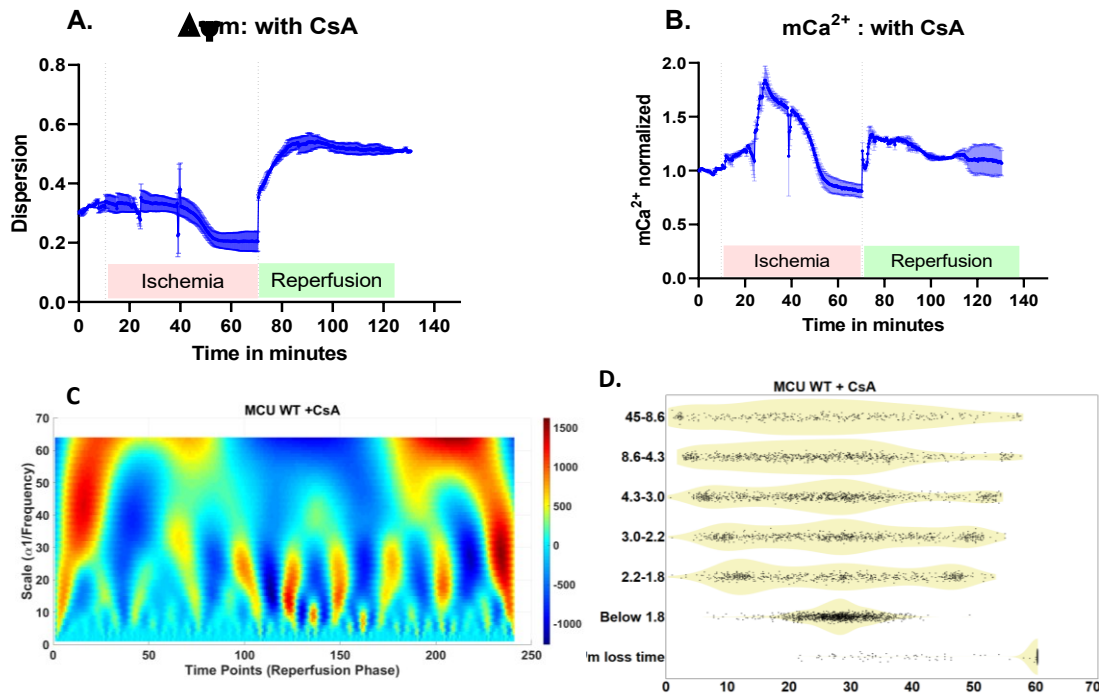


**Figure 3.12: Addition of CsA does not affect  $\Delta\Psi_m$  oscillations.**

0.2 $\mu$ M CsA was added to NMVMs 10 minutes before the start of the I/R protocol. (A)  $\Delta\Psi_m$  during I/R is significantly affected by CsA treatment. (B)  $mCa^{2+}$  with CsA was also not affected. (C) Scalogram of a representative mitochondrial cluster showing oscillations throughout reperfusion phase. (D) Violin plots



showing all oscillating mitochondrial clusters/High frequency oscillators (4.3-45mHz) are present throughout reperfusion phase. (2 coverslip experiments, with 1132 mitochondrial clusters analyzed for oscillation patterns).

### **Behavior of high-frequency oscillators under different conditions**

We show in figures 3.9 E, F, G, H, 3.10 D, H, 3.11 D and 3.12D the overall behavior of  $\Delta\Psi_m$  oscillations during reperfusion. We separated mitochondrial oscillators into different frequency bands and observed that a mitochondrion can switch its frequency during the course of reperfusion. We observed that the high frequency oscillators are strongly influenced by either blocking electron transport chain with rotenone or by replenishing the glutathione pool with a cell-permeable glutathione ethyl ester. We further statistically analyzed the effect of different conditions on high-frequency oscillators (in the 8.6-45mHz frequency band) to see how they vary throughout reperfusion time. Empirical Cumulative Distribution functions, reflecting the cumulative probability of  $\Delta\Psi_m$  stabilization during reperfusion, were plotted against the reperfusion time (Fig 3.13). We performed a non-parametric Kolmogorov-Smirnov test, where the null hypothesis is that the distribution of mitochondrial oscillators under different treatments does not change over the course of reperfusion. We saw that while knocking out MCU or addition of CGP (essentially suppressing  $mCa^{2+}$  influx), did not affect these high frequency oscillators (p not significant, with  $\alpha=0.001$ ), while modulating ROS or the antioxidant capacity of the cells significantly influenced the high-frequency oscillators ( $p<0.000001$ ). Over the course of reperfusion, we observed  $\Delta\Psi_m$  stabilization under conditions where ROS is scavenged by GSHee.

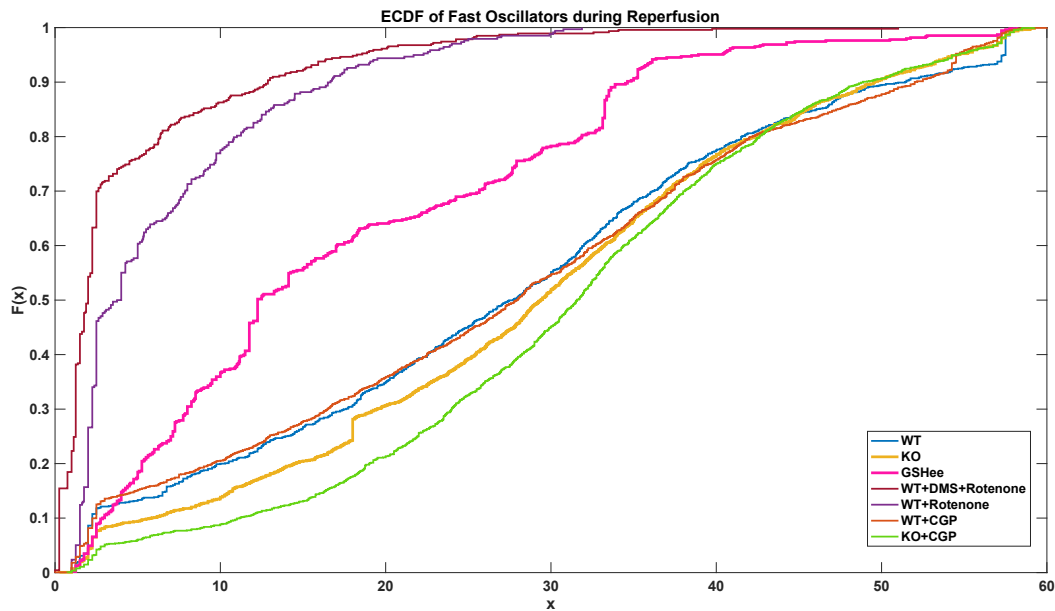


**Figure 3.13: Empirical Cumulative Distribution Functions comparing different treatments on high-frequency  $\Delta\Psi_m$  oscillators during reperfusion.**

The X axis represented by (x) is the time in minutes during reperfusion and Y axis represents the probability of stabilization during reperfusion.

We further analyzed Lactate Dehydrogenase (LDH) levels as a marker for cytotoxicity in supernatants after reperfusion injury. LDH levels were not significantly different between MCU WT and KO cells. CGP or GSHee addition did not affect cytotoxicity levels. Addition of rotenone, although it stabilized early  $\Delta\Psi_m$  oscillations, significantly increased LDH levels, as expected since inhibition of the ETC inhibits oxidative phosphorylation and ATP production, and exacerbates irreversible  $\Delta\Psi_m$  loss on reperfusion.

Taken together, these results show that  $\Delta\Psi_m$  oscillations that occur during reperfusion after Ischemia are triggered by ROS and not by  $mCa^{2+}$ .

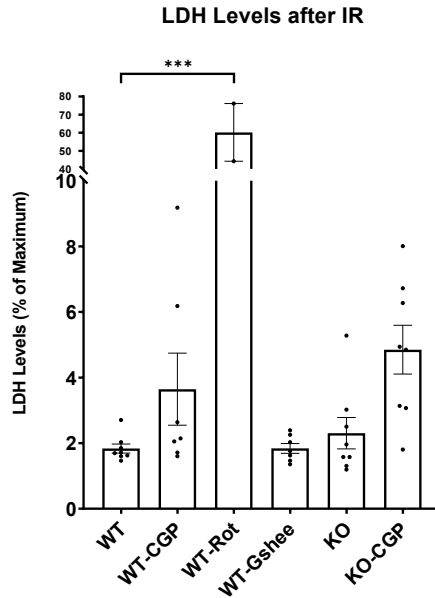


**Figure 3.14: LDH Assay as a measure of cytotoxicity at the end of Reperfusion after Ischemia.**

Supernatants were collected after reperfusion to measure Lactate Dehydrogenase levels. Positive control was supernatant from lysed NMVMs and was considered as 100% of LDH levels released (maximum). All other samples were scaled from this positive control. One-way ANOVA comparing WT with rotenone showed significantly high levels of LDH in rotenone treated cells. WT comparisons with other samples were not significantly different.

## Discussion

In the present work, we acutely knocked out the mitochondrial calcium uniporter in neonatal mouse cardiac myocytes and monitored mitochondrial  $\text{Ca}^{2+}$  and  $\Delta\Psi_m$  during in vitro Ischemia/Reperfusion injury. The main findings were that: 1) the primary trigger for  $\Delta\Psi_m$  instability during reperfusion is reactive oxygen species rather than  $\text{Ca}^{2+}$ , and 2) under ischemic conditions, MCU is not the primary mode of  $\text{Ca}^{2+}$  import into mitochondria. Instead, reverse mode mitochondrial  $\text{Na}^+/\text{Ca}^{2+}$  exchange mediates  $\text{Ca}^{2+}$  uptake. These findings challenge current paradigms of I/R injury, which may lead to new therapeutic approaches in the future.

### Role of MCU & mNCE during Ischemia/Reperfusion

Excess accumulation of  $\text{Ca}^{2+}$  is thought to trigger mitochondrial permeability transition pore opening leading to cell death (122) (123) (124). Several studies have shown that during ischemia,  $\text{Ca}^{2+}$  in mitochondria increases (104). It has been generally assumed that  $\text{Ca}^{2+}$  overload of mitochondria, in this case, occurs through the mitochondrial calcium uniporter (50), (52), (53). In line with this thinking, it was shown that inhibiting the MCU either chemically, with Ru360, or genetically knocking out the cardiac-specific MCU had protective effects in IR injury (125), (58), (59). However global MCU-KO, or even cardiac-specific expression of a dominant negative MCU, did not show any protection in myocardial injury compared to WT mice (55), (60). Our approach was to acutely knockout (in ~5 days of cell culture) MCU to prevent any long-term adaptations in the hope of explaining this inconsistency. We found reduced  $\text{mCa}^{2+}$  transients in beating cells, consistent with findings from other laboratories showing suppression of  $\text{mCa}^{2+}$  transients in NRVMs with MCU knocked-down (57).

We found no differences in basal mCa<sup>2+</sup> levels in our acute MCU-KO model. Similarly, Kwong et. al., also found no differences in matrix [Ca<sup>2+</sup>] in isolated cardiac mitochondria, as well as in permeabilized cardiomyocytes(58) in an adult cardiac-specific MCU-KO model. In contrast, Holmstorm et. al., found a 75% decrease in matrix Ca<sup>2+</sup> levels in isolated mitochondria from global MCU KO cardiomyocytes. These data demonstrate that knocking out MCU does not necessarily eliminate Ca<sup>2+</sup> influx into the mitochondria, indicating that there are other pathways that might contribute to mCa<sup>2+</sup> influx.

Indeed, Fieni et al., showed that the amount of Ca<sup>2+</sup> uptake mediated by the MCU varies between tissues and MCU current density was the smallest in the heart mitochondria (74). Hamilton et al., showed that in brain-mitochondria, deletion of the MCU only partially inhibits calcium uptake and initiation of the permeability transition (Hamilton et al., 2018). The ratio of MCU to its dominant negative form, MCUB, varies among different tissues. For example, in the heart it is 3:1 (MCU:MCUB) and in skeletal muscle it is 40:1 (Raffaello et al., 2013), thus resulting in differential regulation of Ca<sup>2+</sup> into mitochondria. In addition, other modes of Ca<sup>2+</sup> entry into the mitochondria have proposed; such as through the mitochondrial ryanodine receptor (Beutner et al., 2005), (Jakob et al., 2014) and the LETM1- Ca<sup>2+</sup> /H<sup>+</sup> exchanger (Jiang et al., 2013), (Tsai et al., 2014). Moreover, under ischemic conditions, reversal of the mitochondrial Na<sup>+</sup>/Ca<sup>2+</sup>/Li<sup>+</sup> exchanger might allow Ca<sup>2+</sup> entry into the mitochondria (Griffiths, 1999). Further, Nicholls et. al showed that above 10nmol Ca<sup>2+</sup>/mg of mitochondrial protein, Ca<sup>2+</sup> is buffered in the matrix from 1-5μM and stays stable (126) despite additional uptake. Therefore, such multiple factors could take precedence in influencing mCa<sup>2+</sup> uptake, especially when MCU is impaired.

Surprisingly, our in vitro Ischemia/ Reperfusion myocyte monolayer method showed no difference in  $\text{Ca}^{2+}$  uptake between MCU-KO and WT during ischemia, as well as during reperfusion.  $\text{Ca}^{2+}$  influx via MCU requires maintenance of  $\Delta\Psi_m$  (50), (127), which, in our experiments was lost after 30 minutes of ischemia; however, the maximum  $\text{Ca}^{2+}$  increase during ischemia occurred before loss of  $\Delta\Psi_m$  and this peak was also unaffected by MCU knockout. This suggests that other factors may be inhibiting MCU during ischemia, for example, Moreau and Parekh showed that acidification of the mitochondrial matrix inhibits the MCU (128). In addition, our group previously showed that under conditions of elevated cytosolic  $\text{Na}^+$ ,  $\text{Ca}^{2+}$  influx into mitochondria was reduced (129). Under Ischemic conditions, there is  $\Delta\Psi_m$  reduction, a decrease in pH because of ATP breakdown during increased metabolic demand, and elevated cytosolic  $\text{Na}^+$  (9). Therefore, ischemic conditions could favor suppression of MCU activity.

When we added CGP-37157, an inhibitor of the mitochondrial  $\text{Na}^+/\text{Li}^+/\text{Ca}^{2+}$  exchanger (130), we found that the rise of  $\text{mCa}^{2+}$  during ischemia was almost completely eliminated and during reperfusion,  $\text{mCa}^{2+}$  was also suppressed. CGP-37157 is a benzothiazepine with a structure somewhat similar to  $\text{Ca}^{2+}$  channel blockers and there are some reports in the literature that it might also inhibit SR  $\text{Ca}^{2+}$  uptake, ryanodine receptors (131), or L-type  $\text{Ca}^{2+}$  channels (132). None of these potential off-target effects could explain our results, since there was no significant effect of CGP on the cytosolic  $\text{Ca}^{2+}$  response to I/R. Previously, Griffiths et al., showed that addition of clonazepam, a similar derivative of benzothiazepine that inhibits mNCE, blunted  $\text{mCa}^{2+}$  influx during hypoxic conditions, suggesting that mNCE could work in reverse during metabolic inhibition (47). They also reported that that mitochondria in adult cardiomyocytes treated with Ruthenium Red (RuR) still took up  $\text{Ca}^{2+}$  under hypoxia. The explanation for this behavior was

attributed to the loss of  $\Delta\Psi_m$  during Ischemia, causing the electrochemical driving forces to favor mNCE reversal.

The design of our experiments afforded us the rare opportunity to measure mCa<sup>2+</sup> ratiometrically, and  $\Delta\Psi_m$  simultaneously, during I/R, which is not easily accomplished in other model systems. We saw that in MCU-WT and in MCU-KO monolayers, Ca<sup>2+</sup> entered mitochondria during the time  $\Delta\Psi_m$  was still maintained and when  $\Delta\Psi_m$  was lost, mitochondrial Ca<sup>2+</sup> levels rapidly decreased to a level below the normoxic baseline. With CGP treatment, although mCa<sup>2+</sup> accumulation was largely suppressed, we did not see any remarkable change in the time at which  $\Delta\Psi_m$  loss occurred during ischemia in WT and KO cells; it still occurred at 30-40 minutes of ischemia. Hence, changes in  $\Delta\Psi_m$  could not account for the CGP effect on mitochondrial Ca<sup>2+</sup>.

This brings us to the question, if mNCE reverses due to changes in electrochemical driving force during Ischemia, then why do we see a suppression of mCa<sup>2+</sup> accumulation *before*  $\Delta\Psi_m$  loss? If mNCE is indeed electrogenic, shouldn't we see a suppression only when  $\Delta\Psi_m$  depolarizes? If it's not electrogenic, then it could work in reverse if the ion concentrations changed during pathological conditions. The electrogenic nature of NCLX is still debated. Some of the earliest studies favored an electrogenic nature for the exchanger when they found that Ca<sup>2+</sup> efflux from the mitochondria was dependent on [Na<sup>+</sup>] and energy produced from respiration (133)(134). However, some studies favored electroneutral exchange, based on the observation that perturbing  $\Delta\Psi_m$  with an uncoupler did not change steady state Ca<sup>2+</sup> efflux from the mitochondria (135) and that the Na<sup>+</sup> mediated Ca<sup>2+</sup> efflux process did not perturb  $\Delta\Psi_m$  (136). Later studies supported the electrogenic nature of mNCE (137), (138), (139). Nevertheless, under conditions of Ischemia, changes in  $\Delta\Psi_m$ , [Na<sup>+</sup>], and [Ca<sup>2+</sup>] could all influence mNCE behavior. Lower Na<sup>+</sup> and

higher free  $\text{Ca}^{2+}$  in the mitochondrial matrix versus the cytoplasm, together with  $\Delta\Psi_m$ , provide the electrochemical driving force to drive  $\text{Ca}^{2+}$  efflux out of the mitochondria under normal conditions, but under ischemic conditions, it is possible that an electroneutral mode of mNCE takes precedence, leaving only the chemical gradients to determine the direction of ion exchange. The  $K_m$  for  $\text{Na}^+$  of NCLX has been reported to be  $\sim 7\text{-}10\text{mM}$  (140), (141), (142), and changes in cytosolic  $\text{Na}^+$  will affect efflux rates of  $\text{Ca}^{2+}$  via mNCE. During Ischemia, cytosolic  $[\text{Na}^+]$  can reach  $\sim 40\text{mM}$  within a few minutes (9), but, unfortunately, we currently have no information about matrix  $[\text{Na}^+]$ , which will be affected by the pH gradient through an inner membrane  $\text{Na}^+/\text{H}^+$  exchanger, by mNCE activity, and possibly also by  $\text{Na}^+$  leak across the membrane. Similarly, we do not precisely know what the concentration gradient of  $\text{Ca}^{2+}$  is across the inner membrane. It will be important in the future to get more quantitative information on these gradients to determine how the equilibrium potential for mNCE changes during ischemia.

*Based on our findings, it appears that reverse mode mNCE, not MCU, is the primary mode of  $\text{Ca}^{2+}$  entry during ischemia and early reperfusion, while beat-to-beat mitochondrial  $\text{Ca}^{2+}$  entry does require MCU.*

### **$\text{Ca}^{2+}$ vs ROS in triggering $\Delta\Psi_m$ instability during reperfusion**

$\Delta\Psi_m$  instability upon reperfusion can translate to higher organ level fatal arrhythmias (17). The primary trigger for  $\Delta\Psi_m$  instability has been debated, with some groups in support of  $\text{Ca}^{2+}$ -induced mPTP as the primary mediator of  $\Delta\Psi_m$  instability or oscillation (32) (143) (144) (124), while others favor a mechanism involving RIRR, independent of  $\text{Ca}^{2+}$  (14) (27) (4) (15). Our data in NMVMs support ROS-mediated,  $\text{Ca}^{2+}$ -independent,  $\Delta\Psi_m$  instability.  $\Delta\Psi_m$  instability/oscillation



characteristics, in terms of frequency or the time to  $\Delta\Psi_m$  stabilization, did not differ between MCU-KO and WT, ruling out MCU as the key mediator of oscillation. Furthermore, suppressing the influx of  $mCa^{2+}$  with CGP-37157 during ischemia and reperfusion did not alter  $\Delta\Psi_m$  instability, providing evidence that the process was  $Ca^{2+}$  independent. Indeed, the most effective and reproducible stabilizer of  $\Delta\Psi_m$  was inhibition of the electron transport chain at Complex I. A similar effect was observed when NDUFS4, a subunit of Complex I was knocked out in mice, i.e., the number of 'mito-flashes' was reduced (120). This is somewhat paradoxical, since, in highly reduced isolated mitochondria, inhibition of Complex I can increase ROS emission from this site. However, this finding was in agreement with our earlier studies of  $\Delta\Psi_m$  oscillations in adult cardiomyocytes, where inhibition of Complex I, Complex IV (with CN<sup>-</sup>), Complex III (at the Qo site with myxothiazol), or ANT (bongkreikic acid) were all capable of inhibiting oxidative stress and stabilizing whole cell  $\Delta\Psi_m$  oscillations (14). The exception was inhibition of Complex III with Antimycin A, which inhibits the Qi site and causes a large increase in superoxide production from Complex III. The interpretation of these data is that ETC inhibition either upstream or downstream of Complex III prevents RIRR by stopping the source of electron flow to superoxide, and, in turn,  $H_2O_2$ . The primacy of ROS in the process is also supported by the effects of supplementation of the cardiomyocytes with a cell-permeable version of reduced glutathione (glutathione ethyl ester; GSHEE), which stabilized  $\Delta\Psi_m$  within 20 minutes of reperfusion. Notably,  $\Delta\Psi_m$  oscillatory behavior in adult myocytes is also exquisitely sensitive to the cytoplasmic and mitochondrial GSH:GSSG ratio (28).

## Conclusions

We report that during Ischemia and Reperfusion, reverse-mode mitochondrial  $\text{Na}^+/\text{Ca}^{2+}$  exchange, not the MCU, is the primary mode of  $\text{Ca}^{2+}$  import into the mitochondria in Mouse Neonatal Cardiac Myocytes. We also report that  $\Delta\Psi_m$  oscillations persist despite blocking  $\text{mCa}^{2+}$  influx with CGP, showing that  $\Delta\Psi_m$  oscillations are not triggered by  $\text{mCa}^{2+}$  influx. We also show that blocking complex-I with rotenone suppresses  $\Delta\Psi_m$  oscillations, consistent with an RIRR mechanism. Replenishing the glutathione pool with a cell-permeable reduced glutathione ethyl ester to boost the anti-oxidant capacity of the system also stabilizes  $\Delta\Psi_m$  during reperfusion, reinforcing the conclusion that RIRR is the primary trigger for  $\Delta\Psi_m$  instability during reperfusion rather than  $\text{mCa}^{2+}$  influx.

## CHAPTER 4: Future Directions

### Does activating Hypoxia Inducible Factor prior to I/R prevent mitochondrial instability?

#### Motivation

Based on our results so far implicating ROS in mitochondrial  $\Delta\Psi_m$  instability, we wondered if activating the Hypoxia Inducible Factor (HIF) would protect mitochondria against instability during I/R injury. HIFs are transcription regulators whose stabilization depends on  $[O_2]$ . They can bind to hypoxia responsive elements and promote transcription of multiple genes involved in increasing oxygen supply to the affected tissue (145) (146). Since their discovery (147), (148), HIFs have been observed to promote efficient use of available  $O_2$  supply via angiogenesis and erythropoietin production to protect tissues from ischemic damage (149), (150).

To test our hypothesis that stabilizing HIF could prevent mitochondrial instability upon reperfusion, we used a cell-permeable compound, Dimethylxalylglycine (DMOG), a competitive inhibitor of prolyl hydroxylase (PH). PH degrades HIF1 $\alpha$  under normoxic conditions. Under hypoxic conditions, PH is inhibited and HIF1 $\alpha$  is not targeted for degradation. (151), (152).

#### Results and Discussion:

We added 1mM DMOG to NMVMs for 8-12 hours overnight before performing I/R injury to cells. We observed that  $\Delta\Psi_m$  oscillations stopped around 15-20 minutes of reperfusion and the cells regained their beating (Fig 5D and F). In fact, with DMOG, mitochondria exhibited low amplitude high-frequency  $\Delta\Psi_m$  oscillations during Ischemia, which is a indicative of physiological oscillatory

behavior of mitochondria (153), (27). This leads us to speculate that promoting the expression of hypoxia responsive factors with DMOG equips myocytes to resist stress (i.e, ischemia) and therefore, during reperfusion, they are able to cope with increased oxidative stress. Alternatively, HIF1 $\alpha$  activation promotes a shift towards glycolytic metabolism as opposed to oxidative metabolism(145). This could prime cells to function under limited O<sub>2</sub> availability and recover quickly under favorable conditions. Performing these experiments on HIF1 $\alpha$  or HIF2 $\alpha$  knockout myocytes as well as on prolyl hydroxylase knockout myocytes would uncover protective mechanisms that HIFs implement under times of hypoxic stress.

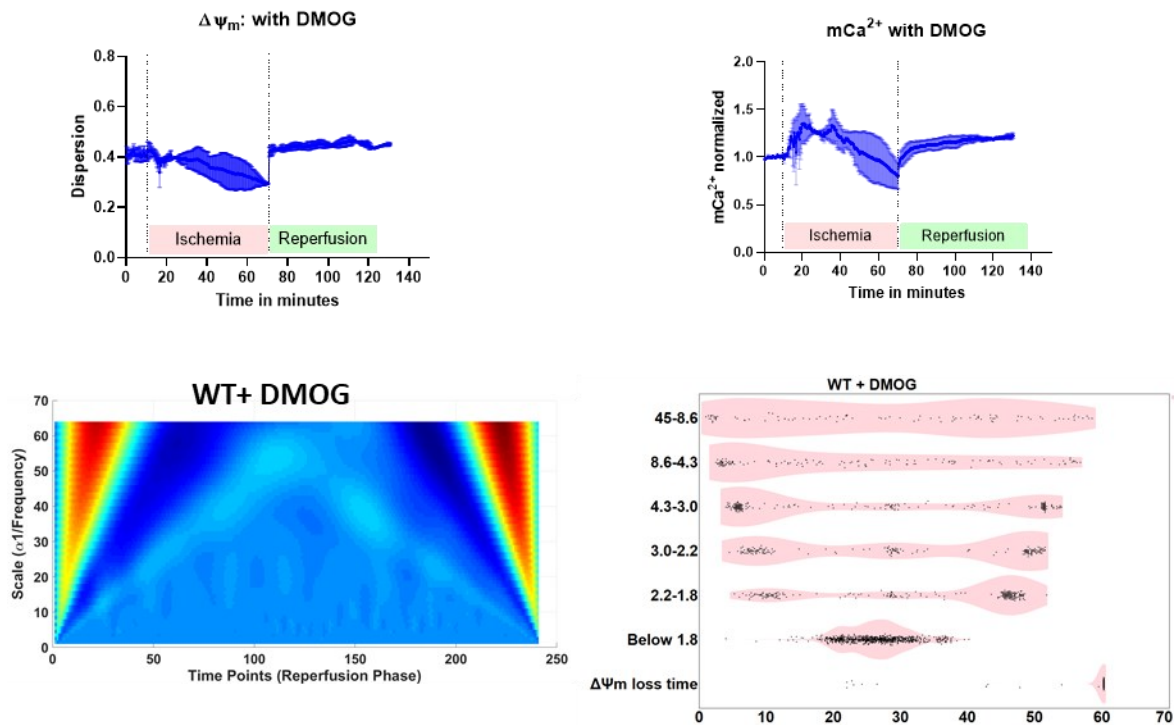


**Figure 4: Addition of DMOG stabilizes  $\Delta\Psi_m$  oscillations.**

A.  $\Delta\Psi_m$  during I/R is not affected. B. mCa<sup>2+</sup> with DMOG is not affected. C. Scalogram of a representative mitochondrial cluster showing absence of oscillations throughout reperfusion phase. D. Violin plots showing all oscillating mitochondrial clusters/ High frequency oscillators (4.3-45mHz) stabilize during reperfusion, but some myocytes resume beating. Therefore, the high-frequency oscillators do not taper off as they do with GSHee. (2 coverslip experiments, with 831 mitochondrial clusters analyzed for oscillation patterns).

## **Does knocking out mitochondrial Na<sup>+</sup>/Li<sup>+</sup>/Ca<sup>2+</sup> exchanger affect mCa<sup>2+</sup> import during Ischemia/Reperfusion?**

Motivation:

Given our observation of mCa<sup>2+</sup> suppression during I/R with CGP-37157 (Fig. 3.7), it would be of immediate interest to evaluate if a genetic knockout of SLC8B1, also known as NCLX, the presumed molecular component of mNCE, affects mCa<sup>2+</sup> import during I/R. CGP-37157 has been shown to inhibit NCLX(130) and, in addition to our findings, reverse mode mNCE has been proposed to mediate mitochondrial Ca<sup>2+</sup> entry during hypoxia/ reoxygenation in adult cardiomyocytes, based on pharmacological sensitivity to clonazepam, a benzothiazepine with a structure similar to CGP (47). Genetic knockout of NCLX may provide additional supporting evidence for the molecular mechanisms involved in mCa<sup>2+</sup> influx during Ischemia and Reperfusion.

## References

1. Nowbar Alexandra N., Gitto Mauro, Howard James P., Francis Darrel P., and Al-Lamee Rasha. 2019. Mortality From Ischemic Heart Disease. *Circulation: Cardiovascular Quality and Outcomes*. 12:e005375.
2. Kalogeris, T., C.P. Baines, M. Krenz, and R.J. Korthuis. 2012. Cell Biology of Ischemia/Reperfusion Injury. *Int Rev Cell Mol Biol*. 298:229–317.
3. Iwai, T., K. Tanonaka, R. Inoue, S. Kasahara, N. Kamo, and S. Takeo. 2002. Mitochondrial Damage During Ischemia Determines Post-Ischemic Contractile Dysfunction in Perfused Rat Heart. *Journal of Molecular and Cellular Cardiology*. 34:725–738.
4. Kim, J.-S., Y. Jin, and J.J. Lemasters. 2006. Reactive oxygen species, but not Ca<sup>2+</sup> overloading, trigger pH- and mitochondrial permeability transition-dependent death of adult rat myocytes after ischemia-reperfusion. *American Journal of Physiology-Heart and Circulatory Physiology*. 290:H2024–H2034.
5. Seidlmayer, L.K., V.V. Juettner, S. Kettlewell, E.V. Pavlov, L.A. Blatter, and E.N. Dedkova. 2015. Distinct mPTP activation mechanisms in ischaemia–reperfusion: contributions of Ca<sup>2+</sup>, ROS, pH, and inorganic polyphosphate. *Cardiovasc Res*. 106:237–248.
6. Handy, D.E., and J. Loscalzo. 2017. Responses to Reductive Stress in the Cardiovascular System. *Free Radic Biol Med*. 109:114–124.
7. Griffiths, E.J. 2012. Mitochondria and Heart Disease. In: Scatena R, P Bottoni, B Giardina, editors. *Advances in Mitochondrial Medicine*. Dordrecht: Springer Netherlands. pp. 249–267.
8. Piper, H.M., K. Meuter, and C. Schäfer. 2003. Cellular mechanisms of ischemia-reperfusion injury. *The Annals of Thoracic Surgery*. 75:S644–S648.
9. Murphy, E., and C. Steenbergen. 2008. Ion Transport and Energetics During Cell Death and Protection. *Physiology (Bethesda)*. 23:115–123.
10. Azzi, A., and G.F. Azzone. 1965. Swelling and shrinkage phenomena in liver mitochondria II. Low amplitude swelling-shrinkage cycles. *Biochimica et Biophysica Acta (BBA) - Enzymology and Biological Oxidation*. 105:265–278.
11. Mustafa, M.G., K. Utsumi, and L. Packer. 1966. Damped oscillatory control of mitochondrial respiration and volume. *Biochemical and Biophysical Research Communications*. 24:381–385.
12. Packer, L., R. Utsumi, and M.G. Mustafa. 1966. Oscillatory states of mitochondria. 1. Electron and energy transfer pathways. *Arch. Biochem. Biophys*. 117:381–393.

13. Chance, B., and T. Yoshioka. 1966. Sustained oscillations of ionic constituents of mitochondria. *Arch. Biochem. Biophys.* 117:451–465.
14. Aon, M.A., S. Cortassa, E. Marbán, and B. O'Rourke. 2003. Synchronized Whole Cell Oscillations in Mitochondrial Metabolism Triggered by a Local Release of Reactive Oxygen Species in Cardiac Myocytes. *J. Biol. Chem.* 278:44735–44744.
15. Aon, M.A., S. Cortassa, and B. O'Rourke. 2008. Mitochondrial Oscillations in Physiology and Pathophysiology. *Adv Exp Med Biol.* 641:98–117.
16. Kurz, F.T., M.A. Aon, B. O'Rourke, and A.A. Arrounadas. 2010. Spatio-temporal oscillations of individual mitochondria in cardiac myocytes reveal modulation of synchronized mitochondrial clusters. *PNAS.* 107:14315–14320.
17. Akar, F.G., M.A. Aon, G.F. Tomaselli, and B. O'Rourke. 2005. The mitochondrial origin of postischemic arrhythmias. *J Clin Invest.* 115:3527–3535.
18. Aon, M.A., S. Cortassa, F.G. Akar, D.A. Brown, L. Zhou, and B. O'Rourke. 2009. FROM MITOCHONDRIAL DYNAMICS TO ARRHYTHMIAS. *Int J Biochem Cell Biol.* 41:1940–1948.
19. Nicholls, D.G. 2013. Bioenergetics. Academic Press.
20. Guo, R., S. Zong, M. Wu, J. Gu, and M. Yang. 2017. Architecture of Human Mitochondrial Respiratory Megacomplex I2III2IV2. *Cell.* 170:1247-1257.e12.
21. Iwata, S., J.W. Lee, K. Okada, J.K. Lee, M. Iwata, B. Rasmussen, T.A. Link, S. Ramaswamy, and B.K. Jap. 1998. Complete structure of the 11-subunit bovine mitochondrial cytochrome bc1 complex. *Science.* 281:64–71.
22. Tsukihara, T., H. Aoyama, E. Yamashita, T. Tomizaki, H. Yamaguchi, K. Shinzawa-Itoh, R. Nakashima, R. Yaono, and S. Yoshikawa. 1996. The Whole Structure of the 13-Subunit Oxidized Cytochrome c Oxidase at 2.8 Å. *Science.* 272:1136–1144.
23. Pebay-Peyroula, E., C. Dahout-Gonzalez, R. Kahn, V. Trézéguet, G.J.-M. Lauquin, and G. Brandolin. 2003. Structure of mitochondrial ADP/ATP carrier in complex with carboxyatractyloside. *Nature.* 426:39–44.
24. O'Rourke, B., B.M. Ramza, and E. Marban. 1994. Oscillations of membrane current and excitability driven by metabolic oscillations in heart cells. *Science.* 265:962–966.
25. Romashko, D.N., E. Marban, and B. O'Rourke. 1998. Subcellular metabolic transients and mitochondrial redox waves in heart cells. *PNAS.* 95:1618–1623.
26. Sasaki, N., T. Sato, E. Marbán, and B. O'Rourke. 2001. ATP consumption by uncoupled mitochondria activates sarcolemmal KATP channels in cardiac myocytes. *American Journal of Physiology-Heart and Circulatory Physiology.* 280:H1882–H1888.



27. Cortassa, S., M.A. Aon, R.L. Winslow, and B. O'Rourke. 2004. A Mitochondrial Oscillator Dependent on Reactive Oxygen Species. *Biophysical Journal*. 87:2060–2073.
28. Aon, M.A., S. Cortassa, C. Maack, and B. O'Rourke. 2007. Sequential Opening of Mitochondrial Ion Channels as a Function of Glutathione Redox Thiol Status. *J. Biol. Chem.* 282:21889–21900.
29. Brookes, P.S., Y. Yoon, J.L. Robotham, M.W. Anders, and S.-S. Sheu. 2004. Calcium, ATP, and ROS: a mitochondrial love-hate triangle. *American Journal of Physiology-Cell Physiology*. 287:C817–C833.
30. Zorov, D.B., C.R. Filburn, L.O. Klotz, J.L. Zweier, and S.J. Sollott. 2000. Reactive oxygen species (ROS)-induced ROS release: a new phenomenon accompanying induction of the mitochondrial permeability transition in cardiac myocytes. *J. Exp. Med.* 192:1001–1014.
31. Aon, M.A., S. Cortassa, and B. O'Rourke. 2004. Percolation and criticality in a mitochondrial network. *Proc Natl Acad Sci U S A*. 101:4447–4452.
32. Wang, W., H. Fang, L. Groom, A. Cheng, W. Zhang, J. Liu, X. Wang, K. Li, P. Han, M. Zheng, J. Yin, W. Wang, M.P. Mattson, J.P.Y. Kao, E.G. Lakatta, S.-S. Sheu, K. Ouyang, J. Chen, R.T. Dirksen, and H. Cheng. 2008. Superoxide Flashes in Single Mitochondria. *Cell*. 134:279–290.
33. Schwarzländer, M., S. Wagner, Y.G. Ermakova, V.V. Belousov, R. Radi, J.S. Beckman, G.R. Buettner, N. Demarex, M.R. Duchon, H.J. Forman, M.D. Fricker, D. Gems, A.P. Halestrap, B. Halliwell, U. Jakob, I.G. Johnston, N.S. Jones, D.C. Logan, B. Morgan, F.L. Müller, D.G. Nicholls, S.J. Remington, P.T. Schumacker, C.C. Winterbourn, L.J. Sweetlove, A.J. Meyer, T.P. Dick, and M.P. Murphy. 2014. The 'mitoflash' probe cpYFP does not respond to superoxide. *Nature*. 514:E12–E14.
34. Halestrap, A.P. 2009. What is the mitochondrial permeability transition pore? *Journal of Molecular and Cellular Cardiology*. 46:821–831.
35. Rasola, A., and P. Bernardi. 2011. Mitochondrial permeability transition in Ca<sup>2+</sup>-dependent apoptosis and necrosis. *Cell Calcium*. 50:222–233.
36. Ong, S.-B., P. Samangouei, S.B. Kalkhoran, and D.J. Hausenloy. 2015. The mitochondrial permeability transition pore and its role in myocardial ischemia reperfusion injury. *Journal of Molecular and Cellular Cardiology*. 78:23–34.
37. Kwong, J.Q., and J.D. Molkenin. 2015. Physiological and pathological roles of the mitochondrial permeability transition pore in the heart. *Cell Metab.* 21:206–214.
38. Beavis, A.D. 1992. Properties of the inner membrane anion channel in intact mitochondria. *J Bioenerg Biomembr.* 24:77–90.

39. Beavis, A.D., and K.D. Garlid. 1987. The mitochondrial inner membrane anion channel. Regulation by divalent cations and protons. *J. Biol. Chem.* 262:15085–15093.
40. Papadopoulos, V., M. Baraldi, T.R. Guilarte, T.B. Knudsen, J.-J. Lacapère, P. Lindemann, M.D. Norenberg, D. Nutt, A. Weizman, M.-R. Zhang, and M. Gavish. 2006. Translocator protein (18kDa): new nomenclature for the peripheral-type benzodiazepine receptor based on its structure and molecular function. *Trends in Pharmacological Sciences.* 27:402–409.
41. Motloch, L.J., J. Hu, and F.G. Akar. 2015. The Mitochondrial Translocator Protein and Arrhythmogenesis in Ischemic Heart Disease. *Oxid Med Cell Longev.* 2015.
42. Brown, D.A., M.A. Aon, F.G. Akar, T. Liu, N. Sorraín, and B. O'Rourke. 2008. Effects of 4'-chlorodiazepam on cellular excitation-contraction coupling and ischaemia-reperfusion injury in rabbit heart. *Cardiovasc Res.* 79:141–149.
43. Ilkan, Z., and F.G. Akar. 2018. The Mitochondrial Translocator Protein and the Emerging Link Between Oxidative Stress and Arrhythmias in the Diabetic Heart. *Front Physiol.* 9.
44. Maack, C., and B. O'Rourke. 2007. Excitation-contraction coupling and mitochondrial energetics. *Basic Res Cardiol.* 102:369–392.
45. Denton, R.M. 2009. Regulation of mitochondrial dehydrogenases by calcium ions. *Biochimica et Biophysica Acta (BBA) - Bioenergetics.* 1787:1309–1316.
46. Wei, A.-C., T. Liu, R.L. Winslow, and B. O'Rourke. 2012. Dynamics of matrix-free Ca<sup>2+</sup> in cardiac mitochondria: two components of Ca<sup>2+</sup> uptake and role of phosphate buffering. *J Gen Physiol.* 139:465–478.
47. Griffiths, E.J., C.J. Ocampo, J.S. Savage, G.A. Rutter, R.G. Hansford, M.D. Stern, and H.S. Silverman. 1998. Mitochondrial calcium transporting pathways during hypoxia and reoxygenation in single rat cardiomyocytes. *Cardiovasc Res.* 39:423–433.
48. Miyata H, Lakatta E G, Stern M D, and Silverman H S. 1992. Relation of mitochondrial and cytosolic free calcium to cardiac myocyte recovery after exposure to anoxia. *Circulation Research.* 71:605–613.
49. Duchen, M.R. 2000. Mitochondria and calcium: from cell signalling to cell death. *J Physiol.* 529:57–68.
50. Kirichok, Y., G. Krapivinsky, and D.E. Clapham. 2004. The mitochondrial calcium uniporter is a highly selective ion channel. *Nature.* 427:360–364.
51. Chaudhuri, D., Y. Sancak, V.K. Mootha, and D.E. Clapham. 2013. MCU encodes the pore conducting mitochondrial calcium currents. *eLife.* 2:e00704.

52. Baughman, J.M., F. Perocchi, H.S. Girgis, M. Plovanich, C.A. Belcher-Timme, Y. Sancak, X.R. Bao, L. Strittmatter, O. Goldberger, R.L. Bogorad, V. Kotliansky, and V.K. Mootha. 2011. Integrative genomics identifies MCU as an essential component of the mitochondrial calcium uniporter. *Nature*. 476:341–345.
53. De Stefani, D., A. Raffaello, E. Teardo, I. Szabò, and R. Rizzuto. 2011. A 40 kDa protein of the inner membrane is the mitochondrial calcium uniporter. *Nature*. 476:336–340.
54. De Stefani, D., M. Patron, and R. Rizzuto. 2015. Structure and function of the mitochondrial calcium uniporter complex. *Biochimica et Biophysica Acta (BBA) - Molecular Cell Research*. 1853:2006–2011.
55. Pan, X., J. Liu, T. Nguyen, C. Liu, J. Sun, Y. Teng, M.M. Fergusson, I.I. Rovira, M. Allen, D.A. Springer, A.M. Aponte, M. Gucek, R.S. Balaban, E. Murphy, and T. Finkel. 2013. The physiological role of mitochondrial calcium revealed by mice lacking the mitochondrial calcium uniporter. *Nat Cell Biol*. 15:1464–1472.
56. Holmström, K.M., X. Pan, J.C. Liu, S. Menazza, J. Liu, T.T. Nguyen, H. Pan, R.J. Parks, S. Anderson, A. Noguchi, D. Springer, E. Murphy, and T. Finkel. 2015. Assessment of cardiac function in mice lacking the mitochondrial calcium uniporter. *J Mol Cell Cardiol*. 85:178–182.
57. Drago, I., D. De Stefani, R. Rizzuto, and T. Pozzan. 2012. Mitochondrial Ca<sup>2+</sup> uptake contributes to buffering cytoplasmic Ca<sup>2+</sup> peaks in cardiomyocytes. *Proceedings of the National Academy of Sciences*. 109:12986–12991.
58. Kwong, J.Q., X. Lu, R.N. Correll, J.A. Schwanekamp, R.J. Vagnozzi, M.A. Sargent, A.J. York, J. Zhang, D.M. Bers, and J.D. Molckentin. 2015. The Mitochondrial Calcium Uniporter Selectively Matches Metabolic Output to Acute Contractile Stress in the Heart. *Cell Reports*. 12:15–22.
59. Luongo, T.S., J.P. Lambert, A. Yuan, X. Zhang, P. Gross, J. Song, S. Shanmughapriya, E. Gao, M. Jain, S.R. Houser, W.J. Koch, J.Y. Cheung, M. Madesh, and J.W. Elrod. 2015. The Mitochondrial Calcium Uniporter Matches Energetic Supply with Cardiac Workload during Stress and Modulates Permeability Transition. *Cell Rep*. 12:23–34.
60. Rasmussen, T.P., Y. Wu, M.A. Joiner, O.M. Koval, N.R. Wilson, E.D. Luczak, Q. Wang, B. Chen, Z. Gao, Z. Zhu, B.A. Wagner, J. Soto, M.L. McCormick, W. Kutschke, R.M. Weiss, L. Yu, R.L. Boudreau, E.D. Abel, F. Zhan, D.R. Spitz, G.R. Buettner, L.-S. Song, L.V. Zingman, and M.E. Anderson. 2015. Inhibition of MCU forces extramitochondrial adaptations governing physiological and pathological stress responses in heart. *PNAS*. 112:9129–9134.
61. Lambert, J.P., T.S. Luongo, D. Tomar, P. Jadiya, E. Gao, X. Zhang, A.M. Lucchese, D.W. Kolmetzky, N.S. Shah, and J.W. Elrod. 2019. MCUB Regulates the Molecular Composition

- of the Mitochondrial Calcium Uniporter Channel to Limit Mitochondrial Calcium Overload During Stress. *Circulation*. 140:1720–1733.
62. Patron, M., V. Checchetto, A. Raffaello, E. Teardo, D. Vecellio Reane, M. Mantoan, V. Granatiero, I. Szabò, D. De Stefani, and R. Rizzuto. 2014. MICU1 and MICU2 Finely Tune the Mitochondrial Ca<sup>2+</sup> Uniporter by Exerting Opposite Effects on MCU Activity. *Mol Cell*. 53:726–737.
  63. Kamer, K.J., and V.K. Mootha. 2014. MICU1 and MICU2 play nonredundant roles in the regulation of the mitochondrial calcium uniporter. *EMBO reports*. 15:299–307.
  64. Mallilankaraman, K., P. Doonan, C. Cárdenas, H.C. Chandramoorthy, M. Muller, R. Miller, N.E. Hoffman, R. Gandhirajan, J. Molgó, M.J. Birnbaum, B. Rothberg, D.-O.D. Mak, J.K. Foskett, and M. Madesh. 2012. MICU1 is an Essential Gatekeeper for MCU-Mediated Mitochondrial Ca<sup>2+</sup> Uptake That Regulates Cell Survival. *Cell*. 151:630–644.
  65. Csordás, G., T. Golenár, E.L. Seifert, K.J. Kamer, Y. Sancak, F. Perocchi, C. Moffat, D. Weaver, S. de la F. Perez, R. Bogorad, V. Koteliensky, J. Adijanto, V.K. Mootha, and G. Hajnóczky. 2013. MICU1 controls both the threshold and cooperative activation of the mitochondrial Ca<sup>2+</sup> uniporter. *Cell Metab*. 17:976–987.
  66. Perocchi, F., V.M. Gohil, H.S. Girgis, X.R. Bao, J.E. McCombs, A.E. Palmer, and V.K. Mootha. 2010. MICU1 encodes a mitochondrial EF hand protein required for Ca<sup>2+</sup> uptake. *Nature*. 467:291–296.
  67. Liu, J.C., J. Liu, K.M. Holmström, S. Menazza, R.J. Parks, M.M. Fergusson, Z.-X. Yu, D.A. Springer, C. Halsey, C. Liu, E. Murphy, and T. Finkel. 2016. MICU1 serves as a molecular gatekeeper to prevent in vivo mitochondrial calcium overload. *Cell Rep*. 16:1561–1573.
  68. Bick, A.G., H. Wakimoto, K.J. Kamer, Y. Sancak, O. Goldberger, A. Axelsson, D.M. DeLaughter, J.M. Gorham, V.K. Mootha, J.G. Seidman, and C.E. Seidman. 2017. Cardiovascular homeostasis dependence on MICU2, a regulatory subunit of the mitochondrial calcium uniporter. *PNAS*. 114:E9096–E9104.
  69. Sancak, Y., A.L. Markhard, T. Kitami, E. Kovács-Bogdán, K.J. Kamer, N.D. Udeshi, S.A. Carr, D. Chaudhuri, D.E. Clapham, A.A. Li, S.E. Calvo, O. Goldberger, and V.K. Mootha. 2013. EMRE is an essential component of the mitochondrial calcium uniporter complex. *Science*. 342:1379–1382.
  70. Liu, J.C., N.C. Syder, N.S. Ghorashi, T.B. Willingham, R.J. Parks, J. Sun, M.M. Fergusson, J. Liu, K.M. Holmström, S. Menazza, D.A. Springer, C. Liu, B. Glancy, T. Finkel, and E. Murphy. 2020. EMRE is essential for mitochondrial calcium uniporter activity in a mouse model. *JCI Insight*. 5.
  71. Mallilankaraman, K., C. Cárdenas, P. Doonan, H.C. Chandramoorthy, K.M. Irrinki, T. Golenár, G. Csordás, P. Madireddi, J. Yang, M. Müller, R. Miller, J.E. Kolesar, J. Molgó, B.

- Kaufman, G. Hajnóczky, J.K. Foskett, and M. Madesh. 2012. MCUR1 is an Essential Component of Mitochondrial Ca<sup>2+</sup> Uptake that Regulates Cellular Metabolism. *Nat Cell Biol.* 14:1336–1343.
72. Tomar, D., Z. Dong, S. Shanmughapriya, D.A. Koch, T. Thomas, N.E. Hoffman, S.A. Timbalia, S.J. Goldman, S.L. Breves, D.P. Corbally, N. Nemani, J.P. Fairweather, A.R. Cutri, X. Zhang, J. Song, F.J. Prado, J. Huang, C. Barrero, J.E. Rabinowitz, T.S. Luongo, S.M. Schumacher, M. Rockman, A. Dietrich, S. Merali, J. Caplan, P. Stathopoulos, R.S. Ahima, J.Y. Cheung, S.R. Houser, W.J. Koch, V. Patel, V.M. Gohil, J.W. Elrod, S. Rajan, and M. Madesh. 2016. MCUR1 is a Scaffold Factor for the MCU Complex Function and Promotes Mitochondrial Bioenergetics. *Cell Rep.* 15:1673–1685.
73. Fan, M., J. Zhang, C.-W. Tsai, B.J. Orlando, M. Rodriguez, Y. Xu, M. Liao, M.-F. Tsai, and L. Feng. 2020. Structure and mechanism of the mitochondrial Ca<sup>2+</sup> uniporter holocomplex. *Nature.* 1–5.
74. Fieni, F., S. Bae Lee, Y.N. Jan, and Y. Kirichok. 2012. Activity of the mitochondrial calcium uniporter varies greatly between tissues. *Nature Communications.* 3:1–12.
75. Raffaello, A., D. De Stefani, D. Sabbadin, E. Teardo, G. Merli, A. Picard, V. Checchetto, S. Moro, I. Szabò, and R. Rizzuto. 2013. The mitochondrial calcium uniporter is a multimer that can include a dominant-negative pore-forming subunit. *EMBO J.* 32:2362–2376.
76. Beutner, G., V.K. Sharma, L. Lin, S.-Y. Ryu, R.T. Dirksen, and S.-S. Sheu. 2005. Type 1 ryanodine receptor in cardiac mitochondria: Transducer of excitation–metabolism coupling. *Biochimica et Biophysica Acta (BBA) - Biomembranes.* 1717:1–10.
77. Jakob, R., G. Beutner, V.K. Sharma, Y. Duan, R.A. Gross, S. Hurst, B.S. Jhun, J. O-Uchi, and S.-S. Sheu. 2014. Molecular and functional identification of a mitochondrial ryanodine receptor in neurons. *Neuroscience Letters.* 575:7–12.
78. Jiang, D., L. Zhao, C.B. Clish, and D.E. Clapham. 2013. Letm1, the mitochondrial Ca<sup>2+</sup>/H<sup>+</sup> antiporter, is essential for normal glucose metabolism and alters brain function in Wolf–Hirschhorn syndrome. *Proc Natl Acad Sci U S A.* 110:E2249–E2254.
79. Tsai, M.-F., D. Jiang, L. Zhao, D. Clapham, and C. Miller. 2014. Functional reconstitution of the mitochondrial Ca<sup>2+</sup>/H<sup>+</sup> antiporter Letm1. *J Gen Physiol.* 143:67–73.
80. Griffiths, E.J. 1999. Reversal of mitochondrial Na/Ca exchange during metabolic inhibition in rat cardiomyocytes. *FEBS Letters.* 453:400–404.
81. Jiang, D., L. Zhao, and D.E. Clapham. 2009. Genome-Wide RNAi Screen Identifies Letm1 as a Mitochondrial Ca<sup>2+</sup>/H<sup>+</sup> Antiporter. *Science.* 326:144–147.
82. Finkel, T., S. Menazza, K.M. Holmström, R.J. Parks, J. Liu, J. Sun, J. Liu, X. Pan, and E. Murphy. 2015. The Ins and Outs of Mitochondrial Calcium. *Circ Res.* 116:1810–1819.

83. Berns, M.W., A.E. Siemens, and R.J. Walter. 1984. Mitochondrial fluorescence patterns in rhodamine 6G-stained myocardial cells in vitro: Analysis by real-time computer video microscopy and laser microspot excitation. *Cell Biophysics*. 6:263–277.
84. Siemens, A., R. Walter, L.H. Liaw, and M.W. Berns. 1982. Laser-stimulated fluorescence of submicrometer regions within single mitochondria of rhodamine-treated myocardial cells in culture. *Proc Natl Acad Sci U S A*. 79:466–470.
85. Hüser, J., and L.A. Blatter. 1999. Fluctuations in mitochondrial membrane potential caused by repetitive gating of the permeability transition pore. *Biochem J*. 343:311–317.
86. Kurz, F.T., M.A. Aon, B. O'Rourke, and A.A. Armoundas. 2010. Wavelet analysis reveals heterogeneous time-dependent oscillations of individual mitochondria. *Am J Physiol Heart Circ Physiol*. 299:H1736–H1740.
87. Kurz, F.T., M.A. Aon, B. O'Rourke, and A.A. Armoundas. 2017. Functional Implications of Cardiac Mitochondria Clustering. *Adv Exp Med Biol*. 982:1–24.
88. Garfinkel, A., M.L. Spano, W.L. Ditto, and J.N. Weiss. 1992. Controlling Cardiac Chaos. *Science*. 257:1230–1235.
89. Mironov, S.L., and D.W. Richter. 2001. Oscillations and hypoxic changes of mitochondrial variables in neurons of the brainstem respiratory centre of mice. *J Physiol*. 533:227–236.
90. Duchen, M.R., A. Leyssens, and M. Crompton. 1998. Transient Mitochondrial Depolarizations Reflect Focal Sarcoplasmic Reticular Calcium Release in Single Rat Cardiomyocytes. *J Cell Biol*. 142:975–988.
91. Nivala, M., P. Korge, M. Nivala, J.N. Weiss, and Z. Qu. 2011. Linking Flickering to Waves and Whole-Cell Oscillations in a Mitochondrial Network Model. *Biophysical Journal*. 101:2102–2111.
92. Buckman, J.F., and I.J. Reynolds. 2001. Spontaneous Changes in Mitochondrial Membrane Potential in Cultured Neurons. *J. Neurosci*. 21:5054–5065.
93. Vergun, O., and I.J. Reynolds. 2004. Fluctuations in Mitochondrial Membrane Potential in Single Isolated Brain Mitochondria: Modulation by Adenine Nucleotides and Ca<sup>2+</sup>. *Biophysical Journal*. 87:3585–3593.
94. Solhjoo, S., and B. O'Rourke. 2015. Mitochondrial instability during regional ischemia–reperfusion underlies arrhythmias in monolayers of cardiomyocytes. *Journal of Molecular and Cellular Cardiology*. 78:90–99.
95. Zhou, L., S. Solhjoo, B. Millare, G. Plank, M.R. Abraham, S. Cortassa, N. Trayanova, and B. O'Rourke. 2014. Effects of Regional Mitochondrial Depolarization on Electrical

- Propagation: Implications for Arrhythmogenesis. *Circ Arrhythm Electrophysiol.* 7:143–151.
96. Kurz, F.T., M.A. Aon, B. O'Rourke, and A.A. Armoundas. 2014. Cardiac mitochondria exhibit dynamic functional clustering. *Front Physiol.* 5.
  97. Pitts, K.R., and C.F. Toombs. 2004. Coverslip hypoxia: a novel method for studying cardiac myocyte hypoxia and ischemia in vitro. *American Journal of Physiology-Heart and Circulatory Physiology.* 287:H1801–H1812.
  98. Marks, R. 1991. Introduction to Shannon Sampling and Interpolation Theory. New York: Springer-Verlag.
  99. Thévenaz, P., U.E. Ruttimann, and M. Unser. 1998. A Pyramid Approach to Subpixel Registration Based on Intensity. *IEEE Transactions on Image Processing.* 7:27–41.
  100. Percival, D.B. 2008. Analysis of Geophysical Time Series Using Discrete Wavelet Transforms: An Overview. In: Donner RV, SM Barbosa, editors. *Nonlinear Time Series Analysis in the Geosciences.* Berlin, Heidelberg: Springer Berlin Heidelberg. pp. 61–79.
  101. Aon, M.A., S. Cortassa, F.G. Akar, and B. O'Rourke. 2006. Mitochondrial criticality: A new concept at the turning point of life or death. *Biochim Biophys Acta.* 1762:232–240.
  102. Termonia, Y., and J. Ross. 1981. Oscillations and control features in glycolysis: numerical analysis of a comprehensive model. *Proc Natl Acad Sci U S A.* 78:2952–2956.
  103. Lyon, A.R., P.J. Joudrey, D. Jin, R.D. Nass, M.A. Aon, B. O'Rourke, and F.G. Akar. 2010. Optical imaging of mitochondrial function uncovers actively propagating waves of mitochondrial membrane potential collapse across intact heart. *J Mol Cell Cardiol.* 49:565–575.
  104. Finkel Toren, Menazza Sara, Holmström Kira M., Parks Randi J., Liu Julia, Sun Junhui, Liu Jie, Pan Xin, and Murphy Elizabeth. 2015. The Ins and Outs of Mitochondrial Calcium. *Circulation Research.* 116:1810–1819.
  105. Brown, D., and B. O'Rourke. 2010. Cardiac mitochondria and arrhythmias. *Cardiovascular research.* 88:241–249.
  106. Aon, M.A., S. Cortassa, F.G. Akar, D.A. Brown, L. Zhou, and B. O'Rourke. 2009. FROM MITOCHONDRIAL DYNAMICS TO ARRHYTHMIAS. *Int J Biochem Cell Biol.* 41:1940–1948.
  107. Zorov, D.B., C.R. Filburn, L.-O. Klotz, J.L. Zweier, and S.J. Sollott. 2000. Reactive Oxygen Species (Ros-Induced) Ros Release. *J Exp Med.* 192:1001–1014.

108. Palmer, A.E., M. Giacomello, T. Kortemme, S.A. Hires, V. Lev-Ram, D. Baker, and R.Y. Tsien. 2006. Ca<sup>2+</sup> Indicators Based on Computationally Redesigned Calmodulin-Peptide Pairs. *Chemistry & Biology*. 13:521–530.
109. de Diego Carlos, Pai Rakesh K., Chen Fuhua, Xie Lai-Hua, De Leeuw Jan, Weiss James N., and Valderrábano Miguel. 2008. Electrophysiological Consequences of Acute Regional Ischemia/Reperfusion in Neonatal Rat Ventricular Myocyte Monolayers. *Circulation*. 118:2330–2337.
110. Lemasters, J.J., and V.K. Ramshesh. 2007. Imaging of Mitochondrial Polarization and Depolarization with Cationic Fluorophores. In: *Methods in Cell Biology*. Academic Press. pp. 283–295.
111. Duchen, M.R., A. Surin, and J. Jacobson. 2003. [17] Imaging mitochondrial function in intact cells. In: *Methods in Enzymology*. Academic Press. pp. 353–389.
112. Wüst, R.C.I., M. Helmes, J.L. Martin, T.J.T. van der Wardt, R.J.P. Musters, J. van der Velden, and G.J.M. Stienen. 2017. Rapid frequency-dependent changes in free mitochondrial calcium concentration in rat cardiac myocytes. *The Journal of Physiology*. 595:2001–2019.
113. Schindelin, J., I. Arganda-Carreras, E. Frise, V. Kaynig, M. Longair, T. Pietzsch, S. Preibisch, C. Rueden, S. Saalfeld, B. Schmid, J.-Y. Tinevez, D.J. White, V. Hartenstein, K. Eliceiri, P. Tomancak, and A. Cardona. 2012. Fiji: an open-source platform for biological-image analysis. *Nature Methods*. 9:676–682.
114. Ashok, D., and B. O'Rourke. 2020. MitoWave: Spatio-temporal analysis of mitochondrial membrane potential fluctuations during ischemia-reperfusion. *bioRxiv*. 2020.05.21.108670.
115. Gunter, T.E., and D.R. Pfeiffer. 1990. Mechanisms by which mitochondria transport calcium. *American Journal of Physiology-Cell Physiology*. 258:C755–C786.
116. Kwong, J.Q., J. Huo, M.J. Bround, J.G. Boyer, J.A. Schwanekamp, N. Ghazal, J.T. Maxwell, Y.C. Jang, Z. Khuchua, K. Shi, D.M. Bers, J. Davis, and J.D. Molkentin. 2018. The mitochondrial calcium uniporter underlies metabolic fuel preference in skeletal muscle. *JCI Insight*. 3:e121689.
117. Hobai, I.A., and B. O'Rourke. 2000. Enhanced Ca<sup>2+</sup>-Activated Na<sup>+</sup>-Ca<sup>2+</sup> Exchange Activity in Canine Pacing-Induced Heart Failure. *Circulation Research*. 87:690–698.
118. Halestrap, A.P., S.J. Clarke, and S.A. Javadov. 2004. Mitochondrial permeability transition pore opening during myocardial reperfusion—a target for cardioprotection. *Cardiovasc Res*. 61:372–385.



119. Venable, P.W., T.G. Taylor, K.J. Sciuto, J. Zhao, J. Shibayama, M. Warren, K.W. Spitzer, and A.V. Zaitsev. 2013. Detection of mitochondrial depolarization/recovery during ischaemia-reperfusion using spectral properties of confocally recorded TMRM fluorescence: Spectral method to detect mitochondrial depolarization. *The Journal of Physiology*. 591:2781–2794.
120. Zhang, H., G. Gong, P. Wang, Z. Zhang, S.C. Kolwicz, P.S. Rabinovitch, R. Tian, and W. Wang. 2018. Heart Specific Knockout of Ndufs4 Ameliorates Ischemia Reperfusion Injury. *J Mol Cell Cardiol*. 123:38–45.
121. Hausenloy, D.J., M.R. Duchon, and D.M. Yellon. 2003. Inhibiting mitochondrial permeability transition pore opening at reperfusion protects against ischaemia–reperfusion injury. *Cardiovasc Res*. 60:617–625.
122. Hunter, D.R., and R.A. Haworth. 1979. The Ca<sup>2+</sup> Induced Membrane Transition in Mitochondria. *Archives of Biochemistry and Biophysics*. 195:453–459.
123. Halestrap, A.P., and A.P. Richardson. 2015. The mitochondrial permeability transition: A current perspective on its identity and role in ischaemia/reperfusion injury. *Journal of Molecular and Cellular Cardiology*. 78:129–141.
124. Bernardi, P., and S. von Stockum. 2012. The permeability transition pore as a Ca<sup>2+</sup> release channel: New answers to an old question. *Cell Calcium*. 52:22–27.
125. de J García-Rivas, G., K. Carvajal, F. Correa, and C. Zazueta. 2006. Ru360, a specific mitochondrial calcium uptake inhibitor, improves cardiac post-ischaemic functional recovery in rats in vivo. *Br J Pharmacol*. 149:829–837.
126. Nicholls, D.G., and M. Crompton. 1980. Mitochondrial calcium transport. *FEBS Letters*. 111:261–268.
127. Drago, I., P. Pizzo, and T. Pozzan. 2011. After half a century mitochondrial calcium in- and efflux machineries reveal themselves. *EMBO J*. 30:4119–4125.
128. Moreau, B., and A.B. Parekh. 2008. Ca<sup>2+</sup>-Dependent Inactivation of the Mitochondrial Ca<sup>2+</sup> Uniporter Involves Proton Flux through the ATP Synthase. *Current Biology*. 18:855–859.
129. Maack, C., S. Cortassa, M. Aon, A. Ganesan, T. Liu, and B. O’Rourke. 2006. Elevated Cytosolic Na<sup>+</sup> Decreases Mitochondrial Ca<sup>2+</sup> Uptake During Excitation-Contraction Coupling and Impairs Energetic Adaptation in Cardiac Myocytes. *Circulation Research*. 99:172–182.
130. Cox, D.A., L. Conforti, N. Sperelakis, and M.A. Matlib. 1993. Selectivity of Inhibition of Na<sup>+</sup>-Ca<sup>2+</sup> Exchange of Heart Mitochondria by Benzothiazepine CGP-37157. *Journal of Cardiovascular Pharmacology*. 21:595–599.

131. Neumann, J.T., P.L. Diaz-Sylvester, S. Fleischer, and J.A. Copello. 2011. CGP-37157 Inhibits the Sarcoplasmic Reticulum Ca<sup>2+</sup> ATPase and Activates Ryanodine Receptor Channels in Striated Muscle. *Mol Pharmacol*. 79:141–147.
132. Thu, L.T., J.R. Ahn, and S.-H. Woo. 2006. Inhibition of L-type Ca<sup>2+</sup> channel by mitochondrial Na<sup>+</sup>–Ca<sup>2+</sup> exchange inhibitor CGP-37157 in rat atrial myocytes. *European Journal of Pharmacology*. 552:15–19.
133. Wolkowicz, P.E., L.H. Michael, R.M. Lewis, and J. McMillin-Wood. 1983. Sodium-calcium exchange in dog heart mitochondria: effects of ischemia and verapamil. *American Journal of Physiology-Heart and Circulatory Physiology*. 244:H644–H651.
134. Crompton, M., M. Künzi, and E. Carafoli. 1977. The Calcium-Induced and Sodium-Induced Effluxes of Calcium from Heart Mitochondria. *European Journal of Biochemistry*. 79:549–558.
135. Brand, M.D. 1985. The stoichiometry of the exchange catalysed by the mitochondrial calcium/sodium antiporter. *Biochem J*. 229:161–166.
136. Affolter, H., and E. Carafoli. 1980. The Ca<sup>2+</sup>-Na<sup>+</sup> antiporter of heart mitochondria operates electroneutrally. *Biochemical and Biophysical Research Communications*. 95:193–196.
137. Baysal, K., D.W. Jung, K.K. Gunter, T.E. Gunter, and G.P. Brierley. 1994. Na(+)-dependent Ca<sup>2+</sup> efflux mechanism of heart mitochondria is not a passive Ca<sup>2+</sup>/2Na<sup>+</sup> exchanger. *American Journal of Physiology-Cell Physiology*. 266:C800–C808.
138. Jung, D.W., K. Baysal, and G.P. Brierley. 1995. The Sodium-Calcium Antiport of Heart Mitochondria Is Not Electroneutral. *Journal of Biological Chemistry*. 270:672–678.
139. Kim, B., and S. Matsuoka. 2008. Cytoplasmic Na<sup>+</sup>-dependent modulation of mitochondrial Ca<sup>2+</sup> via electrogenic mitochondrial Na<sup>+</sup>–Ca<sup>2+</sup> exchange. *The Journal of Physiology*. 586:1683–1697.
140. Paucek, P., and M. Jabůrek. 2004. Kinetics and ion specificity of Na<sup>+</sup>/Ca<sup>2+</sup> exchange mediated by the reconstituted beef heart mitochondrial Na<sup>+</sup>/Ca<sup>2+</sup> antiporter. *Biochimica et Biophysica Acta (BBA) - Bioenergetics*. 1659:83–91.
141. Wei, A.-C., T. Liu, S. Cortassa, R.L. Winslow, and B. O'Rourke. 2011. Mitochondrial Ca<sup>2+</sup> Influx and Efflux rates in Guinea Pig Cardiac Mitochondria: Low and High Affinity Effects of Cyclosporine A. *Biochim Biophys Acta*. 1813:1373–1381.
142. Palty, R., M. Hershinkel, and I. Sekler. 2012. Molecular Identity and Functional Properties of the Mitochondrial Na<sup>+</sup> /Ca<sup>2+</sup> Exchanger. *J. Biol. Chem*. 287:31650–31657.

143. O-Uchi, J., B.S. Jhun, J. Mishra, and S.-S. Sheu. 2018. Organellar Ion Channels and Transporters. In: *Cardiac Electrophysiology: From Cell to Bedside*. Philadelphia, PA: Elsevier. pp. 66–79.
144. Gong, G., X. Liu, H. Zhang, S.-S. Sheu, and W. Wang. 2015. Mitochondrial flash as a novel biomarker of mitochondrial respiration in the heart. *Am J Physiol Heart Circ Physiol*. 309:H1166–H1177.
145. Semenza, G.L. 2014. Oxygen Sensing, Hypoxia-Inducible Factors, and Disease Pathophysiology. *Annual Review of Pathology: Mechanisms of Disease*. 9:47–71.
146. Dengler, V.L., M. Galbraith, and J.M. Espinosa. 2014. Transcriptional Regulation by Hypoxia Inducible Factors. *Crit Rev Biochem Mol Biol*. 49:1–15.
147. Semenza, G.L., and G.L. Wang. 1992. A nuclear factor induced by hypoxia via de novo protein synthesis binds to the human erythropoietin gene enhancer at a site required for transcriptional activation. *Mol Cell Biol*. 12:5447–5454.
148. Wang, G.L., B.H. Jiang, E.A. Rue, and G.L. Semenza. 1995. Hypoxia-inducible factor 1 is a basic-helix-loop-helix-PAS heterodimer regulated by cellular O<sub>2</sub> tension. *Proc Natl Acad Sci U S A*. 92:5510–5514.
149. Pugh, C.W., and P.J. Ratcliffe. 2003. Regulation of angiogenesis by hypoxia: role of the HIF system. *Nature Medicine*. 9:677–684.
150. Semenza, G.L. 2011. Hypoxia-Inducible Factor 1: Regulator of Mitochondrial Metabolism and Mediator of Ischemic Preconditioning. *Biochim Biophys Acta*. 1813:1263–1268.
151. Cunliffe, C.J., T.J. Franklin, N.J. Hales, and G.B. Hill. 1992. Novel inhibitors of prolyl 4-hydroxylase. 3. Inhibition by the substrate analog N-oxaloglycine and its derivatives. *J. Med. Chem*. 35:2652–2658.
152. Jaakkola, P., D.R. Mole, Y.-M. Tian, M.I. Wilson, J. Gielbert, S.J. Gaskell, A. von Kriegsheim, H.F. Hebestreit, M. Mukherji, C.J. Schofield, P.H. Maxwell, ‡ Christopher W. Pugh, and ‡ Peter J. Ratcliffe. 2001. Targeting of HIF- $\alpha$  to the von Hippel-Lindau Ubiquitylation Complex by O<sub>2</sub>-Regulated Prolyl Hydroxylation. *Science*. 292:468–472.
153. Aon, M.A., S. Cortassa, and B. O'Rourke. 2006. The Fundamental Organization of Cardiac Mitochondria as a Network of Coupled Oscillators. *Biophys J*. 91:4317–4327.

## Appendices

### Appendix I: Macros and MATLAB codes for MitoWave Analysis Routine

- This routine requires switching between ImageJ (OR FIJI) and MATLAB.
- Language written for ImageJ is ImageJ Macro or .ijm. They run on FIJI.
- Comments and annotations are in `//Green or %Green.`
- Modifications must be made if sampling rate is different from what we used. We sampled at the rate of 1 image every 15 seconds to get 241 images in a period of 60.25 minutes. Modification points are highlighted in blue.
- Arrays containing required data for Ischemia  $\Delta\Psi_m$  depolarization time, Average frequency of each cell, mitochondrial frequencies and associated timepoints, mitochondrial cluster areas, mitochondrial  $\Delta\Psi_m$  depolarization time, cellular depolarization time are in **Bold** and Highlighted in yellow.
- Step III point 13 gives a summary of the final results with the names of the arrays where the relevant data are stored

#### STEP I: CELLULAR SEGMENTATION (ON FIJI)

1. Run StackReg plugin to align the images in the image stack

#### **2. Macro 1: Creating a mask**

```
run("Duplicate...", "title= MASK2 duplicate");
run("Duplicate...", "title=MASK1");
selectWindow("");
close();
run("Median...", "radius=2");
run("8-bit");
run("Enhance Contrast...");
run("Auto Local Threshold", "method=Niblack radius=40 parameter_1=0 parameter_2=0
white");
selectWindow("MASK1");
run("Analyze Particles...", "size=60.00-Infinity display clear include add");
```

```
// save the ROIs after creating a mask of the segmented cells.
// Apply this ROI to the image stack to obtain Fluorescence Intensity
```

#### **3. Macro 2: Obtain fluorescence intensity per cell**

```
run("Set Measurements...", "mean redirect=None decimal=3");
roiManager("Show None");
roiManager("Show All");
roiManager("Multi Measure");
```

#### STEP II: DETERMINATION OF ISCHEMIA DEPOLARIZATION TIME (ON MATLAB)

1. Input TMRM fluorescence intensity signal from each cell into MATLAB as an array.
2. Run this code (Ischemia Depolarization time point results are in the array "IPT\_2MAT\_Depolarization\_minutes" in minutes :

```

TMRM_Ischemia=TMRM(42:282, :); % Change according to the time points of
Ischemia
%%Multi-level Signal Reconstruction
numberofcells= size(TMRM_Ischemia,2);
modwtc_2={};
for k= 1: numberofcells
    k
    local={};
    levelForReconstruction = [false, false, false, false, true];
    wt = modwt(TMRM_Ischemia(:,k), 'sym4', 4);
    mra = modwtmra(wt, 'sym4');
    TMRM1 = sum(mra(levelForReconstruction,:),1);
    % n
    local{k}= TMRM1;
modwtc_2{k} = TMRM1;
end
modwtc_2= modwtc_2'

%%findchangepeints
IPTs_2={};
for k= 1: numberofcells
    ipt1=findchangepts(modwtc_2{k});
    IPTs_2{k}=ipt1;
end
IPTs_2=IPTs_2';
%%
%Plot Figure
figure;histogram(cell2mat(IPTs_2), 'BinWidth', 5);
ylabel({'Counts of Cells Depolarizing'});

% Create xlabel
xlabel({'Time Points'});

% Create title
title({'Time taken for \Delta \psim depolarization during Ischemia'});

%%
% Finding the corresponding yvalue to plot the changed point
IPTs_2_MAT=cell2mat(IPTs_2);
IPT_2MAT_Depolarization_minutes= IPTs_2_MAT.*0.25; %% these are the values we
need to determine the depolarization time point during Ischemia %change the
multiplication factor based on the sampling period. I sampled @ 1 image every
15 seconds.
for x= 1: size(TMRM_Ischemia, 2)
    local_corr_y(x)= TMRM_Ischemia(IPTs_2_MAT(x), x);
end
local_corr_y= local_corr_y';
IPT_2MAT_addbaseline= IPTs_2_MAT+42;

%%
%plotting the figure of the Ischemia depolarization moment on the TMRM

```

```

%Fluorescence
figure; plot(TMRM, 'DisplayName', 'TMRM')
hold on; plot(IPT_2MAT_addbaseline, local_corr_y, 'k.', 'MarkerSize', 12);
hold off

```

### STEP III: MITOCHONDRIAL $\Delta\Psi_m$ OSCILLATION ANALYSIS

1. Create 8 folders with the following names to save data from each step:

- (i) CroppedCells\_1 // To separate each cell in the I/R imagestack and save
- (ii) ReperfusionStack\_2 // Separate and save reperfusion phase for each cell
- (iii) DifferentialStack\_3 // Save Differential stack (n-(n+1)<sup>th</sup> image
- (iv) ROIofMitoClusters\_4
- (v) AreaMean\_5
- (vi) CWT\_6
- (vii) CWTtoImageJ\_7
- (viii) ApplyingThreshold\_8; with 3 subfolders "Results", "TIFF", "ROI".

2. ON IMAGEJ: TO SEPARATE EACH CELL

//CHANGE THE REPERFUSION DUPLICATE STACK ACCORDING TO WHEN REPERFUSION HAPPENED

```

dir1 = getDirectory("Choose Directory "); // Choose the "CroppedCells_1" folder
dir2 = getDirectory("Choose Directory "); // Choose the "ReperfusionStack_2" folder
roicount= roiManager("count");
T=getTitle();
print(T);
print(roicount);
setBatchMode(true);
for (i = 0; i < roicount; i++)
{

selectWindow(T);
run("Duplicate...", "title=[IR copy] duplicate");
roiManager("Select", i);
run("Clear Outside", "stack");
roiManager("Select", i);
run("Duplicate...", "title=copy duplicate");
selectWindow("IR copy");
roiManager("Select", i);
run("Duplicate...", "title=[copy reperfusion] duplicate range=283-523");
selectWindow("copy");
saveAs("Tiff", dir1+"Cell_"+i+1);
selectWindow("copy reperfusion");
saveAs("Tiff", dir2+"Reper_"+i+1);

```

```

selectWindow("IR copy");
close("IR copy");
selectWindow(T);
}
setBatchMode(false);

```

### 3. ON MATLAB: TO CREATE A DIFFERENTIAL STACK

```

%%% change filenames of Reperfusion
changefilename_dir= uigetdir; %% the "ReperfusionStack_2" folder
filestochangenames = dir([ changefilename_dir '/*.tif']);
for l=1:length(filestochangenames)
    1
    oldFileName = filestochangenames(l).name;
    oldFileName
    startunderSym = strfind(oldFileName, '_');
    startPerSym = strfind(oldFileName, '.');
    if ~isempty(startunderSym) && ~isempty(startPerSym)
        fileNumber = str2num(oldFileName(startunderSym(1)+1:startPerSym(1)-
1));
        fileNumber
        newFileName = sprintf('Reper_%03d.tif',fileNumber);
        newFileName
        if exist(newFileName, 'file')
            continue
        else
            movefile(oldFileName,newFileName);
        end
    end
end
end

%%% WITH CORRECT FILENAME%%%%%%%%
Image_folder= uigetdir; %% select the ReperfusionStack_2 folder
Diff_stack_folder=uigetdir; %% select the DifferentialStack_3 folder
Image_Dir=dir([Image_folder '/*.tif']);
total_images=size(Image_Dir, 1);
for n= 1: total_images
    n
    filename= Image_Dir(n).name;
    info = imfinfo(filename);
    num_images = numel(info);
    for k = 1:(num_images-1)
        startunderSym = findstr(filename, '_');
        startPerSym = findstr(filename, '.');
        if ~isempty(startunderSym) && ~isempty(startPerSym)
            fileNumber = str2num(filename(startunderSym(1)+1:startPerSym(1)-1));
            new_name = sprintf('test_%03d.tif',fileNumber);
        end
        fullDestination = fullfile(Diff_stack_folder,new_name);
        A = imread(filename, k, 'Info', info);
        B = imread(filename, k + 1, 'Info', info);
        Q = A - B;
        imshow(Q, []);
        imwrite(Q,fullDestination,'WriteMode', 'append');
    end
end

```

```

        end
    n
    fclose('all');
    n
    end
    %%%%%%%%%%%

```

#### 4. ON FIJI: TO CREATE OUTLINES FOR EACH MITOCHONDRIAL CLUSTER

```

dir3 = getDirectory("Choose Directory "); // Choose the "DifferentialStack_3" folder
dir4 = getDirectory("Choose Directory "); // Choose the "ROIofMitoClusters_4" folder
list = getFileList(dir3);

setBatchMode(true);
for (i=0; i<list.length; i++) {
file = dir3 + list[i];
open(dir3+list[i]);
T= getTitle();
selectWindow(T);
run("Z Project...", "projection=[Max Intensity]");
run("Duplicate...", " ");
run("Enhance Contrast...", "saturated=0.3");
run("8-bit");
run("Auto Local Threshold", "method=Niblack radius=15 parameter_1=0 parameter_2=0
white");
run("Median...", "radius=2");
//run("Make Binary");
run("Watershed");
run("Analyze Particles...", "size=4-Infinity display clear include summarize add");
run("Set Measurements...", "mean redirect=None decimal=3");
roiManager("Show None");
roiManager("Show All");
roiManager("Multi Measure");

titleX=T+"_RoiSet.zip";
roiManager("Save", dir4+titleX);
//saveAs("Results", dir4+titleY);
close(T);
roiManager("reset");

};
setBatchMode(false);

```

#### 5. ON FIJI : TO GET THE AREA AND MEAN FOR EACH MITOCHONDRIAL CLUSTER

```

roiManager("reset");
dir_4 = getDirectory("Choose a Directory"); // Choose the "ROIofMitoClusters_4" folder

```



```

dir_2 = getDirectory("Choose a Directory");// Choose the "ReperfusionStack_2" folder
dir_5 = getDirectory("Choose a Directory");// Choose the "AreaMean_5" folder
list = getFileList(dir_2);
setBatchMode(true);
    for (i=0; i<list.length; i++) {
        showProgress(i, list.length);
        fileR = dir_2 + list[i];
        open(dir_2+list[i]);
        R=getTitle();
        selectWindow(R);
        print(R);
        print("The image title is " + R);
        run("Set Measurements...", "mean redirect=None decimal=3");
        ROList= getFileList(dir_4);
            run("ROI Manager...");
        roiManager("Open", dir_4+ROList[i]);
        getInfo("selection.name");

        selectWindow(R);
        roiManager("Show None");
        roiManager("Show All");
        roiManager("Multi Measure");
        run("Input/Output...", "jpeg=85 gif=-1 file=.csv use_file copy_column save_column");
        titleM=R+"_MeanResults.csv";
        saveAs("Results", dir_5+titleM);
        run("Set Measurements...", "area redirect=None decimal=3");
        selectWindow(R);
        roiManager("Show None");
        roiManager("Show All");
        roiManager("measure");
        titleA=R+"_AreaResults.csv";
        saveAs("Results", dir_5+titleA);
    roiManager("reset");

        selectWindow(R);
        close(R);
    //    close(M);

    };
setBatchMode(false);

```

6. ON MATLAB: IMPORT EACH MITO CLUSTER'S TMRM INTENSITY AND AREA INTO AND PERFORM CONTINUOUS WAVELET TRANSFORM OF THE TMRM SIGNAL.

```

%%GETTING AREA AND MEAN INTENSITY OF EACH CLUSTER DURING REPERFUSION INTO AN
ARRAY FOR CWT
EachCellsMitoROI=uigetdir; %% SELECT DIRECTORY "AreaMean_5" get the directory
where every cell's mitochondria's TMRM intensity and area, during reperfusion
are saved as a .csv results file
Reper_results_dir=dir([EachCellsMitoROI '*MeanResults.csv']);
zz=size(Reper_results_dir, 1); %% get the number of files in that folder,
i.e. number of cells
for z=1:zz
    z
AllcellsandMitos_Mean = sprintf('Reper_%03d.tif_MeanResults.csv', z);
AllcellsandMitos_Mean
AllcellsandMitos_Results{z} = importdata(AllcellsandMitos_Mean);
end

AllcellsandMitos_Resultsmat=cell2mat(AllcellsandMitos_Results);

%% STEP_6: CWTs OF MITOCHONDRIA FROM EACH CELL
numberofcells= size(AllcellsandMitos_Resultsmat,2);
    cwtc={};
for k= 1: numberofcells
    k
    local={};
for n= 1:size(AllcellsandMitos_Resultsmat(k).data, 2)
    % n
    local{n}= cwt(AllcellsandMitos_Resultsmat(k).data(:,n), 1:64, 'sym8');
end
cwtc{k} = local;
end
cwtc= cwtc'

%%

%% STEP_7: WRITE CWTs TO CSV (FOR IMAGEJ TO READ)
selpath= uigetdir; %% CHOOSE DIRECTORY "CWT_6"
[jc, jm] = size(cwtc);
for k= 1: jc
    k
    eachrow= cwtc{k};
    for er=1:size(eachrow, 2)
        er
        ffs= fullfile(selpath, sprintf('Cell_%03d_Cluster_%02d.csv', k, er));
        csvwrite(ffs, eachrow{er});
    end
end

%%

```

## 7. ON FIJI: OPENING THE COEFFICIENTS OF THE CWT AS AN IMAGE ON IMAGEJ

```

dir1 = getDirectory("Choose Directory "); // CHOOSE DIRECTORY "CWT_6" with all the CWTs
written as CSVs
dir2 = getDirectory("Choose Directory "); // CHOOSE DIRECTORY "CWTtoImageJ_7" to save
CWTs as a .tiff file for Imagej to read
list = getFileList(dir1);

```

```

setBatchMode(true);
for (i=0; i<list.length; i++) {
  file = dir1 + list[i];
  run("Text Image... ", "open=&file");
  saveAs("Tiff", dir2+list[i]);
};
setBatchMode(false);

```

8. a. ON FIJI: APPLY THRESHOLD TO THE CWT SCALOGRAM IMAGES

```

dir1 = getDirectory("Choose Directory "); // CHOOSE FOLDER "CWTtoImageJ_7"
dir2 = getDirectory("Choose Directory "); // CHOOSE THE FOLDER "Results" INSIDE
"ApplyingThreshold_8" folder to save .csv files
dir3 = getDirectory("Choose Directory "); // CHOOSE THE FOLDER "Tiff" INSIDE
"ApplyingThreshold_8" FOLDER to save .TIFF files
dir4 = getDirectory("Choose Directory "); // CHOOSE THE FOLDER "ROI" INSIDE
"ApplyingThreshold_8" FOLDER to save THE ROI files
list = getFileList(dir1);
setBatchMode(true);
for (i=0; i<list.length; i++) {
  file = dir1 + list[i];
  open(dir1+list[i]);
  T= getTitle();
  run("Flip Vertically");
  run("Duplicate...", "title=Copy.tif ");
  selectWindow("Copy.tif");
  run("16-bit");
  selectWindow("Copy.tif");
  run("Auto Threshold", "method=Mean white");
  run("Set Measurements...", "area min centroid center perimeter bounding shape skewness
stack invert redirect=None decimal=3");
  run("Analyze Particles...", "display clear include add");
  close("Copy.tif");
  selectWindow(T);
  roiManager("Show None");
  roiManager("Show All");
  roiManager("multi-measure measure_all");
  run("Input/Output...", "jpeg=85 gif=-1 file=.csv use_file copy_column save_column");
  titleX=T+"_RoiSet.zip";
  titleY=T+"_Results.csv";
  saveAs("Tiff", dir3+list[i]);
  roiManager("Save", dir4+titleX);
  saveAs("Results", dir2+titleY);
  roiManager("reset");
};

```

```
setBatchMode(false);
```

#### 8. b. ON FIJI: EXTRACTING CO-ORDINATES OF THE HIGEST COEFFICIENT PEAKS IN THE SCALOGRAM

```
roiManager("reset");
dir1 = getDirectory("Choose Directory "); // CHOOSE THE FOLDER "Results"
dir2 = getDirectory("Choose Directory "); // CHOOSE THE FOLDER "TIFF"
dir3 = getDirectory("Choose Directory "); // CHOOSE THE FOLDER "ROI"
list = getFileList(dir2);

setBatchMode(true);
for (i=0; i<list.length; i++) {
    showProgress(i, list.length);

file = dir2 + list[i];
open(dir2+list[i]);
R=getTitle();
    selectWindow(R);
    ROList= getFileList(dir3);
        run("ROI Manager...");
    roiManager("Open", dir3+ROList[i]);
    getInfo("selection.name");
    selectWindow(R);
    roiManager("Show None");
roicount= roiManager("count");
//titleZ="/Test.txt";
titleZ= R+"_Brightest.txt";
fileZ=File.open(dir1+titleZ);
    for (j = 0; j < roicount; j++) {
        roiManager("Select", j);
        getRawStatistics(nPixels, mean, min, max);
        run("Find Maxima...", "noise="+max+" output=[Point Selection]");
        getSelectionBounds(x, y, w, h);
        print(fileZ,x+", "+y+", "+getPixel(x,y));
    }
    File.close(fileZ);
    roiManager("reset");
}
```

#### 9. ON MATLAB: IMPORT DATA OF SCALOGRAM COEFFICIENTS INTO MATLAB

```
% convert brightest points .txt file to .csv file for importing into MATLAB
```

```

Brightestpoints=uigetdir
Brightestpoints_dir= dir([Brightestpoints '*Brightest.txt']);
numberoffiles= size(Brightestpoints_dir,1);
for m=1: numberoffiles
    m
    eachrow= cwtc{m}
    eachcell= {};
    for er = 1: size(eachrow, 2);
        er
myfilename = sprintf('Cell_%03d_Cluster_%02d.tif_Brightest.txt', m, er);
myfilename
fileID = fopen(myfilename,'r');
dataArray = textscan(fileID, '%n%n%n', 'Delimiter', ',');
fclose(fileID);
newfilename= sprintf('Cell_%03d_Cluster_%02d.tif_Brightest.csv', m, er);
csvwrite(newfilename, dataArray)
    end
end

%%%%%%%%% import CO-ORDINATES OF COEFFICIENT PEAKS THAT WERE THRESHOLDED ON
IMAGEJ

MeanThresholded=uigetdir
MeanThresholded_dir= dir([MeanThresholded '*.csv']);
numberoffiles= size(MeanThresholded_dir,1);
MeanThresholded_Results = {};
    for m=1: numberoffiles
        m
        eachrow= cwtc{m}
        eachcell= {};
        for er = 1: size(eachrow, 2);
            er
myfilename = sprintf('Cell_%03d_Cluster_%02d.tif_Results.csv', m, er);
myfilename
eachcell{er}= importdata(myfilename);
        end
        MeanThresholded_Results{m}= eachcell;
    end
    MeanThresholded_Results= MeanThresholded_Results' %% Contains the
coordinates of the peak coefficients that were thresholded in the scalogram.

%%%%%%%%% import BRIGHTEST Point

MeanThresholded=uigetdir
MeanThresholded_dir= dir([MeanThresholded '*.csv']);
numberoffiles= size(MeanThresholded_dir,1);
Brightest_Results = {};
    for m=1: numberoffiles
        m
        eachrow= cwtc{m}
        eachcell= {};
        for er = 1: size(eachrow, 2);
            er
myfilename = sprintf('Cell_%03d_Cluster_%02d.tif_Brightest.csv', m, er);

```

```

myfilename
eachcell{er}= importdata(myfilename);
    end
    Brightest_Results{m}= eachcell;
    end
Brightest_Results= Brightest_Results'

```

```

%%

```

**10. ON MATLAB: DATA REDUCTION PROCESS TO SEPARATE FREQUENCIES OF MITOCHONDRIAL CLUSTERS INTO 6 FREQUENCY BANDS AND OBTAIN THEIR ASSOCIATED TIME. (The final frequencies and associated time are averages within a particular frequency band).**

```

MeanThresholded_ResultsCopy= repmat(MeanThresholded_Results,1); %% duplicate
the array containing co-ordinates of peak coefficients
for i = 1:size(MeanThresholded_ResultsCopy,1) %% i= number of cells
    dead_mito_count=0; %% assign as 0 and count if there are dead mitos
    current_cell=MeanThresholded_ResultsCopy{i,1}; %% current_cell is the
whole current cell with many mitos
    current_brightest_cell= Brightest_Results{i, 1}; %% using the
brightest points and not the centroid to obtain Xm and Ym
    mito_death_time_array=[]; %% when each mito of a cell dies during
reperfusion
    for j = 1:size(current_cell,2) %% j is the number of columns,
equivalent to the number of mitos in a cell
        col_header=current_cell{1,j}.Properties.VariableNames; %%1 HAS
BEEN ASSIGNED TO THEM- TO START THEM OFF.SOMETHING LIKE A PRE-ALLOCATION.
AFTER THAT, DIFFERENT NUMBERS WILL BE ASSIGNED TO THEM BASED ON WHAT COMES
OUT OF THE FORLOOP IN THE NEXT SET OF CODES.
        col_Area=1;
        col_BX=1;
        col_Width=1;
        col_max_coeff=1;
        col_XM=1;
        col_YM=1;
        local_max=-1000; %% TO INITIALIZE; THIS IS THE LOWEST VALUE AND
EVERY VALUE WE LOOK AT WILL BE ABOVE THIS

        index=2;

        for k=1:size(col_header,2) %% k is the number of columns of
all the parameters from nanmean thresholded results (from 1 to 18). With this
for loop we want to get the number assigned to a particular column.
            if strcmp(col_header{1,k},'Area') %% asking for which
col_header matches 'Area'. Usually its the first column.
                col_Area=k; %% usually col_Area is 1.
            end
            if strcmp(col_header{1,k},'BX')
                col_BX=k;
            end
            if strcmp(col_header{1,k},'Width')
                col_Width=k;
            end
            if strcmp(col_header{1,k},'Max')

```

```

        col_max_coeff=k;
    end
end

    current_data1=current_cell{1,j};%% NOW WE WILL GO THROUGH EVERY
MITO AND ITS CHARACTERESTICS OF A SIGNLE CELL. current_data has the
information for a single mito
    current_data = current_data1{:,1:12};

    current_brightest_data= current_brightest_cell{1, j}; %%
current_brightest_cell has the information for a single mito, but has Xm and
Ym from the brightest points, and not from the centroid/ center of maximum
(since those are just averages and not the actual brightest points..
    BX_Width_sum = current_data(:,9) + current_data(:,11);
    for k = 1:size(BX_Width_sum) %% from the second largest area
(leaving out the first because thats the begining of the reperfusion phase)
        if (local_max < BX_Width_sum(k))
            local_max = BX_Width_sum(k); %% its considering the
maximum coefficient after discarding the 1st maximum coefficient and the next
maximum coefficient from the maximum area
            index = k
        end
    end
    relevant_max = -1000;
    for k = 2:size(current_data,1) %% from the second largest area
(leaving out the first because thats the begining of the reperfusion phase)
        if (k ~= index && relevant_max <
current_data(k,col_max_coeff))
            relevant_max = current_data(k,col_max_coeff);
        end
    end
    end
    %%%%%%%%%%%%%%%%%%%%%%%%%%%%%%%%%%%%%%%%%%

    if (size(current_data,1)<=2 | (local_max==241 &&
relevant_max<=80))
        MeanThresholded_ResultsCopy{i,1}{1,j}{:,'classification'} =
{'dead'};
        %% if the max coefficient of the second or third largest area is
less than 80, then the mito is dead.
        mito_death_time=0; %% the mito death time is 0, because it
has been dead from the beginning
        dead_mito_count=dead_mito_count+1; %% we start counting the
dead mitos as 1
    else
MeanThresholded_ResultsCopy{i,1}{1,j}{:,'classification'}={'not dead'}; %% if
the coefficient of that largest area is more than 80, the mito is classified
as 'not dead'.

        local_max=-1000;
        index = 2;
        for k = 2:size(current_data,1) %% from the second largest
area (leaving out the first because thats the begining of the reperfusion
phase)
            if (current_data(k,col_Area)>=1000&& local_max <
current_data(k,col_max_coeff))

```

```

        local_max = current_data(k,col_max_coeff); %% its
considering the maximum coefficient after discarding the 1st maximum
coefficient and the next maximum coefficient from the maximum area
        index = k
    end
end

time_pt=current_data(index,col_BX)+current_data(index,col_Width);%% its
finding the time point at which the mito dies, by considering the largest
area's end X location
    time_pt
    if time_pt<= 240 %% depending on the time points of the
reperfusion experiment, this value may need to be changed. If the time point
is less than 240, then we need to know when the mito died.
        MeanThresholded_ResultsCopy{i,1}{1,j}(:,
'mito_death_time')={time_pt};
        mito_death_time_array(j)=time_pt;
        %cell_classification{i,2}=time_pt;
    else

MeanThresholded_ResultsCopy{i,1}{1,j}(:, 'mito_death_time')={241};%% if the
mito didn't die, then just write 241 (or whatever the end of reperfusion time
point is)
        mito_death_time_array(j)=241;
    end

    osc_data_array=[];%% PREALLOCATING FOR WRITING IN THE
LOCATION OF THE BRIGHTEST SPOTS IN THE CWT- WHICH CORRESPONDS TO THE SCALE
AND TIME
    osc_index=0;
    for k = 2:size(current_data,1) %% considering only the rows
that are not the begining or the ending (ones with largest areas and
coefficients)

local_sum=current_data(k,col_BX)+current_data(k,col_Width); %% incase the
mito dies during the experiment, we still need the scale and time before it
dies. So this local_sum considers the points before the mito dies
        if (k~=index && local_sum<=time_pt)
            osc_index=osc_index+1; %% when the mito is not dead
yet, then osc_index is atleast 1 (and not 0).

osc_data_array(osc_index,1)=current_brightest_data(k,1); %% takes the k-th
row and the first column which has the X coordinate (for the time)
            osc_data_array(osc_index,2)=64-
current_brightest_data(k,2); %% takes the k- th row and the second column
which has the Y co-ordinate for the scale. But since the Y-axis is inverted
(a bug in image j??), we'd have to subtract the Y value from 64 to get the
actual scale value corresponding to the time.
            osc_data_array(osc_index, 3)=
current_brightest_data(k, 3);
        end
    end
    if (osc_index==0)

MeanThresholded_ResultsCopy{i,1}{1,j}(:, 'classification')={'noise'};
    else

```



```

        osc_data_avg_XM=nanmean(osc_data_array(:, 1)); %% for a
particular mito, we get the average time (by getting the nanmean of all the
rows in the first column, with X-cordinates)
        osc_data_std_XM=std(osc_data_array(:, 1));
        osc_data_avg_YM=nanmean(osc_data_array(:,2));%% for a
particular mito, we get the average scale (by getting the nanmean of all the
rows in the second column, with the Y-cordinates subtracted from 64)
        osc_data_std_YM=std(osc_data_array(:, 2));

        XM_list= osc_data_array(:, 1);
        YM_list= osc_data_array(:, 2);
        BrightestCoeff_list= osc_data_array(:, 3);
        YM_real_fast_mean= nanmean(YM_list(YM_list>=0. &
YM_list<=5));
        XM_real_fast_time =nanmean(XM_list(find(YM_list>=1 &
YM_list<=5)));
        BrightestCoeff_real_fast_mean=
nanmean(BrightestCoeff_list(find(YM_list>=1 & YM_list<=5)));
        YM_fast_mean      =nanmean(YM_list(YM_list>5 &
YM_list<=10));
        XM_fast_time      =nanmean(XM_list(find(YM_list>5 &
YM_list<=10)));
        BrightestCoeff_fast_mean=
nanmean(BrightestCoeff_list(find(YM_list>5 & YM_list<=10)));
        YM_moderate_mean =nanmean(YM_list(YM_list >10 &
YM_list<=15));
        XM_moderate_time  =nanmean(XM_list(find(YM_list >10 &
YM_list<=15)));
        BrightestCoeff_moderate_mean=
nanmean(BrightestCoeff_list(find(YM_list >10 & YM_list<=15)));
        YM_slow_mean      =nanmean(YM_list(YM_list>15 &
YM_list<=20));
        XM_slow_time      =nanmean(XM_list(find(YM_list>15 &
YM_list<=20)));
        BrightestCoeff_slow_mean=
nanmean(BrightestCoeff_list(find(YM_list>15 & YM_list<=20)));
        YM_slower_mean    =nanmean(YM_list(YM_list>20 &
YM_list<=25));
        XM_slower_time    =nanmean(XM_list(find(YM_list>20 &
YM_list<=25)));
        BrightestCoeff_slower_mean=
nanmean(BrightestCoeff_list(find(YM_list>20 & YM_list<=25)));
        YM_nonoscillating_mean=nanmean(YM_list(YM_list>25));
        XM_nonoscillating_time=nanmean(XM_list(find(YM_list>25)));
        BrightestCoeff_nonoscillating_mean=
nanmean(BrightestCoeff_list(find(YM_list>25)));
        real_fast_XM= osc_data_array(osc_data_array(:, 2)>1 &
osc_data_array(:, 2)<5); %finds the corresponding Xms; finding scale values
of only fast oscillations (scale below 5)

        MeanThresholded_ResultsCopy{i,1}{1,j}(:,
'Real_fast_mean')= {YM_real_fast_mean};
        MeanThresholded_ResultsCopy{i,1}{1,j}(:,
'Real_fast_TIME')={XM_real_fast_time};

```

```

        MeanThresholded_ResultsCopy{i,1}{1,j}(:,
'BrightestCoeff_real_fast_mean')={BrightestCoeff_real_fast_mean};
        MeanThresholded_ResultsCopy{i,1}{1,j}(:, 'Fast_mean')=
{YM_fast_mean};
        MeanThresholded_ResultsCopy{i,1}{1,j}(:,
'Fast_TIME')={XM_fast_time};
        MeanThresholded_ResultsCopy{i,1}{1,j}(:,
'BrightestCoeff_fast_mean')={BrightestCoeff_fast_mean};
        MeanThresholded_ResultsCopy{i,1}{1,j}(:,
'Moderate_mean')= {YM_moderate_mean};
        MeanThresholded_ResultsCopy{i,1}{1,j}(:,
'Moderate_TIME')= {XM_moderate_time};
        MeanThresholded_ResultsCopy{i,1}{1,j}(:,
'BrightestCoeff_moderate_mean')={BrightestCoeff_moderate_mean};
        MeanThresholded_ResultsCopy{i,1}{1,j}(:, 'Slow_mean')=
{YM_slow_mean};
        MeanThresholded_ResultsCopy{i,1}{1,j}(:, 'Slow_TIME')={
XM_slow_time};
        MeanThresholded_ResultsCopy{i,1}{1,j}(:,
'BrightestCoeff_slow_mean')= {BrightestCoeff_slow_mean};
        MeanThresholded_ResultsCopy{i,1}{1,j}(:, 'Slower_mean')=
{YM_slower_mean};
        MeanThresholded_ResultsCopy{i,1}{1,j}(:,
'Slower_TIME')={XM_slower_time};
        MeanThresholded_ResultsCopy{i,1}{1,j}(:,
'BrightestCoeff_slower_mean')={BrightestCoeff_slower_mean};
        MeanThresholded_ResultsCopy{i,1}{1,j}(:,
'NonOscillating_mean')= {YM_nonoscillating_mean};
        MeanThresholded_ResultsCopy{i,1}{1,j}(:,
'NonOscillating_TIME')={XM_nonoscillating_time};
        MeanThresholded_ResultsCopy{i,1}{1,j}(:,
'BrightestCoeff_nonoscillating_mean')={BrightestCoeff_nonoscillating_mean};

        MeanThresholded_ResultsCopy{i,1}{1,j}(:, 'avg_osc_XM')=
{osc_data_avg_XM}; %% with this line, we are introducing the parameters of
scale and time to save along with every mito

MeanThresholded_ResultsCopy{i,1}{1,j}(:, 'std_osc_XM')={osc_data_std_XM};

MeanThresholded_ResultsCopy{i,1}{1,j}(:, 'avg_osc_YM')={osc_data_avg_YM};

MeanThresholded_ResultsCopy{i,1}{1,j}(:, 'std_osc_YM')={osc_data_std_YM};

        if (osc_data_avg_YM < 15) %% we classify every mito as
'slow', 'fast' or 'non oscillating' based on the average scale value we
obtain
MeanThresholded_ResultsCopy{i,1}{1,j}(:, 'osc_classification')={'fast'};
        else
            if (15<=osc_data_avg_YM && osc_data_avg_YM<=25)
MeanThresholded_ResultsCopy{i,1}{1,j}(:, 'osc_classification')={'slow'};
            else
MeanThresholded_ResultsCopy{i,1}{1,j}(:, 'osc_classification')={'non
oscillating'};

```

```

end
end
end
end
end
if dead_mito_count/size(MeanThresholded_ResultsCopy{i,1},2) >= 0.6 %%
if more than 60% of the mitos in each cell are dead, then the whole cell is
considered as dead
    cell_classification{i,1}='dead'; %% we have a separate
cell_classification array to record which cells are dead and when they died.
    cell_classification{i,2} = 0;
else
    cell_classification{i,1}='not dead'; %% if more than 60% of the
mitos of a cell are not dead, then the whole cell is considered as alive. If
some of the mitos did die along the way, their mito_death_time were
considered and the mito that held out the longest was used as the time for
the cell death
    cell_classification{i,2} = max(mito_death_time_array);
end
end
end

```

## 11. ON MATLAB: COMPILING REQUIRED INFORMATION FROM ABOVE DATA REDUCTION PROCESS

```

%%
Cell_YMs= {};
for i= 1: size(MeanThresholded_ResultsCopy, 1);
    local_cell_YMs={};
    for j= 1: size(MeanThresholded_ResultsCopy{i,1}, 2)
        if
strcmp(MeanThresholded_ResultsCopy{i,1}{1,j}.('classification')(1,1),'not
dead')
            local_cell_YMs{j, 1}=
MeanThresholded_ResultsCopy{i,1}{1,j}.('Real_fast_mean')(1);
            local_cell_YMs{j, 2}=
MeanThresholded_ResultsCopy{i,1}{1,j}.('Fast_mean')(1);
            local_cell_YMs{j, 3}=
MeanThresholded_ResultsCopy{i,1}{1,j}.('Moderate_mean')(1);
            local_cell_YMs{j, 4}=
MeanThresholded_ResultsCopy{i,1}{1,j}.('Slow_mean')(1);
            local_cell_YMs{j, 5}=
MeanThresholded_ResultsCopy{i,1}{1,j}.('Slower_mean')(1);
            local_cell_YMs{j, 6}=
MeanThresholded_ResultsCopy{i,1}{1,j}.('NonOscillating_mean')(1);
        else
            local_cell_YMs{j, 1}= NaN;%% changed from 'dead' to NaN,
since the term 'dead' is not compatible with an Array for the next step
            local_cell_YMs{j, 2}= NaN;
            local_cell_YMs{j, 3}= NaN;
            local_cell_YMs{j, 4}= NaN;
            local_cell_YMs{j, 5}= NaN;
            local_cell_YMs{j, 6}= NaN;
        end
    end
    Cell_YMs{i}=local_cell_YMs;
end
end

```

```

Cell_YMs= Cell_YMs';
%%%
Cell_YM_averages=-ones(size(Cell_YMs, 1),1);
for i= 1: size(Cell_YMs, 1)
    current_YM_array= [];
    YM_array_index=0;
    for j= 1: size(Cell_YMs{i, 1}, 2)
        if strcmp(cell_classification{i, 1}, 'dead')
            continue
        else
            YM_array_index= YM_array_index+1;
            current_YM_array(YM_array_index)= Cell_YMs{i,1}{1,j};
        end
    end
    if (size(current_YM_array) >0)
        Cell_YM_averages(i)= nanmean(current_YM_array);
    end
end
Cell_YM_averages_withNaN= Cell_YM_averages;
Cell_YM_averages_withNaN(Cell_YM_averages_withNaN==-1)=NaN;

%%%%%%%%%%%%%%%%%%%%%%%%%%%%%%%%%%%%%%%%%%%%%%%%%%%%%%%%%%%%%%%%%%%%%%%%

for i= 1: size(Cell_YMs, 1)
    cell_classification{i,3}=Cell_YM_averages(i);
end

%%%%%%%%%%%%%%%%%%%%%%%%%%%%%%%%%%%%%%%%%%%%%%%%%%%%%%%%%%%%%%%%%%%%%%%%
all_dead_count=0;
dead_with_some_alive=[];
some_alive_index=0;
not_dead=[];
not_dead_index=0;
for i= 1: size(cell_classification, 1)
    if cell_classification{i,2}==0
        if cell_classification{i,3}==-1
            all_dead_count=all_dead_count+1;
        else
            some_alive_index=some_alive_index+1;
            dead_with_some_alive(some_alive_index)=cell_classification{i,3};
        end
    else
        not_dead_index=not_dead_index+1;
        not_dead(not_dead_index)=cell_classification{i,3};
    end
end
dead_with_some_alive_avg=nanmean(dead_with_some_alive);
not_dead_avg=nanmean(not_dead);

%%
%MITO DEATH TIME
mitodeathtime_percell={};
for i= 1: size(MeanThresholded_ResultsCopy, 1);
    local_cell_mitodeathtime={};
    for j= 1: size(MeanThresholded_ResultsCopy{i,1}, 2)

```

```

        if
strcmp(MeanThresholded_ResultsCopy{i,1}{1,j}.('classification')(1,1),'not
dead')
            local_cell_mitodeathtime{j}=
MeanThresholded_ResultsCopy{i,1}{1,j}.('mito_death_time')(1);
        else
            local_cell_mitodeathtime{j}=0;
        end
    end
    mitodeathtime_percell{i}=local_cell_mitodeathtime;
end
%%
%GETTING THE TIME ASSOCIATED WITH DIFFERENT FREQUENCIES AND CONVERTING SCALE
TO PSEUDOFREQUENCIES
death_timefornotdeadcell=[];
death_timefornotdeadmito=[];
freq_notdeadcell=[];
freq_notdeadmito=[];
cellindex=0;
cellindex
mitoindex=0;
mitoindex
for i= 1: size(cell_classification, 1)
    i
    if cell_classification{i,2}~=0
        cellindex=cellindex+1;
        cellindex
        death_timefornotdeadcell(cellindex)=cell_classification{i,2};
        death_timefornotdeadcell(cellindex)
        freq_notdeadcell(cellindex)=cell_classification{i,3};
        freq_notdeadcell(cellindex)
        for j= 1: size(MeanThresholded_ResultsCopy{i,1}, 2)
            j
            if
strcmp(MeanThresholded_ResultsCopy{i,1}{1,j}.('classification')(1,1),'not
dead')
                mitoindex=mitoindex+1;
                mitoindex
                death_timefornotdeadmito(mitoindex)=
MeanThresholded_ResultsCopy{i,1}{1,j}.('mito_death_time')(1);

                freq_notdeadmito(mitoindex,1)=MeanThresholded_ResultsCopy{i,1}{1,j}.('Real_fa
st_mean')(1);

                freq_notdeadmito(mitoindex,2)=MeanThresholded_ResultsCopy{i,1}{1,j}.('Real_fa
st_TIME')(1);

                freq_notdeadmito(mitoindex,3)=MeanThresholded_ResultsCopy{i,1}{1,j}.('Fast_me
an')(1);

                freq_notdeadmito(mitoindex,4)=MeanThresholded_ResultsCopy{i,1}{1,j}.('Fast_TIME')(1);

                freq_notdeadmito(mitoindex,5)=MeanThresholded_ResultsCopy{i,1}{1,j}.('Moderat
e_mean')(1);

```

```

freq_notdeadmito(mitoindex,6)=MeanThresholded_ResultsCopy{i,1}{1,j}.('Moderate_TIME')(1);

freq_notdeadmito(mitoindex,7)=MeanThresholded_ResultsCopy{i,1}{1,j}.('Slow_mean')(1);

freq_notdeadmito(mitoindex,8)=MeanThresholded_ResultsCopy{i,1}{1,j}.('Slow_TIME')(1);

freq_notdeadmito(mitoindex,9)=MeanThresholded_ResultsCopy{i,1}{1,j}.('Slower_mean')(1);

freq_notdeadmito(mitoindex,10)=MeanThresholded_ResultsCopy{i,1}{1,j}.('Slower_TIME')(1);

freq_notdeadmito(mitoindex,11)=MeanThresholded_ResultsCopy{i,1}{1,j}.('NonOscillating_mean')(1);

freq_notdeadmito(mitoindex,12)=MeanThresholded_ResultsCopy{i,1}{1,j}.('NonOscillating_TIME')(1);
    freq_notdeadmito(mitoindex,13)= MitoAreas{1,i}(j, 1);

freq_notdeadmito(mitoindex,14)=MeanThresholded_ResultsCopy{i,1}{1,j}.('BrightestCoeff_real_fast_mean')(1);

freq_notdeadmito(mitoindex,15)=MeanThresholded_ResultsCopy{i,1}{1,j}.('BrightestCoeff_fast_mean')(1);

freq_notdeadmito(mitoindex,16)=MeanThresholded_ResultsCopy{i,1}{1,j}.('BrightestCoeff_moderate_mean')(1);

freq_notdeadmito(mitoindex,17)=MeanThresholded_ResultsCopy{i,1}{1,j}.('BrightestCoeff_slow_mean')(1);

freq_notdeadmito(mitoindex,18)=MeanThresholded_ResultsCopy{i,1}{1,j}.('BrightestCoeff_slower_mean')(1);

freq_notdeadmito(mitoindex,19)=MeanThresholded_ResultsCopy{i,1}{1,j}.('BrightestCoeff_nonoscillating_mean')(1);

    end
    end
end

time_points= 1:time_pt;
time_points=time_points';
time=time_points.*.25;
death_timefornotdeadmito=death_timefornotdeadmito';
Freqconvertedfromscale_MITO_real_fast=scal2frq(freq_notdeadmito(:,1),
'sym8', 15);
Freqconvertedfromscale_MITO_fast=scal2frq(freq_notdeadmito(:,3), 'sym8',
15);

```

```

Freqconvertedfromscale_MITO_moderate=scal2frq(freq_notdeadmito(:,5), 'sym8',
15);
Freqconvertedfromscale_MITO_slow=scal2frq(freq_notdeadmito(:,7), 'sym8',
15);
Freqconvertedfromscale_MITO_slower=scal2frq(freq_notdeadmito(:,9), 'sym8',
15);
Freqconvertedfromscale_MITO_nonoscillating=scal2frq(freq_notdeadmito(:,11),
'sym8', 15);

BrightestCoeff_RF_MITO=freq_notdeadmito(:, 14);
BrightestCoeff_F_MITO=freq_notdeadmito(:, 15);
BrightestCoeff_M_MITO=freq_notdeadmito(:, 16);
BrightestCoeff_S_MITO=freq_notdeadmito(:, 17);
BrightestCoeff_RS_MITO=freq_notdeadmito(:, 18);
BrightestCoeff_NO_MITO=freq_notdeadmito(:, 19);

Freqconvertedfromscale_CELL=scal2frq(Cell_YM_averages_withNaN, 'sym8', 15);
%change according to sampling rate
MitoAreasArray=freq_notdeadmito(:,13); %% Mitochondrial Cluster Area
death_timefornotdeadmito_minutes= death_timefornotdeadmito.*.25; %change
according to sampling rate
death_timefornotdeadcell= death_timefornotdeadcell';
death_timefornotdeadcell_minutes= death_timefornotdeadcell.*0.25; %change
according to sampling rate
%% To get Time Component of the different oscillation frequencies
Freq associated time= freq_notdeadmito(:, [2:2:12]);
Freq associated time minutes= Freq_associated_time.*.25;

Freqconvertedfromscale_MITO=cat(2, Freqconvertedfromscale_MITO_real_fast,
Freqconvertedfromscale_MITO_fast, Freqconvertedfromscale_MITO_moderate,
Freqconvertedfromscale_MITO_slow, Freqconvertedfromscale_MITO_slower,
Freqconvertedfromscale_MITO_nonoscillating);

Freq_average_MITO= nanmean(Freqconvertedfromscale_MITO, 2);

BrightestCoeff_AllFreq_MITO=cat(2, BrightestCoeff_RF_MITO,
BrightestCoeff_F_MITO, BrightestCoeff_M_MITO, BrightestCoeff_S_MITO,
BrightestCoeff_RS_MITO,BrightestCoeff_NO_MITO);
MultiplicationofFreqCoeff=
Freqconvertedfromscale_MITO.*(abs(BrightestCoeff_AllFreq_MITO));
WeightedMean_Hz= nansum(MultiplicationofFreqCoeff, 2)./
nansum(abs(BrightestCoeff_AllFreq_MITO), 2);
WeightedMean_mHz= WeightedMean_Hz.*1000;

%FIGURE
figure; histogram(Freqconvertedfromscale_MITO_real_fast,'DisplayName','real
fast', 'FaceColor',[1 0.701960784313725 0], 'BinWidth',0.00025);hold on;
histogram(Freqconvertedfromscale_MITO_fast,'DisplayName','fast','FaceColor',[
1 0 0], 'BinWidth',0.00025);hold on;
histogram(Freqconvertedfromscale_MITO_moderate,'DisplayName','moderate','Face
Color',[1 1 0], 'BinWidth',0.00025); hold on;
histogram(Freqconvertedfromscale_MITO_slow,'DisplayName','slow','FaceColor',[
0 0 1], 'BinWidth',0.00025);hold on;
histogram(Freqconvertedfromscale_MITO_slower,'DisplayName','slower','FaceColo
r',[1 1 1], 'BinWidth',0.00025); hold on;

```

```

histogram(Freqconvertedfromscale_MITO_nonoscillating,'DisplayName','non-
oscillating','FaceColor',[1 0 1], 'BinWidth',0.00025);

Freqconvertedfromscale_MITO_mHz= Freqconvertedfromscale_MITO.*1000;
Freq_MITO= Freqconvertedfromscale_MITO_mHz(:, 1);
indexNaN= find((isnan(Freq_MITO)));
Freq_MITO(isnan(Freq_MITO))= Freqconvertedfromscale_MITO_mHz(indexNaN, 2);
indexNaN= find((isnan(Freq_MITO)));
Freq_MITO(isnan(Freq_MITO))= Freqconvertedfromscale_MITO_mHz(indexNaN, 3);
indexNaN= find((isnan(Freq_MITO)));
Freq_MITO(isnan(Freq_MITO))= Freqconvertedfromscale_MITO_mHz(indexNaN, 4);
indexNaN= find((isnan(Freq_MITO)));
Freq_MITO(isnan(Freq_MITO))= Freqconvertedfromscale_MITO_mHz(indexNaN, 5);
indexNaN= find((isnan(Freq_MITO)));
Freq_MITO(isnan(Freq_MITO))= Freqconvertedfromscale_MITO_mHz(indexNaN, 6);

```

## 12. ON MATLAB: CLEARING VARIABLES THAT ARE NOT REQUIRED

```

%%% CLEARING UNECESSARY VARIABLES FROM WORKSPACE
clear EachCellsMitoROI
clear eachrow
clear er
clear ffs
clear jc
clear jm
clear local
clear Reper_results_dir
clear selpath
clear z
clear zz
%%%
clear ans
clear dataArray
clear eachcell
clear eachrow
clear er
clear fileID
clear k
clear m
clear myfilename
clear n
clear newfilename
clear AllcellsandMitos_Mean
clear Brightestpoints
clear MeanThresholded
clear current_brightest_cell
clear current_brightest_data
clear col_Area
clear col_BX
clear col_header
clear col_max_coeff
clear col_Width
clear col_XM
clear col_YM
clear current_cell
clear current_data

```



```
clear i
clear index
clear j
clear k
clear local_max
clear local_sum
clear YM_array_index
clear osc_index
clear local_cell_mitodeathtime
clear fileNumber
clear changefilename_dir
clear Brightestpoints_dir
```

```
clear Brightestpoints_dir
clear changefilename_dir
clear current_YM_array
clear fileNumber
clear local_cell_mitodeathtime
clear local_cell_YMs
clear MeanThresholded_dir
clear total_images
clear numberoffiles
```

```
clear A
clear B
clear filename
clear filestochangenames
clear fullDestination
clear i
clear Image_Dir
clear Image_folder
clear index
clear info
clear j
clear k
clear l
clear local_max
clear local_sum
clear Diff_stack_folder
clear new_name
clear newFileName
clear num_images
clear oldFileName
clear Q
clear startPerSym
clear startunderSym
```

```
%% if you want to check/ debug, then don't delete these variables. Go through
them to check where there may be a problem
```

```
clear osc_data_avg_XM
clear osc_data_avg_YM
clear osc_data_std_XM
clear osc_data_std_YM
clear some_alive_index
clear XM_fast_time
clear XM_nonoscillating_time
```

```

clear XM_moderate_time
clear XM_real_fast_time
clear XM_slow_time
clear XM_slower_time
clear YM_fast_mean
clear YM_moderate_mean
clear YM_nonoscillating_mean
clear YM_real_fast_mean
clear YM_slow_mean
clear YM_slower_mean
clear localArea
clear current_data1
clear real_fast_XM
clear XM_list
clear YM_list
clear time_pt
%%
clear delimiter
clear startRow
clear CabcksubRatio
clear CabcksubRatio_dir
clear CacliiumCalibration
clear CalciumCalib_dir

```

### 13. RESULTS ARE IN THE FOLLOWING ARRAYS:

- (i) **IPT\_2MAT\_Depolarization\_minutes** - Has the time point at which a cell depolarized during Ischemia
- (ii) **cell\_classification** - Column 1 has the state of each cell at the beginning of reperfusion, Column 2 has the time at which the cell depolarized (based on if 60% of mitochondria depolarized in that cell), Column 3 has the average frequency of that cell (based on average frequency of the oscillating clusters)
- (iii) **death\_timefornotdeadmito\_minutes** - Has the timepoint at which a mitochondrial cluster exhibited irreversible  $\Delta\Psi_m$  depolarization during Reperfusion
- (iv) **Freqconvertedfromscale\_MITO**- Has the average frequency of a mitochondrial cluster separated into different frequency bands and associated with a particular timepoint during reperfusion. Column 1 has frequencies ranging from 8.6-45mHz, Column 2 has 8.6-4.3mHz, Column 3 has 4.3-3mHz, Column 4 has 3-2.2 mHz, Column 5 has 2.2-1.8mHz and Column 6 has frequencies below 1.8 mHz.
- (v) **Freq\_associated\_time\_minutes** - Has the timepoint associated with the particular frequency of a mitochondrial cluster. Column 1 has frequencies ranging from 8.6-45mHz, Column 2 has 8.6-4.3mHz, Column 3 has 4.3-3mHz, Column 4 has 3-2.2 mHz, Column 5 has 2.2-1.8mHz and Column 6 has frequencies below 1.8 mHz. Along with the  $\Delta\Psi_m$  depolarization time, these values are used to make the violin

plots to obtain a complete graphical visualization of the dynamic oscillatory behavior of mitochondrial  $\Delta\Psi_m$ .

- (vi) **MitoAreasArray** - Contain area of each mitochondrial cluster
- (vii) **Freq\_MITO** - Has the predominant frequency exhibited by the mitochondrial cluster

## Curriculum Vitae

# DEEPTHI ASHOK

Johns Hopkins University School of  
Medicine  
720, Rutland Ave  
Baltimore 21205  
dashok1@jhmi.edu

## Education

- |              |  |
|--------------|--|
| 2013-Current | Ph.D Candidate, Cellular and Molecular Medicine<br>Johns Hopkins University School of Medicine, U.S.A<br>Advisor: Brian O'Rourke, Ph.D., Professor<br>Thesis Title: Role of Mitochondrial Calcium Uniporter in<br>Mitochondrial Membrane Potential Instability in Ischemia<br>Reperfusion Injury |
| 2008         | Master of Research in Medical and Molecular Biology<br>Newcastle University, Newcastle upon Tyne, U.K<br>Thesis title: Association Study of Mitochondrial Haplogroups with<br>Aging  |
| 2006         | Advisor: Patrick Chinnery, Ph.D., Professor<br>Bachelor of Science (Biotechnology, Chemistry and Botany)<br>Mount Carmel College, Bangalore University, Bangalore, India   |

## Awards/Funding offered

- American Heart Association, Scientific Sessions, BCVS Abstract Travel Award, 2018
- NIH Ruth L. Kirschstein National Research Service Award/ Predoctoral Fellowship  
September, 2016- 2019 (accepted)
- American Heart Association Predoctoral Fellowship, 2016 (declined)
- Pollard Scholar for Molecular Signaling Pathways and Cell Structure- 2015
- Newcastle University International Postgraduate Scholarship- 2007

## Major Research Experience

PhD. CANDIDATE

September 2013- Current

Cellular and Molecular Medicine Program  
Johns Hopkins University School of Medicine

Research Description:

- Characterizing mitochondrial behavior and developing wavelet-based approaches to uncover dominant frequencies of mitochondrial oscillations during ischemia/reperfusion injuries.
- Developing CRISPR-based adenoviral vectors for targeted gene regulation of mitochondrial proteins that are down-regulated in heart failure.

RESEARCH ASSOCIATE

August 2010 - June 2013

Buck Institute for Research on Aging, Novato, California, U.S.  
Supervisor: Martin Brand. Ph.D., Professor

Research Description:

- Evaluating bioenergetic differences between cybrids of African and European mitochondrial haplogroup background.
- High-Throughput screen for site-specific inhibitors of mitochondrial reactive oxygen species production
- Determining glutamate dehydrogenase activity from Sirtuin3 knock-out and wild-type mice

RESEARCH ASSISTANT August 2008 - February 2010

Newcastle University, Newcastle upon Tyne, U.K.

Supervisor: Patrick Chinnery, Ph.D., Professor

Research Description:

- Developing methods to quantify superoxide levels and mitochondrial membrane potential in lymphocytes in an aged population using flowcytometry. This work is an extension of my master's thesis (published in PLoS one, 2014)
- Candidate nuclear gene screening for Leber's Heredity Optic: Designed primers and optimized PCR conditions to sequence eight candidate genes in eight patients with LHON.
- Candidate region sequencing for neurodegeneration with brain iron accumulation: Sequenced the c19orf12 region (published Movement Disorders, 2012).

MASTER'S STUDENT

August 2007 - August 2008

Newcastle University, Newcastle upon Tyne, U.K.

Supervisor: Patrick Chinnery, Ph.D., Professor

Thesis Research Description: Determining if mitochondrial haplogroups influence aging phenotypes (published in Neurobiology of Aging, 2013)

## Publications

### Published

- Roman, Barbara, Pawandeep Kaur, **Deepthi Ashok**, Mark Kohr, Roopa Biswas, Brian O'Rourke, Charles Steenbergen, Samarjit Das. 2020. Nuclear-mitochondrial communication involving miR-181c plays an important role in cardiac dysfunction during obesity. *Journal of Molecular and Cellular Cardiology*. 144:87–96.
- Kyriakos N. Papanicolaou, **Deepthi Ashok** Ting Liu, Tyler M. Bauer, Junhui Sun, Zhen Li, Eduardo da Costa, Charles Crepy D'Orleans, Sara Nathan, David J. Lefer, Elizabeth Murphy, Nazareno Paolocci, D. Brian Foster, Brian O'Rourke. 2020. Global knockout of ROMK potassium channel worsens cardiac ischemia-reperfusion injury but cardiomyocyte-specific knockout does not: Implications for the identity of mitoKATP. *Journal of Molecular and Cellular Cardiology*. 139:176–189
- Laura Wiley, **Deepthi Ashok**, Carmen Martin-Ruiz, Duncan CS Talbot, Joanna Collerton, Andrew Kingston, Karen Davies, Patrick F Chinnery, Michael Catt, Carol Jagger, Thomas BL Kirkwood, Thomas von Zglinicki. Reactive oxygen species production and mitochondrial dysfunction in whiteblood cells are not valid biomarkers of ageing in the very old. *PLoS ONE*, 2014, 9(3): e91005. doi:10.1371/journal.pone.0091005
- Adam L. Orr, **Deepthi Ashok**, Akos A. Gerencser, Melissa R. Sarantos, Judy Shi, Robert E. Hughes, Martin D. Brand. Novel inhibitors of mitochondrial sn-glycerol 3-phosphate dehydrogenase. *PLoS ONE*, 2014 9(2): e89938. doi:10.1371/journal.pone.0089938
- Joanna Collerton, **Deepthi Ashok**, Carmen Martin-Ruiz, Angela Pyle, Gavin Hudson, Mohammad Yadegarfar, Karen Davies, Carol Jagger, Thomas von Zglinicki, Thomas BL Kirkwood, Patrick F Chinnery. Frailty and mortality are not influenced by mitochondrial DNA haplotypes in the very old. *Neurobiology of Aging*, 2013, 34(12), 2889.e1-2889.
- Adam L. Orr, **Deepthi Ashok**, Akos A. Gerencser, Melissa R. Sarantos, Judy Shi, Robert E. Hughes, Martin D. Brand. Inhibitors of ROS production by the ubiquinone-binding site of mitochondrial complex I identified by chemical screening. *Free Radical Biology and Medicine*, 2013, 65, 1047-1059
- Rita Horvath, Elke Holinski-Feder, Vivienne C.M. Neeve, Angela Pyle, Helen Griffin, **Deepthi Ashok**, Charlotte Foley, Gavin Hudson, Bernd Rautenstrauss, Gudrun Nürnberg, Peter Nürnberg, Jorg Kortler, Birgit Neitzel, Ingelore Bäßmann, Thahira Rahman, Bernard Keavney, John Loughlin, Sophie Hambleton, Benedikt Schoser, Hanns Lochmüller, Mauro Santibanez-Koref, Patrick F. Chinnery. A new phenotype of brain iron accumulation with

dystonia, optic atrophy and peripheral neuropathy. *Movement Disorders* 2012, 76(6), 789-793.

- George W. Rogers, Martin D. Brand, Susanna Petrosyan, **Deepthi Ashok**, Alvaro Elorza, David A. Ferrick, Anne N Murphy. High throughput microplate respiratory measurements using minimal quantities of isolated mitochondria. *PLoS One* 2011, Vol 6 (7), doi; 10.1371/journal.pone.0021746

### Submitted

- **Deepthi Ashok** and Brian O'Rourke. 2020. MitoWave: Spatio-temporal analysis of mitochondrial membrane potential fluctuations during ischemia-reperfusion. bioRxiv. 2020.05.21.108670.

### In preparation

- **Deepthi Ashok**, Kyriakos Papanicolaou, Michelle Wang, Ting Liu, Brian O'Rourke Mitochondrial Membrane Potential instability persists in Ischemia/Reperfusion injury in MCU-KO cardiomyocytes.

## Conference posters

Mitochondrial Membrane Potential Oscillations Persist During Reperfusion After Ischemia in MCU Knockout Cardiomyocytes. **Deepthi Ashok**, Kyriakos Papanicolaou, Brian O'Rourke *Circulation* 138 (Suppl 1), A13164-A13164, 2018

Enhancing Mitochondrial Biogenesis with a CRISPR/ndCas9 Adenoviral Vector System in Cardiomyocytes. **Deepthi Ashok**, Agnieszka Sidor, Brian O'Rourke. *Biophysical Journal* 114 (3), 662a Biophysical Society, 2018

miR-181c Regulates Mitochondrial Calcium Influx by targeting Cytochrome C Oxidase subunit 1 Soroosh Solhjoo, Sangeetha Kannan, **Deepthi Ashok**, Brian O'Rourke, Charles Steenbergen, Samarjit Das. *Journal of Molecular and Cellular Cardiology*. 112, 15, 2017

Crispr/ndcas9 Adenoviral Vector System as a Tool for Promoting Mitochondrial Biogenesis in Cardiomyocytes. **Deepthi Ashok**, Agnieszka Sidor, Brian O'Rourke. *Circulation* 136 (Suppl 1), A21011-A21011, 2017

CRISPR-mediated Transcriptional Regulation of Mitochondrial Proteins. **Deepthi Ashok**, Agnes Sidor, Ting Liu, Brian O'Rourke. *Cellular and Molecular Medicine Retreat*, 2015

## Teaching/Mentoring Experience

- Mentored Undergraduate students (Michelle Wang, Aditi Biswas, Lauren Parker) for summer research projects at Johns Hopkins University.
- Pollard Scholar for Signaling Pathways and Cell Structure (2015): Tutored lower year Cellular and Molecular Medicine PhD students on Pathways and Cell Structure course at Johns Hopkins University.
- Seahorse XF Analyzer advanced course at Buck Institute for Research on Aging (3 days) (April 2011 and April 2012):
  - Taught and demonstrated isolation of mitochondria from mouse liver.
  - Taught users to perform a coupling and electron flow experiment using isolated mitochondria.
  - Assisted users in performing bioenergetic assays on intact cells to study mitochondrial and glycolytic function.

## References

Brian O'Rourke, Ph.D.  
Professor of Medicine  
Vice Chair of Basic and Translational Research,  
Department of Medicine  
Johns Hopkins University School of Medicine  
720 Rutland Avenue  
Ross 1060  
Baltimore, MD 21205  
Phone: 410-614-0034  
[bor@jhmi.edu](mailto:bor@jhmi.edu)

Rajini Rao Ph.D.  
Director, Graduate Program in Cellular and Molecular  
Medicine  
Professor of Physiology  
Johns Hopkins University School of Medicine  
Room 201 Wood Basic Science Building  
Baltimore, MD 21205  
Phone: 410-955-4732  
[rrao@jhmi.edu](mailto:rrao@jhmi.edu)

Mark Edward Anderson, M.D., Ph.D.  
Director, Department of Medicine,  
Johns Hopkins University School of  
Medicine  
Professor of Medicine  
855 N. Wolfe St  
Baltimore, MD 21205  
[Mark.Anderson@jhmi.edu](mailto:Mark.Anderson@jhmi.edu)

David A. Kass, M.D.  
Abraham and Virginia Weiss Professor  
of Cardiology  
Professor of Biomedical Engineering  
Professor of Pharmacology and  
Molecular Sciences  
Director, Institute of CardioScience  
Johns Hopkins University School of  
Medicine  
Ross Building, 858, 720 Rutland  
Avenue, Baltimore MD  
410-955-7153  
[dkass@jhmi.edu](mailto:dkass@jhmi.edu)